KYB

Our Precision, Your Advantage

KYB Corporation

KYB TECHNICAL REVIEW No. 62 APR. 2021

KYB TECHNICAL REVIEW

ISSN 1880-7410

APR. 2021

No.62

KYB Corporation

(Kayaba Industry Co., Ltd. employed “KYB Corporation” as the popular name from October 1st, 2015.)

As of February 1, 2021

Head Office World Trade Center Bldg., 2-4-1, Hamamatsu-cho,
Minato-ku, Tokyo 105-6111, Japan Tel：(81)3-3435-3511

Basic Technology R&D Center	1-12-1, Asamizodai, Minami-ku, Sagamihara-shi, Kanagawa 252-0328, Japan	TEL:(81)42-745-8111
Production Technology R&D Center	60, Dota, Kani-shi, Gifu 509-0206, Japan	TEL:(81)574-26-1453
Developmental Experiment Center	1185, Kashio, Sirosuna, Kawabe-machi, Kamo-gun, Gifu 509-0307, Japan	TEL:(81)574-52-1323
Machine Tools Center	60, Dota, Kani-shi, Gifu 509-0206, Japan	TEL:(81)574-26-5310
Nagoya Branch	3-11-22, Meieki, Nakamura-ku, Nagoya-shi, Aichi 450-0002, Japan	TEL:(81)52-587-1760
Osaka Branch	TEK No. 2 Bldg., 1-23-20, Esaka-cho, Suita-shi, Osaka 564-0063, Japan	TEL:(81)6-6387-3221
Fukuoka Branch	Yasukawa Sangyou Bldg., 2-6-26, Hakataekihigashi, Hakata-ku, Fukuoka-shi, Fukuoka, 812-0013, Japan	TEL:(81)92-411-2066
Hamamatsu Sales Office	Hamamatsu Shimizu Bldg., 315-1 Shinmei-cho, Naka-ku, Hamamatsu-shi, Shizuoka, 430-0931 Japan	TEL:(81)53-454-5321
Hiroshima Sales Office	Hiroshima Bldg., 1-12-16 Hikari-machi, Higashi-ku, Hiroshima-shi, Hiroshima, 732-0052 Japan	TEL:(81)82-567-9166
SAGAMI PLANT	1-12-1, Asamizodai, Minami-ku, Sagamihara-shi, Kanagawa 252-0328, Japan	TEL:(81)42-746-5511
KUMAGAYA PLANT	2050, Nagazaike, Fukaya-shi, Saitama 369-1193, Japan	TEL:(81)48-583-2341
GIFU NORTH PLANT	2548, Dota, Kani-shi, Gifu 509-0298, Japan	TEL:(81)574-26-5111
GIFU SOUTH PLANT	505, Dota, Kani-shi, Gifu 509-0297, Japan	TEL:(81)574-26-1111
GIFU EAST PLANT	60, Dota, Kani-shi, Gifu 509-0206, Japan	TEL:(81)574-26-2135
KAYABA SYSTEM MACHINERY Co., Ltd.	1129-11, Kumozunagatsune-cho, Tsu-shi, Mie 514-0396, Japan	TEL:(81)59-234-4111
KYB Stage Engineering Co., Ltd.	1129-11, Kumozunagatsune-cho, Tsu-shi, Mie 514-0396, Japan	TEL:(81)59-234-9260
KYB TRONDULE Co., Ltd.	3090, Ura, Nagaoka-shi, Niigata, 949-5406, Japan	TEL:(81)258-92-6903
TAKAKO Industries, INC.	1-32-1 Hosononishi, Seika-cho, Souraku-gun, Kyoto, 619-0240, Japan	TEL:(81)774-95-3336
KYB Kanayama Co., Ltd.	4350-130 Tobe, Kanayama-cho, Gero-shi, Gifu, 509-1605 Japan	TEL:(81)576-35-2201
KTB-YS Co., Ltd.	9165 Sakaki, Sakaki-machi, Hanishina-gun, Nagano, 389-0688 Japan	TEL:(81)268-82-2850
KYB Motorcycle Suspension Co., Ltd.	2548, Dota, Kani-shi, Gifu 509-0298, Japan	TEL:(81)574-27-1170
KYB ENGINEERING & SERVICE Co., Ltd.	Sumitomo Fudousan Landmark Plaza 1-6-7 Shibakoen, Minato-ku, Tokyo 105-0011, Japan	TEL:(81)3-6895-1260
KYB Logistics Co., Ltd.	2-16, Himegaoka, Kani-shi, Gifu 509-0249, Japan	TEL:(81)574-26-6427
JAPAN ANALYSTS Co., Ltd.	KYB Corporation SAGAMI PLANT 1-12-1, Asamizodai, Minami-ku, Sagamihara-shi, Kanagawa 252-0328, Japan	TEL:(81)42-749-7512
Kensiyuu Co., Ltd.	NBC Hamamatsu-cho Bldg., 2-9-3, Hamamatsu-cho, Minato-ku, Tokyo 105-0013, Japan	TEL:(81)3-3437-1955

Overseas Subsidiaries and Affiliates

【Americas】

KYB Americas Corporation
2625 North Morton, Franklin, Indiana 46131, U.S.A.
TEL: (1)317-736-7774

Takako America Co., Inc.
715 Corey Road Hutchinson, Kansas 67504-1642, U.S.A.
TEL: (1)620-663-1790

KYB International America, Inc.
2625 North Morton, Franklin, Indiana 46131, U.S.A.
TEL: (1)317-346-6719

KYB Mexico S.A. de C.V.
Circuito San Roque Norte #300 Santa Fe II, Puerto Interior, Silao Guanajuato, CP 36275, Mexico
TEL: (52)472-748-5000

KYB Latinoamerica, S.A. de C.V.
Blvd. Manuel Avila Camacho No. 32, Int. 403, Col. Lomas de Chapultepec, Del. Miguel Hidalgo, DF, 11000, Mexico
TEL: (52)55-5282-5770

KYB Manufacturing do Brasil Fabricante de Autopeças S.A.
Rua Francisco Ferreira da Cruz, 3000, Fazenda Rio Grande-Parana, CEP 83820-293, Brazil
TEL: (55)41-2102-8204

Comercial de AutopeÇas KYB do Brasil Ltda.
Rua Cyro Correia Pereira, 2400 Suite 07-Cidade Industrial, Curitiba-PR, 81460-050, Brazil
TEL: (55)41-3012-3620

【Europe】

KYB Europe GmbH
Langfeldstrasse.11 80939 Munich, Germamy
TEL: (49)-89-5480188-0

KYB Suspensions Europe, S.A.U.
Ctra, Irurzun S/No, 31171 Ororbia Navarra, Spain
TEL: (34)948-421700

KYB Steering Spain, S.A.U.
Poligono Ipertegui No. 2, nave 12, CP-31160, ORKOIEN Navarra, Spain
TEL: (34)948-3121004

KYB Advanced Manufacturing Spain, S.A.U.
Poligono Industrial Perguita Calle B, No. 15, 31210 Los Arcos Navarra, Spain
TEL: (34)948-640336

KYB Manufacturing Czech, s.r.o.
U Panasonicu 277, Stare Civice, 530 06 Pardubice, Czech Republic
TEL: (420)466-812-233

KYB CHITA Manufacturing Europe s.r.o.
Prumyslova 1421, 53701 Chrudim, Czech Republic
TEL: (420)469-363-302

LLC KYB Eurasia
117638 Odesskaya street 2 building A, Moscow, Russian Federation
TEL: (7)495-7716010

【Asia】

KYB Steering (Thailand) Co., Ltd.
700/829 Moo 6, T. Nongtamlueng Amphur Panthong, Chonburi 20160,Thailand
TEL: (66)3-818-5559

KYB(Thailand)Co., Ltd.
700/363 Moo 6, Amata Nakorn Industrial Park2, Bangna-Trad Road, K.M. 57, Tambol Don Hua Roh, Amqhur Muang, Chonburi 20000, Thailand
TEL: (66)3-846-9999

KYB Asian Pacific Corporation Ltd.
No. 4345 Bhiraj Tower at BITEC, Unit 1209-1211, 12th Floor, Sukhumvit Road, Bangnatai Sub-District, Bangna District, Bangkok 10260, Thailand
TEL: (66)2-300-9777

KYB-UMW Malaysia Sdn. Bhd.
Lot 8, Jalan Waja 16, Telok Panglima Garang, 42500 Kuala Langat, Selangor, Malaysia
TEL: (60)3-3322-0800

PT. KYB Hydraulics Manufacturing Indonesia
JL. Irian X blok RR2 Kawasan MM2100, Cikarang Barat 17520, Indonesia
TEL: (62)21-28080145

PT. Kayaba Indonesia
JL, Jawa Blok ii No. 4 Kawasan MM2100, Cikarang Barat 17520, Indonesia
TEL: (62)21-8981456

PT. Chita Indonesia
JL, Jawa Blok ii No. 4 Kawasan MM2100, Cikarang Barat 17520, Indonesia
TEL: (62)21-89983737

KYB Manufacturing Vietnam Co., Ltd.
Plot I 10-I 11-I 12, Thang Long Industrial Park, Dong Anh District, Hanoi, Vietnam
TEL: (84)24-3881-2773

Takako Vietnam Co., Ltd.
27 Dai Lo Doc Lap, Vietnam Singapore Industrial Park, Thuan An District, Binh Duong, Vietnam
TEL: (84)274-378-2954

永華機械工業股份有限公司
KYB Manufacturing Taiwan Co., Ltd.
No. 493, Guang Hsing Road, Bade District, Taoyuan City, 33454, Taiwan
TEL: (886)3-368-3123

KYB Motorcycle Suspension India Pvt. Ltd.
Pilot No. 6, Sipcot Industrial Park, Vallam Vadagal Village, Sriperumbudur Taluk, Kancheepuram District 631604 Tamil Nadu, India
TEL: (91)44-3012-4301

KYB-Conmat Pvt. Ltd.
702-703, Beside N. H. No. 8, Por, Vadodara 391243, Gujatat, India
TEL: (91)960-1551608

KYB Corporation Chennai Branch
No. 408, Height 1, Temple Green Project, Mathur Village, Sriperumbudur Taluk, Kancheepuram District, India 602105
TEL: (91)2568-0501

KYB Middle East FZE
Office No. 2010 20th Floor, Tower-A
JAFZA One, Jebel Ali Free Zone,
PO.BOX:261819, Dubai, UAE
TEL: (971)4-887-2448

【China】

凱迩必(中国)投資有限公司
KYB (China) Investment Co., Ltd.
No. 121, Wei 3 Road, Dingmao, Zhenjiang New Zone, Zhenjiang, Jiangsu, 212009, China
TEL: (86)511-8558-0300

凱迩必機械工業(鎮江)有限公司
KYB Industrial Machinery (Zhenjiang) Ltd.
No. 38, Wei 3 Road, Dingmao, Zhenjiang New Zone, Zhenjiang, Jiangsu, 212009, China
TEL: (86)511-8889-1008

無錫凱迩必拓普減震器有限公司
Wuxi KYB Top Absorber Co., Ltd.
No. 2 Xikun North Road, Singapore Industrial Zone, Xinwu District, Wuxi, Jiangsu, 214028, China
TEL: (86)510-8528-0118

常州朗鋭凱迩必減振技術有限公司
Changzhou KYB Leadrun Vibration Reduction Technology Co., Ltd.
No. 19 Shunyuan Road, New District, Changzhou, Jiangsu 213125 China
TEL: (86)519-8595-7206

湖北恒隆凱迩必汽車電動転向系統有限公司
Hubei Henglong & KYB Automobile Electric Steering System Co., Ltd.
108 Shacen Road, Economic and Technological Development Zone, Jingzhou, Hubei, China. 434000
TEL: (86)716-416-7951

知多弾簧工業(鎮江)有限公司
CHITA KYB Manufacturing (Zhenjiang) Co., Ltd.
No. 8 Building-1F, New Energy Industrial Park (North Park), No. 300, Gangnan Road, Zhenjiang New District, Jiangsu 212132, China
TEL: (86)511-8317-2570

KYB TECHNICAL REVIEW

No. 62 APR. 2021

CONTENTS

The cover of this issue

<Comment by the cover designer>

"The beautiful sunrise from the sea line makes us image the dawn of something new. I designed this cover, being aware of KYB's strong commitment to transfer of its engineering expertise to next generation for maintaining this beautiful globe environment."

Foreword

Magnetic Functional Fluid Research and Interdisciplinary Research

IDO Yasushi*

A magnetic fluid is a type of artificial fluid that was developed in the 1960s. The fluid consists of ferromagnetic fine particles, such as magnetite or manganese zinc ferrite, of a particle size of about 10 nm whose surface is coated with a surfactant such as oleic acid that are stably distributed within a carrier fluid, usually water or oil. The magnetic fluid has very interesting characteristics: it is attracted by a magnet and develops many protruding structures ("the spike structure") along the magnetic fluid interfaces. Apart from the magnetic fluid, there exists a magnetorheological (MR) fluid that ferromagnetic particles of a submicron to several micron grain size are distributed in a carrier fluid. This is a magnetic functional fluid that reacts with a magnetic field. As an example, Fig. 1 shows a droplet of an MR fluid that micron-sized ferromagnetic particles are distributed in a magnetic carrier fluid prepared in my laboratory. As shown in the figure, when a droplet is dropped on an acrylic plate and is applied with a magnetic field of a permanent magnet placed under the plate, the droplet shows a type of interfacial deformation. The photo shows that the droplet has a number of thorn-like projections. With its response characteristic in a magnetic field (i.e., it changes in viscosity when subjected to a magnetic field), the MR fluid has found its application in and been commercialized as adjustable shock absorbers and other products.

I started my carrier as a researcher in a university's laboratory where I encountered "the magnetic fluid". Although the term "nanotechnology" did not exist at that time, we knew that particles distributed in a magnetic carrier fluid were of nanometer size. That might be the early days of nanotechnology. When I was a student in a graduate school, I reported findings from my research in an academic conference for magnetic fluid specialists. The participants included, not only mechanical engineering researches specialized in fluid engineering and thermal engineering including me, but also researchers from material engineering, physics, chemistry or electrical engineering. The conference was also joined even by artists who tried to express the interfacial deformation of a magnetic fluid as a work of art. As I reported my research results mainly in this type of conferences in my school age, I took it granted that specialists and researchers from a variety of fields come together. Actually, it was when I found a job at a university for another academic field that I noticed it had been very rare for specialists from various fields to gather together under one roof. At that time (and probably even today as well), researchers generally tended to focus on their own field of research and would not interfere with the other fields so much. Communications with specialists from other fields have helped me promote subsequent interdisciplinary research a lot. Thereafter a social (particularly political?) pressure to promote research for an amalgam of different fields rose, but not so many successful cases have been apparently found. One of the problems with the promotion of an amalgam of different fields is that specialists from different fields use their own popular but specific words and terms if their fields are quite apart from each other. One from a field may not be able to understand what others from another field is talking, Still I think the most difficult barrier is that they believe they "cannot do it" or "have no time to try another field now" to begin with.

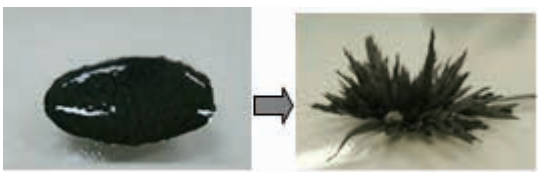

Fig. 1 Interfacial deformation of magnetic functional fluid when subjected to a magnetic field

I think it will be possible for a group of specialists to promote a series of research including from material development, development of mechanisms/principles using the developed materials, to application research for commercialization, if a division of work among them is established well. I hope that the current situation in which researchers are loudly encouraged to be involved in interdisciplinary research but produce nothing is getting to be better even slightly.

Finally, we faced many difficulties with the pandemic of COVID-19 during 2020. The society not only in Japan but also worldwide has totally changed. In universities, professors and students are forced to face changing circumstances as in most classes held online. I definitely wish we will be able to recover from this tough situation as soon as possible.

* Professor, Nagoya Institute of Technology

Editorial

Magneto-Rheological Technologies

NAKANO Masami*

1. Introduction

The science of the phenomenon that a material changes its viscoelasticity when subjected to a magnetic field is called Magneto-Rheology. The function of it is called the Magnetorheological Effect or the MR effect. Typical materials of this kind include a Magneto-Rheological Fluid, which is one of the functional fluids. The MR fluid is a suspension containing micro-sized ferromagnetic particles densely dispersed within a type of oil, such as silicone oil, as a carrier medium. The MR fluid has a special feature: its viscosity (more exactly, yield shear stress) can be changed electrically, reversibly and continuously in several milliseconds order when subjected to a magnetic field [1]. In other words, the MR fluid behaves like a solid with the application of a magnetic field and becomes a liquid with fluidity in the absence of such a field. Fluid power equipment and systems can effectively use the functionality of the MR fluid to deliver functions that have not ever been seen before and to have several significant features including high-speed, easy-to-use, compactness and intelligence. Thus, fluid power systems are expected to be "smart". Technologies to create different functional materials delivering the MR effect and their application technologies are collectively called Magneto-Rheological (MR) Technology, as in the title of this article.

In addition to the MR fluid, this article also covers an MR fluid porous composite consisting of porous material impregnated with an MR fluid for higher MR effect and less sedimentation of the dispersed particles, a high-fluidity dry MR fluid consisting of oil-free ferromagnetic particles for higher MR effect and higher environmental resistance, and an MR elastomer consisting of ferromagnetic fine particles dispersed and cured within a carrier matrix such as silicone rubber. Mainly by introducing the author's research and development cases, the article discusses advanced MR technologies to create and evaluate various functional fluids and soft materials delivering the MR effect including those described above as well as technologies to apply these fluids or materials in different fields.

* Professor, New Industry Creation Hatchery Center (NICHe), Tohoku University

2. MR Fluid and Its Applications

2.1 MR Effect of MR Fluid

An MR fluid can change its rheological properties quickly and reversibly when it is applied with a magnetic field. This function relies on a mechanism that ferromagnetic particles having a number of magnetic domains are polarized with the application of a magnetic field and the particles are connected together to form clusters as shown in Fig. 1. This mechanism to deliver the MR effect causes the MR fluid to behave like a Bingham fluid that has a yield shear stress τ_y with the application of a magnetic field. This induced shear stress τ can be expressed by the equation below:

$$\tau = \tau_y + \eta\dot{\gamma} \quad (1)$$

Where, η is the plastic viscosity of the MR fluid and $\dot{\gamma}$ is the shear rate of the fluid. Fig. 2 shows the typical magneto-rheological property (flow curve: shear rate $\dot{\gamma}$ - shear stress τ curve) of a commercially available MR fluid

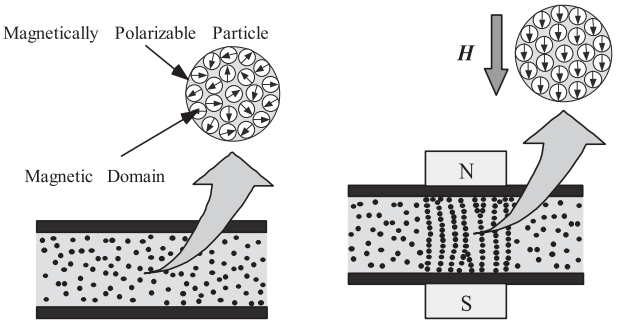

(a) No magnetic field (b) Under a magnetic field

Fig. 1 Formation of particle clusters in MR fluid under a magnetic field

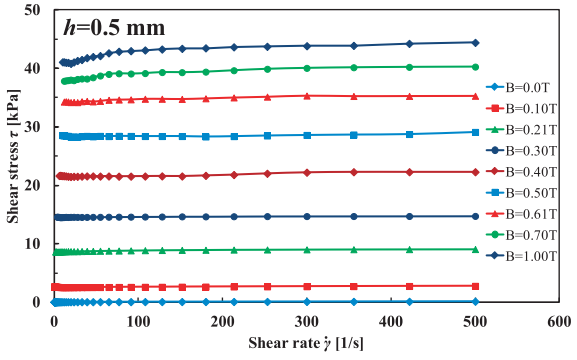

Fig. 2 Flow curves of MR fluid (MRF-132DG)

(MRF-132DG, Lord Co.) measured with a parallel double disc rheometer (the inter-disc distance h = 0.5 mm) [2]. According to the figure, the shear stress shows an almost constant value not depending on the shear rate for all the levels of the applied magnetic flux density B, except in the low shear rate region under a relatively high magnetic field. The yield shear stress at a shear rate of $\dot{\gamma} = 0s^{-1}$ (the shear stress value at the point of intersection of the flow curve and the vertical axis) increases roughly proportionately with the applied flux density. However, the stress tends to be magnetically saturated when B is about 0.7T or higher. With B = 1.0T, the shear stress τ reaches about 45 kPa, which means that the MR fluid can deliver a considerably high induced shear stress.

2.2 MR Fluid Application Technologies

At present, the annual production/sales of MR fluids are on the order of 300 tons, and various equipment and systems using MR fluids, notably shock absorbers for vehicle suspension, have been commercialized and popularly used [3]. This section explains the application of MR fluid in fluid power components including dampers, brakes and clutches, and introduces different types of smart machine systems that make use of them.

To realize an MR fluid damper that can be operated reliably even during power interruption, the MR fluid damper not using any electrical control system that can change its damping force in response to the product (positive or negative) of displacement and velocity using permanent magnets and check valves, has been developed, proving the effectiveness of its application in seismic base isolation systems of building structures [4]. As shown in Fig. 3, this damper has two piston heads, each of which has an annular orifice that is applied with a magnetic field according to the opened/closed operation of a magnetic circuit depending on the displacement, and a magnetic-free bypass orifice with a check valve that is opened or closed according to the direction of flow (positive/negative damper speed). With this structure, the damper can control its damping force f according to the sign of the product of displacement x and velocity v (increases f if the product of x and y is below 0 or decreases f if the product of x and y is above 0).

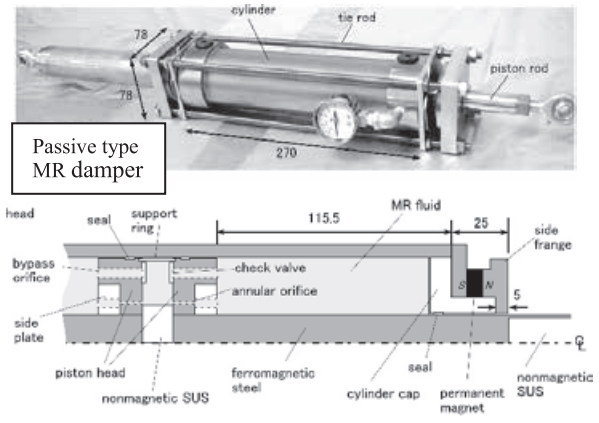

Fig. 3 Illustration of MR damper whose damping force is variable depending on the product of displacement and velocity

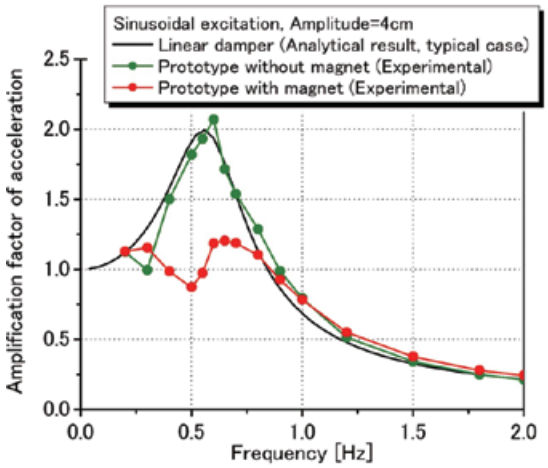

Fig. 4 Seismic control property of SDOF base isolation system consisting of the developed MR dampers

According to the seismic control property of the single-degree-of-freedom (SDOF) base isolation system consisting of the developed MR damper (Fig. 4), the amplification factor of acceleration substantially decreases only at around the resonance frequency, proving the effectiveness of the seismic isolation control.

With the application of a magnetic field (a coil current), the MR fluid clutch can deliver the torque limiting function and the slip rotation function with a certain torque. Combining this clutch with a motor or other power source will ensure back drivability, which can be expected to contribute to higher safety and security of robots used in contact with human. An MR fluid actuator consisting of a servo motor, a multi-disc MR fluid clutch and reduction gears for power-assisted leg orthosis for rehabilitation with back drivability has been developed, in order to improve the safety and security (Fig. 5) [5]. The developed MR fluid clutch adequately meets the target design torque (approx. 4.5 Nm) and can deliver a high response speed.

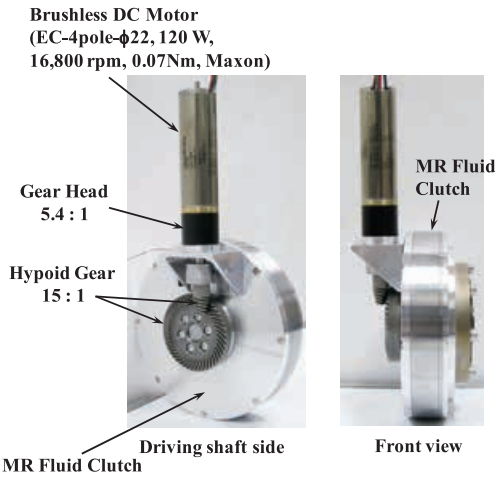

Fig. 5 MR fluid actuator developed for use in power-assisted leg orthosis

In addition, the clutch is not dependent on the rotation speed so much and the transmission torque can be freely set only with the applied current, offering high controllability. Because of the structural safety of the MR fluid clutch with the torque limiting function, the developed MR fluid actuator can ensure back drivability and is suitable for use in the power-assisted equipment.

As a first step to apply MR fluid clutches and brakes to power transmission and control systems, we designed and developed an MR fluid brake for compact electric vehicles (EVs). We have investigated the braking characteristics and road-tested a car (super-compact EV) equipped with the brakes on the four wheels. The test has demonstrated that the MR fluid brake for this vehicle has adequate braking performance, adequate high-speed responsivity and high controllability realizing the application of the brake feeling control and the anti-lock braking control system (ABS) (Fig. 6) [6]. The MR fluid brake is expected to be commercially applied to smart mobility.

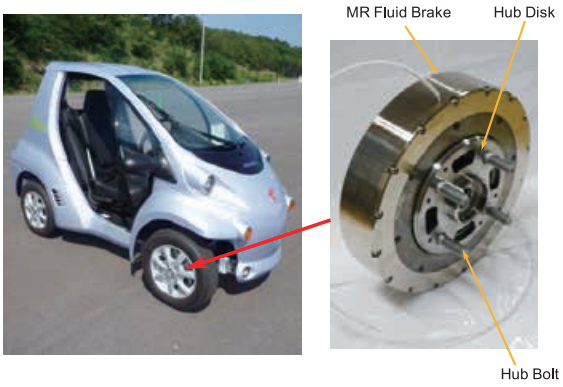

Fig. 6 MR fluid brake for vehicles and its installation on a compact EV

3. MR Fluid Porous Composite and Its Application Technologies

3.1 MR Effect of MR Fluid Porous Composite

To prevent the sedimentation of dispersed particles in the MR fluid, we have developed an MR fluid porous composite consisting of a nonwoven fabric impregnated with an MR fluid since the fluid can be retained in porous material [7]. This also eliminates the necessity of using leakage prevention seals. Two types of nonwoven fabric of different lateral modulus G and different porous structures (Fig. 7(a) and (b)) were selected as porous materials, and then impregnated these nonwoven fabrics were impregnated with an MR fluid (MRF-132DG) to fabricate an MR fluid porous composite. The MR effect of the composites in an oscillating shear mode under a uniform magnetic field was evaluated. Fig 7(c) shows how the maximum induced shear stress τ_{max} on the displacement-shear stress hysteresis curve obtained changes with the applied flux density B. To investigate whether the maximum shear stress is affected by the magnetism of the contact material or not, two types of oscillating sliding plates were used: iron and aluminum. Fig.7(c) shows that

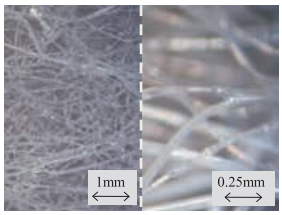

(a) KN-60-3, t=0.8mm

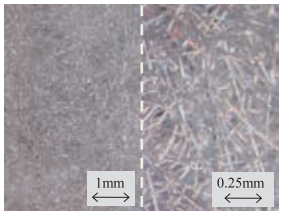

(b) TRF-50H, t=0.5mm

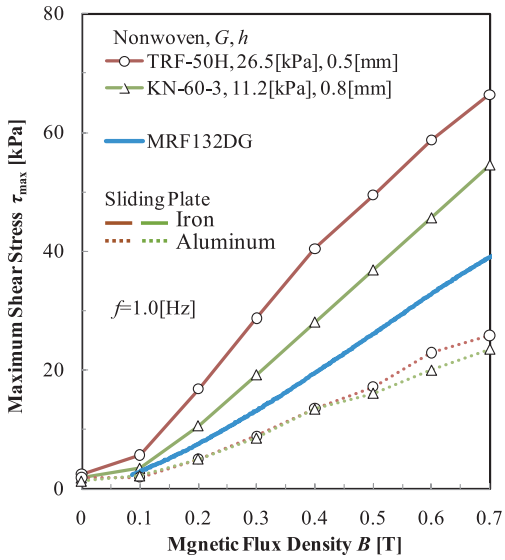

(c) Curves of maximum shear stress τ_{max} against applied flux density B

Fig. 7 MR effect of test unwoven fabrics and MR fluid porous composite (depending on the material of contact sliding plate)

for the composites using both types of nonwoven fabric, the maximum shear stress with the iron sliding plate was generally about 2.0 to 2.5 times higher than that with the non-magnetic aluminum sliding plate, and was about 1.4 to 1.7 times higher than that of the MR fluid. Therefore, the MR fluid porous composite can be expected to remarkably improve the MR effect. It should also be noted that the nonwoven fabric of a higher lateral modulus in which finer fibers are intertwined with each other in a more complexed way (TRF-50H) shows a higher maximum shear stress.

3.2 MR Fluid Porous Composite Application Technologies

Coil winding may have a break or irregular winding attributable to an improper or fluctuating tension of the wire. To control the wire tension of coil winding during the production process, some equipment designed to control the pulleys for the wire with a mechanical friction or hysteresis brake are commonly used. The equipment always involves a fundamental problem related to the rotational inertia of the pulley and brake system. For non-circular coil winding in which the wire velocity substantially varies, it is unavoidable for the wire to have fluctuating tension. Fig. 8 shows a brake that was developed to resolve this fundamental problem [8]. The brake uses a mechanism that the wire is directly run through the

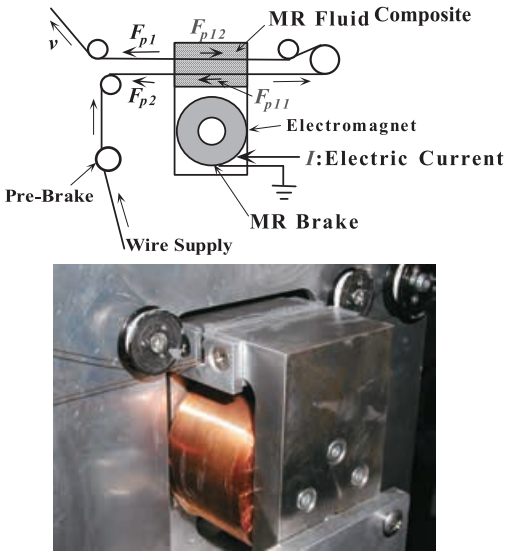

Fig. 8 MR fluid porous composite brake developed for wire tension control system for coil winding

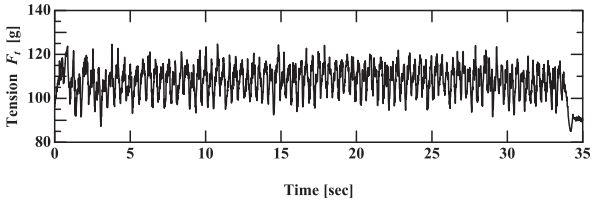

(a) Wire tension controller using conventional mechanical friction brake

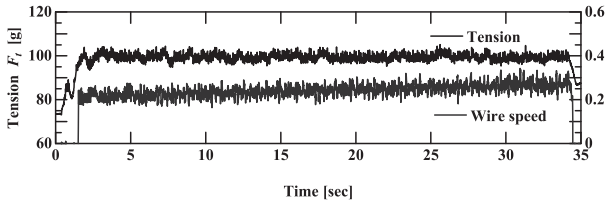

(b) Wire tension controller using MR fluid porous composite brake applied with PID tension feedback control

Fig. 9 Temporal tension fluctuation during non-circular coil winding test

MR fluid porous (66Nylon polyurethane foam) composite to receive braking due to the drag force (a rectangular annular electromagnet has a clearance of 2.5 mm whose both pole faces are affixed with a sheet of MR fluid porous composite each, between which the wire is run through). It has been verified that the wire tension increases roughly in proportion to the magnetic field intensity of the magnetic field applied to the MR fluid porous composite brake, thereby causing the brake to effectively serve as a tension control brake. This tension controller with the developed MR fluid porous composite brake was mounted on an actual coil winding machine to conduct tests to wind a square-shaped noncircular coil (wire diameter d = 0.21 mm), for which the wire velocity always varies, at an average wire velocity v = 0.28 m/sec. The tension fluctuation during the winding is shown in Fig. 9. For the tension control using a mechanical friction brake with conventional pulleys (Fig. 9(a)), the tension fluctuates with an amplitude as large as about 10 g over the whole range. On the other hand, for the tension control using the developed MR fluid porous composite brake applied with PID tension feedback control (Fig. 7(b)), the tension fluctuates with an amplitude as very small as about 2 g, which is equivalent to about 1/5 of that for the mechanical brake control. Furthermore, the temporal variation of the average tension is also suppressed to show good control performance partially because of the PID control to keep the tension almost to the setting [8].

When applying the MR fluid damper to the seismic base isolation or vibration control system of a building structure, the sedimentation of ferromagnetic fine particles dispersed in the MR fluid when it is left at rest for a long time poses a practical problem related to the reliability issue. This particle sedimentation problem can be solved by making use of the MR fluid porous composite consisting of a nonwoven fabric impregnated with an MR fluid. A 20 kN class linear motion variable damping MR damper (maximum total length 800 mm, stroke +/- 100 mm) for seismic base isolation or vibration control systems using the MR fluid porous composite based multi-disc rotary

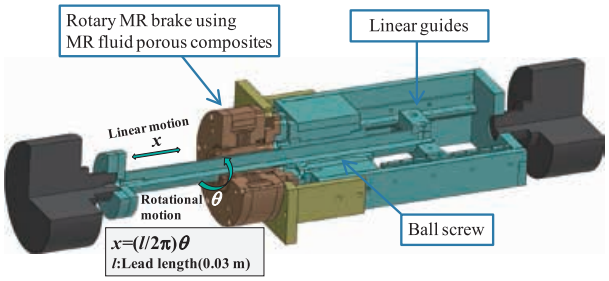

Fig. 10 Linear motion variable damping force MR damper using MR fluid porous composite multi-disc rotary brake

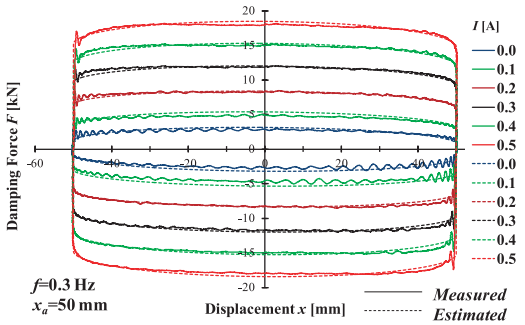

Fig. 11 Changes of hysteresis curves of displacement x - damping force F with coil current I at sinusoidal excitation

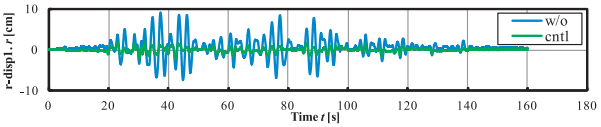

Fig. 12 Response of SDOF isolation system using MR fluid porous composite linear motion MR dampers to Sannomaru seismic wave

MR brake and a ball screw that converts the rotation into a linear motion (Fig. 10) [9]. Fig. 11 shows the hysteresis curves of the generated damping force F vs. the displacement x at sinusoidal excitations (f = 0.3 Hz, x_a = 50 mm). The hysteresis curves show a rectangular loop for every applied coil current I for all coils. The maximum damping force increases as I increases and almost reaches the design value of 20 kN at I = 0.5A. Fig. 12 gives an example of seismic control performance of the SDOF base isolation system using the linear motion MR damper with the MR fluid porous composite brake, which shows the responses to the Sannomaru (an enceinte in Nagoya Castle) seismic wave. The vibration displacement of an object (a building structure in this case) can be substantially reduced by applying the relative speed feedback control.

4. Dry MR Fluid and Its Application to Vehicle's Power Transmission/Braking System

4.1 MR Effect of Dry MR Fluid

When applying the conventional MR fluid to various devices, it is required that the fluid can be used properly within environmental temperatures ranging from around -40°C to 160°C. Since the carrier medium of the MR fluid is liquid such as oil, the higher viscosity at lower temperature often poses a problem. Particularly when using the MR fluid in a power transmission/braking system such as clutches and brakes, the drag torque due to the MR fluid of a higher viscosity at lower temperature substantially increases. As a solution to this problem, we have proposed and developed an oil-free dry MR fluid that uses a carrier gas, instead of the carrier liquid such as oil, within which micro-sized ferromagnetic fine particles core-shell-coated with nano SiO_2 fine particles are dispersed to deliver high fluidity [10]. The optimal fraction of SiO_2 for the greatest MR effect while maintaining the higher fluidity is about 0.49 wt%. Fig. 13 shows how the flow curve (shear stress - shear rate curve) for the dry MR fluid of SiO_2 = 0.49 wt% changes with the applied magnetic field. The shear stress shows an almost constant valve, independent of the shear rate for every applied magnetic flux density B. The shear stress τ almost reaches about 50 kPa with B = 0.9T.

4.2 Application of Dry MR Fluid to Vehicle Brakes

We have tried to apply the developed dry MR fluid to vehicle's wheel brakes. We have developed a multi-layer disc type dry MR fluid brake for compact electric vehicles (EVs). We have demonstrated that the brake has good braking performances by road-testing of a compact EV equipped with the brakes on the four wheels (Fig. 14). Fig. 15 shows the steady-state torque characteristics of the developed dry MR fluid brake. When the coil is applied with a current I A for 20 seconds, a braking torque is quickly rose up and kept at an almost constant level. When the current is removed, it is quickly returned to the drag torque. The steady-state braking torque increases as the coil current increases and reaches the maximum braking torque of 180 Nm, which is higher than the target design torque of 160 Nm, in the application of I = 2.5 A.

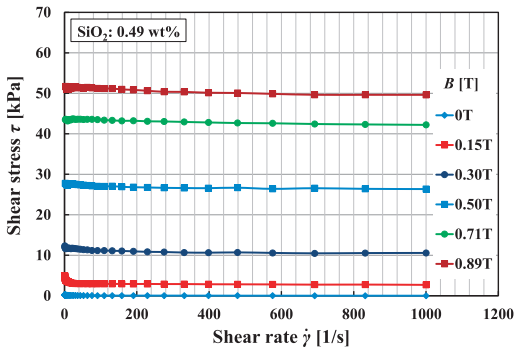

Fig. 13 Flow curve of dry MR fluid (SiO_2: 0.49 wt%)

Fig. 14 Compact EV with dry MR fluid brakes on the four wheels

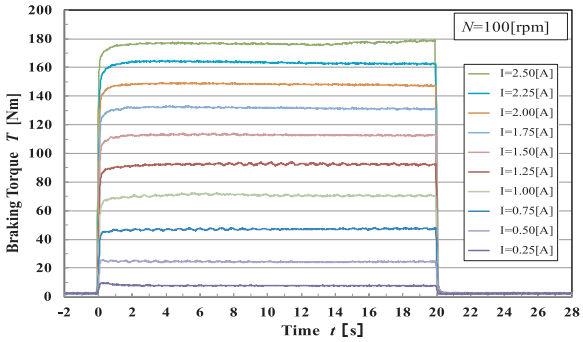

Fig. 15 Steady-state torque characteristics of dry MR fluid brake for compact EVs

5. MR Elastomer and Its Application to Variable Stiffness Devices

The MR fluid normally uses a liquid such as oil as the carrier medium. Silicone rubber or other similar matrix can also be used as a carrier medium, in which ferromagnetic particles are dispersed, and is cured to fabricate an MR elastomer (MRE) mainly whose elasticity (or stiffness) is variable with the application of a magnetic field [11]. A laminated MRE isolator for building base isolation has been developed that consists of alternately laminated MRE and steel layers, a permanent magnet located in the midst of the lamination and an electromagnet surrounding the lamination to make up a magnet circuit, as shown in Fig. 16(a) [12]. In this seismic base isolator, the magnetic field applied to the laminated elastomer can be increased (Fig. 16(b)) or decreased (Fig. 16(c)) depending on the direction of the application of the coil current to the electromagnet. This mechanism can provide extra control to additionally increase or decrease the primary stiffness

generated with the magnetic field applied by the permanent magnet only. Fig. 17 shows the frequency transmissibility characteristics of the laminated MRE seismic base isolator depending on the current I A applied to the coil. According to the figure, the resonance frequency of 14 Hz (I = 0A) increases with a positive current applied or decreases with a negative current applied, showing the variability from about 3 Hz to 20 Hz. An SDOF seismic isolation system consisting of four MR seismic base isolators on which an object (a building structure model) is mounted has been prepared and provided with skyhook control, demonstrating that the system can deliver effective seismic isolation control [13].

6. Concluding Remarks

One of the motive forces bring about technical innovation in the 21st century is new materials, particularly smart materials. The MR fluid and soft material causing the MR effect as described in this article also have a potential for achieving a great industrial or engineering breakthrough in creating high-value-added products too. Using these materials, higher-cost-performance advanced equipment and systems can be developed and commercialized to deliver unique functions by making full use of the rare smartness that the viscoelasticity can be varied with the application of a magnetic field. I hope this article will help realize the expectation.

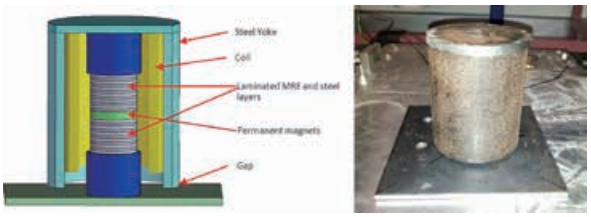

(a) Laminated MRE seismic base isolator

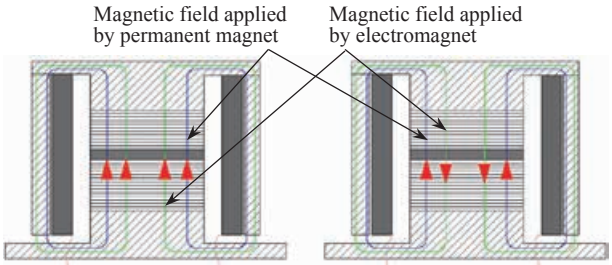

(b) Application in a same direction

(c) Application in different directions

Fig. 16 Laminated MRE seismic base isolator and its magnetic field control by the direction of application of coil current

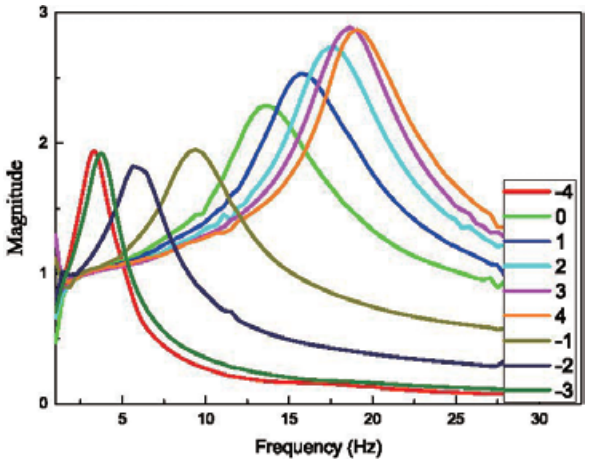

Fig. 17 Frequency transmissibility characteristics of laminated MRE seismic base isolator with variable rigidity feature (resonance frequency change with coil current I A)

References

1) Nakano, M., Yamamoto, H., Jolly, M.R.: Dynamic viscoelasticity of a magnetorheological fluid in oscillatory slit flow, Int. J. of Modern Physics B, Vol. 13, No. 14, 15&16, 2068/2076 (1999)
2) Nakano M.: Development of a magnetic-field-applicable rheometer and magneto-rheology measurement of MR fluid, Fluid Power System, Vol. 48, No. 2, 78/81 (2017)
3) Nakano M.: Trend of research & development and practical use of functional fluids, Fluid Power System, Vol. 47, No. 6, 265/271 (2016)
4) Murakami T, Sakai M, Nakano M.: Development of a passive type MR damper with variable damping characteristics dependent on the displacement and velocity, Transactions of the Japan Society of Mechanical Engineers (JSME), Series C, Vol. 77, No. 774, 257/269 (2011)
5) Nakano M.: MR fluid actuator for power-assisted equipment, Hydraulics & Pneumatics, Vol. 54, No. 3, 34/39 (2015)
6) Nakano M, Michitsuji Y.: Development of an MR fluid brake and its application to electric vehicles, Motion control and dynamic wireless power transfer for electric vehicles, Hori Y. and Yokoi Y. (editors), NTS, 116/129 (2019)
7) Nakano M.: Development of MR fluid composite and its application, Fluid Power System, Vol. 42, No. 1, 41/45 (2011)
8) Nakano M., Kumasaka T., Kudou R.: Development of MR fluid composite brake and its application to wire tension control system for coil winding, Transactions of the Japan Society of Mechanical Engineers (JSME), Series B, Vol. 75, No. 753, 993/999 (2009)
9) Nakano M, Yang J., Sun S., Totsuka A., Fukukita A.: Development and damping properties of a seismic linear motion damper with MR fluid porous composite rotary brake, Smart Materials and Structures, Vol. 29, No. 11, Article No. 115043, 1/13 (2020)
10) Nakano, M., et al.: Magneto-rheological effects and fluidity improvement of novel dry MR fluids, Proceedings of the 10th JFPS International Symposium on Fluid Power, Fukuoka, Japan, Paper No. 1B11, 1/5 (2017)
11) Tian T., Nakano M.: Fabrication and dynamic viscoelastic properties of silicone rubber-based MR elastomers with silicone oil, International Journal of Applied Electromagnetics and Mechanics, Vol. 59, No. 1, 349/355 (2019)
12) Sun S., Deng H., Yang J., Li W., Du H., Alici G., Nakano M.: An adaptive tuned vibration absorber based on multilayered MR elastomers, Smart Materials and Structures, Vol. 24, No. 4, Article No. 045045, 1/13 (2015)
13) Yang J., Sun S., Tian T., Li W., Du H., Alici G., Nakano M.: Development of a novel multi-layer MRE isolator for suppression of building vibrations under seismic events, Mechanical Systems and Signal Processing, Vol. 70-71, 811/820 (2016)

Technology Explanation

Prototype of Electric Mechanical Actuator for Replacing Hydraulic Equipment

SATO Kosuke, SHIBAHARA Daichi, HAKAMADA Shinichiro

Abstract

A prototype of an electric mechanical actuator with a cylindrical linear motor was verified, and the actuator is for replacing hydraulic equipment and the motor is jam free.

In order to increase the force density of the actuator, an airgap area was expanded by layout of the outer stator (magnet) and inner armature, and the Halbach arrangement on the stator and trapezoid teeth on the armature were applied to the motor. And in order to eliminate any inner force between the stator and armature, a movable armature was placed in a sleeve with wear rings.

A verification test showed that the maximum force was 4,741N@240mm/s, the mass was 9.49kg and the force density of the actuator was 499.6N/kg. We expect that the electric mechanical actuator can replace hydraulic equipment.

1 Introduction

Electrification of aircraft equipment has been promoted to improve the fuel efficiency and serviceability [1]. Because of jamming of the electric mechanical actuators attributable to the ball screws, however, the critical equipment including the flight control system still use hydraulic actuators [2]. The authors have then focused on the cylindrical linear motor that can be characterized by its jam free feature. However, this motor involves a problem that the force density is lower than that of hydraulic equipment (commercially available electric actuator: 56 to 133 N/kg, hydraulic equipment: 6,000 N/kg [3]).

Previous prototyping (Table 1) showed a force density of 109 N/kg for the primary prototype or 292.8 N/kg [4] for the secondary prototype, both of which are still below the target level of 600 N/kg [5] for the electric mechanical actuator to be able to replace the hydraulic equipment.

This paper discusses problems with the secondary prototype to set up improvement measures and then derive a structure of a tertiary prototype along with its calculation model with a target force density of 600 N/kg. The paper also provides the results of a verification test.

Table 1 Previous prototyping

	Force density	Improvements
Commercially available product	56N/kg	(Benchmark)
Primary prototype	109N/kg	Higher drive current (5.6 A → 11.2 A)
Secondary prototype	292.8N/kg	Multipolar (8p24s → 16p24s) Coreless → Core type Lighter structure (4.3 kg → 1.5 kg)

2 What is the Cylindrical Linear Motor?

The operating principle of the cylindrical linear motor is shown in Fig. 1. The motor consists of a shaft that serves as a field magnet and a case that serves as an armature. The shaft is installed inside the case in such a manner that can be axially operated. Thus, the motor has a very simple basic structure.

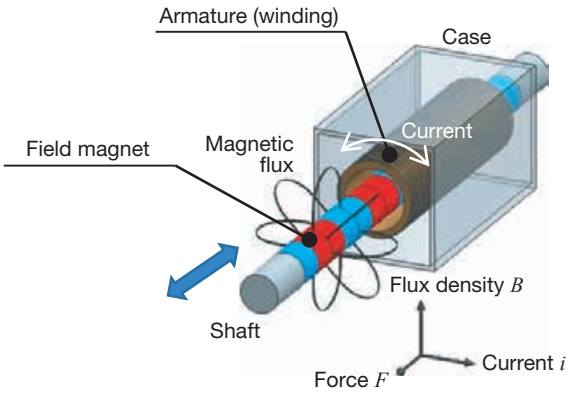

Fig. 1 Operating principle of cylindrical linear motor

The magnetic flux (flux density B) occurs in the radial direction of the shaft and the current i flows along the winding inside the case. When the magnetic flux interlinks with the current, a force F occurs in the axial direction of the shaft according to the Fleming's left-hand rule for electric motors. The direction of the force F can be changed by phase control of the current i.

The force F can be expressed by Equation (1) (where B is the flux density, L the winding length and i the current):

$$F = BiL \quad (1)$$

The force density cannot always be increased just by increasing the winding length L since this will also increase the mass. The current i has been already set to the upper limit current density in the primary and secondary prototypes. Therefore, to increase the force density, the flux density B must be increased. In other words, the number of lines of magnetic flux that interlink with the current needs to be increased by modifying the magnetic circuit of the motor. The core structure employed in the secondary prototype shown in Fig. 2 is an example of modifications with a substantially improved magnetic flux density B.

3 Structure of Tertiary Prototype

3.1 Problems with Secondary Prototype

The problems with the secondary prototype can be summarized as follows. As in Fig. 1, the movable magnet is located inside the stationary armature with an airgap between them so that they can slide with each other. This structure involves two problems:

- Insufficient force density
- Occurrence of an inner force between the magnet and armature

As described in section 1, the electric mechanical actuator has an insufficient force density to replace the hydraulic equipment.

The inner force between the magnet and armature is well balanced if the magnet is perfectly aligned. In reality, however, the magnet may be slightly eccentric due to its own deflection. According to the results of a calculation of the eccentricity and inner force shown in Fig. 3, the inner force is approx. 1,200 N on an assumption that the allowable magnet eccentricity is 0.5 mm. For the secondary prototype, a polycarbonate pipe was inserted between the magnet and armature as a provisional measure to structurally control the allowable eccentricity to 0.1 mm.

3.2 Improvement of Motor Structure

An improved motor structure for the tertiary prototype is shown in Fig. 4. The specifications of the secondary and tertiary prototypes are listed in Table 2. All figures shown in Table 2 indicate design values except mass which indicates actual measurements. Because of the limitations by the internal potentiometer, the tertiary prototype has a stroke of 90 mm in spite of the mechanical stroke of 162 mm, and similarly has a total length of 731.84 mm in spite of the mechanical total length of 641.84 mm.

The tertiary prototype is different in structure from the secondary prototype mainly in two points:

- Arrangement with the outer stator/magnet and the inner armature
- A sleeve inserted between the stator/magnet and armature

Improvement measures related to these structural differences include to expand the airgap area to make up for the insufficient force density, the Halbach arrangement of the stator/magnet, the trapezoid teeth of the armature, and the sleeve structure to decrease the inner force between the armature and stator/magnet.

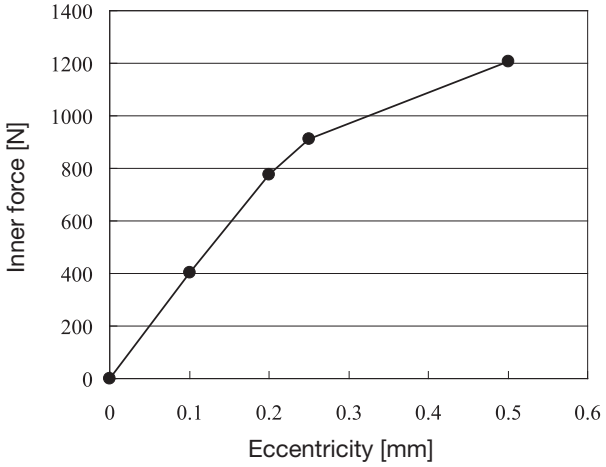

Fig. 3 Inner force between magnet and armature (analysis)

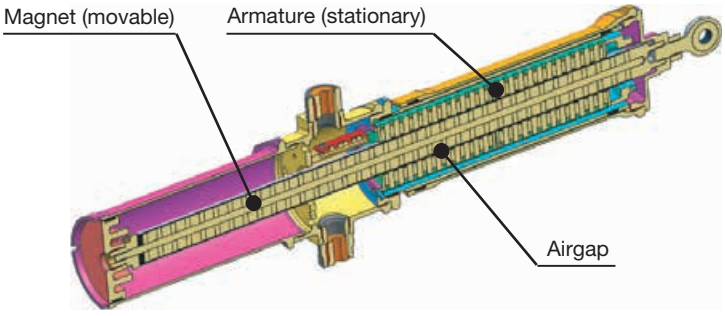

Fig. 2 Structure of secondary prototype

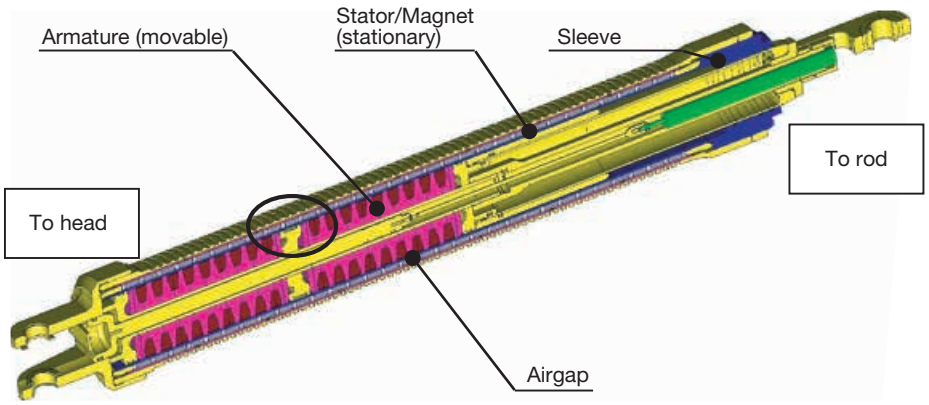

(a) Overview

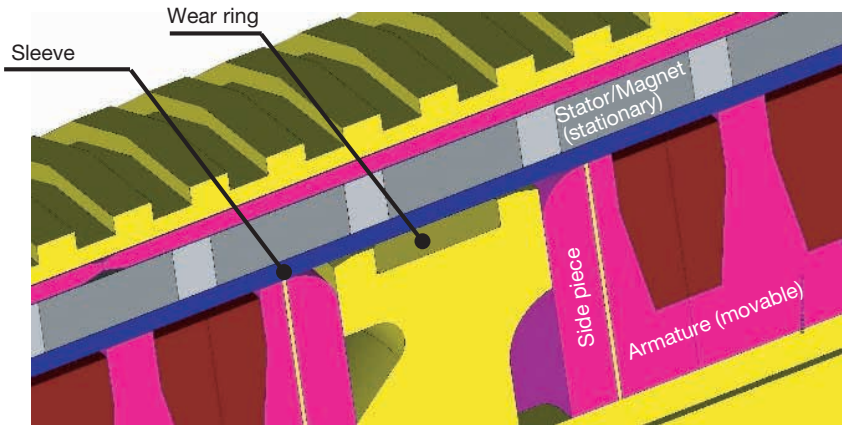

(b) Enlarged view of elliptical part

Fig. 4 Structure of tertiary prototype

Table 2 Specifications

	Tertiary prototype	Secondary prototype
Actuator		
Mount	Rod end	Trunnion
Total length - Outer dia.	731.84(641.84)mm - ø89mm	555.7mm-ø90mm
Stroke	90(162)mm	162.2mm
Mass	9.49kg	6.9kg
Motor		
Structure	16p18s, core type	16p24s, core type
Arrangement (In-Out)	Armature-Magnet	Magnet-Armature
Power supply	DC 270V	DC 707V
Allowable magnet temperature	150°C	90°C
Cooling	Natural air cooling	Natural air cooling
Stroke sensor	Potentiometer	Hall device

3.2.1 Larger Airgap Area

Increasing the airgap area will enlarge the magnet surface area, resulting in more lines of magnetic flux generated by the magnet. Naturally, the flux density B in Equation (1) is higher. With the stator/magnet located outside, the tertiary prototype has an airgap area of ø61 mm x 247.94 mm, which is larger than that of the secondary prototype (ø24 mm x 208.98 mm). The airgap area of the tertiary prototype is 3.01 times larger than that of the secondary prototype.

However, the inner-armature arrangement with the actuator's outer diameter almost equivalent to that of the secondary prototype (Table 2) makes the outer diameter of the armature core smaller, which causes the armature core to be more likely to have magnetic saturation. Countermeasures to this problem are the trapezoid teeth described in 3.2.3 and the phase lead compensator for current control stated in 4.1.

3.2.2 Halbach Arrangement

The motor magnets can be arranged in different ways depending on the direction of magnetization: Halbach and counter arrangements. The tertiary prototype uses the Halbach arrangement. Fig. 5(a) shows the flow of magnetic flux for the Halbach arrangement and Fig. 5(b) for the counter arrangement. Triangles appearing in the figures show the direction of magnetization of the magnet.

Since the Halbach arrangement of magnets generates deflected magnetic flux, installing an armature on the deflected side of the magnetic flux will obtain more flux linkage with a same magnet volume. Furthermore, different magnet materials are used for the radial and axial

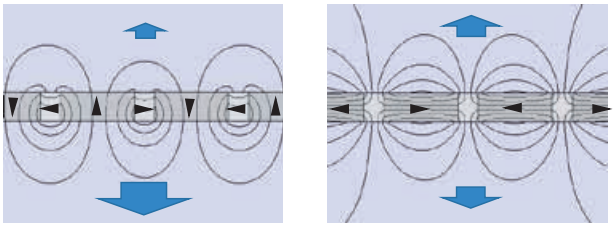

(a) Halbach arrangement (b) Counter arrangement

Fig. 5 Magnetic flux from magnets

magnetizations to achieve the allowable magnet temperature of 150˚C while keeping the force at a certain level (Patent public No. 2019-122072).

3.2.3 Trapezoid Teeth

Fig. 6 shows the distribution of flux density of trapezoid teeth used in the tertiary prototype and that of rectangular teeth as a comparison target. Magnetic saturation is colored in red. Note that both the windings for trapezoid and rectangular teeth have a same cross-sectional area.

For the rectangular teeth, the magnetic flux is concentrated in the root, causing a bottleneck of the flux. For the trapezoid teeth with an almost uniform area of the radial magnetic path, the magnetic flux is distributed in the whole teeth to realize a smooth flow of magnetic flux. The trapezoid teeth has an advantage of a higher flux density B (WO2019/102761A1, Patent public No. 2019-097377).

3.2.4 Sleeve Structure

As shown in Fig. 4, the armature is installed together with wear rings inside the aluminium alloy sleeve so that the armature can slide in the axial direction via the rings. The inner surface of the sleeve is coated with a hard anodic oxide to ensure the sliding property. The wear rings is made of aircraft fluoroplastic.

The sleeve structure prevents the armature from becoming eccentric and the inner force between the stator/magnet and armature is balanced in the radial direction, resulting in almost zero (Patent public No. WO2019/202758A1).

3.3 Motor Assembly

The motor assembly is shown in Photo 1.

Photo 1(a) shows the motor being assembled in which 56 magnets, among the total 63, and 6 back yokes, among the total 8, have been assembled into the sleeve.

Photo 1(b) shows the armature assembly with 18 (exactly 24, because of 2 windings per slot) windings installed in the armature core and with 3 green wear rings: two on the both sides of the armature and one at the midpoint.

(a) Stator/magnet (being assembled) (b) Armature

Photo 1 Motor assembly

4 Calculation Model

To determine the theoretical performance of the tertiary prototype, the following sections derive a magnetic field analysis model and a dynamic operation model.

4.1 Magnetic Field Analysis Model

Fig. 7 shows the profile of a magnetic field analysis model used to calculate the stall characteristics and also shows the winding connection.

The model consists of a stator/magnet and an armature and is symmetric with respect to a two-dimensional axis. The sleeve and middle piston use non-magnetic metal.

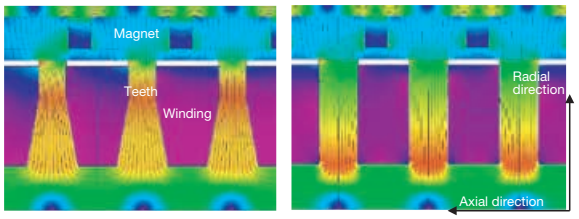

(a) Trapezoid teeth (b) Rectangular teeth

Fig. 6 Flux density of armature

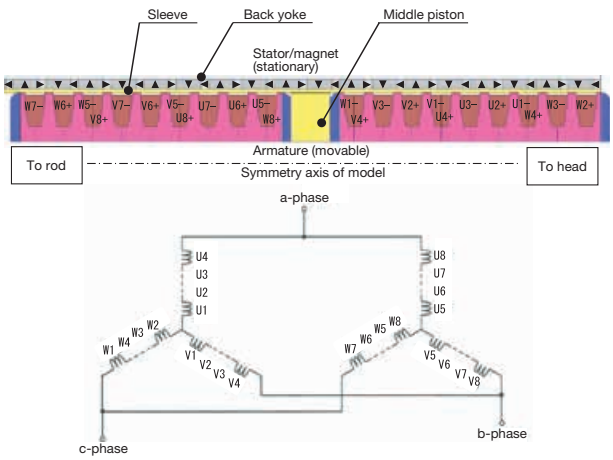

Fig. 7 Magnetic field analysis model

The magnet characteristics values are those at a temperature of 22.9˚C and no eddy current loss in the armature core is not considered.

The winding connection is a parallel configuration of a core assembly on the rod side and another on the head side. The current control has been provided with phase lead compensator of 30° to suppress the magnetic saturation in the armature core.

4.2 Dynamic Operation Model

A dynamic operation model is used to calculate the force-velocity and damping characteristics. Fig. 8 shows the controller, the inverter and the motor. Table 3 shows physical constants used for the calculation. The q-axis flux linkage Φ_q decreases as the current increases, approximating the effect of the magnetic saturation in the armature core.

Table 3 Physical constants

F_c	Current compensator corner frequency
F_{mr}	Frictional force
K_{id}	d-axis control gain
K_{iq}	q-axis control gain
L_d	d-axis inductance
L_q	q-axis inductance
M_ℓ	Inertial mass
R_m	Phase resistance
$R_{\theta 2x}$	Stroke/Angle conversion factor
V_{dc}	Supply voltage of invertor
V_{pw}	PWM voltage
V_{rd}	d-axis command
η_m	Inverter efficiency
Φ_q	q-axis flux linkage

Input to the dynamic operation model is the current command i_m* and output from the model is the stroke x_m and the force f_ℓ. The equation of motion related to the mass M_ℓ can be expressed by Equation (2):

$$M_\ell \ddot{x}_m + F_{mr}\,\mathrm{sgn}\,(\dot{x}_m) = f_\ell - f_c \tag{2}$$

Where, the force f_ℓ is given by Equation (3):

$$f_\ell = \frac{\Phi_q}{R_{\theta 2x}} i_q \tag{3}$$

The motor voltage equation for d-/q-axis models is expressed by Equation (4):

$$\begin{bmatrix} v_d \\ v_q \end{bmatrix} = R_m \begin{bmatrix} i_d \\ i_q \end{bmatrix} + \begin{bmatrix} L_d & 0 \\ 0 & L_q \end{bmatrix} \begin{bmatrix} \dot{i}_d \\ \dot{i}_q \end{bmatrix} + \dot{\theta} \begin{bmatrix} 0 & -L_q \\ L_d & 0 \end{bmatrix} \begin{bmatrix} i_d \\ i_q \end{bmatrix} + \dot{\theta}\Phi_q \begin{bmatrix} 0 \\ 1 \end{bmatrix} \tag{4}$$

Where,

$$i_m = \frac{i_q}{\sqrt{3}} \tag{5}$$

$$\begin{bmatrix} i_d \\ i_q \end{bmatrix} = \sqrt{\frac{2}{3}} \begin{bmatrix} \cos\theta & \cos\left(\theta - \frac{2}{3}\pi\right) & \cos\left(\theta - \frac{4}{3}\pi\right) \\ -\sin\theta & -\sin\left(\theta - \frac{2}{3}\pi\right) & -\sin\left(\theta - \frac{4}{3}\pi\right) \end{bmatrix} \begin{bmatrix} i_a \\ i_b \\ i_c \end{bmatrix} \tag{6}$$

$$\begin{bmatrix} v_a \\ v_b \\ v_c \end{bmatrix} = \sqrt{\frac{2}{3}} \begin{bmatrix} \cos\theta & -\sin\theta \\ \cos\left(\theta - \frac{2}{3}\pi\right) & -\sin\left(\theta - \frac{2}{3}\pi\right) \\ \cos\left(\theta - \frac{4}{3}\pi\right) & -\sin\left(\theta - \frac{4}{3}\pi\right) \end{bmatrix} \begin{bmatrix} v_d \\ v_q \end{bmatrix} \tag{7}$$

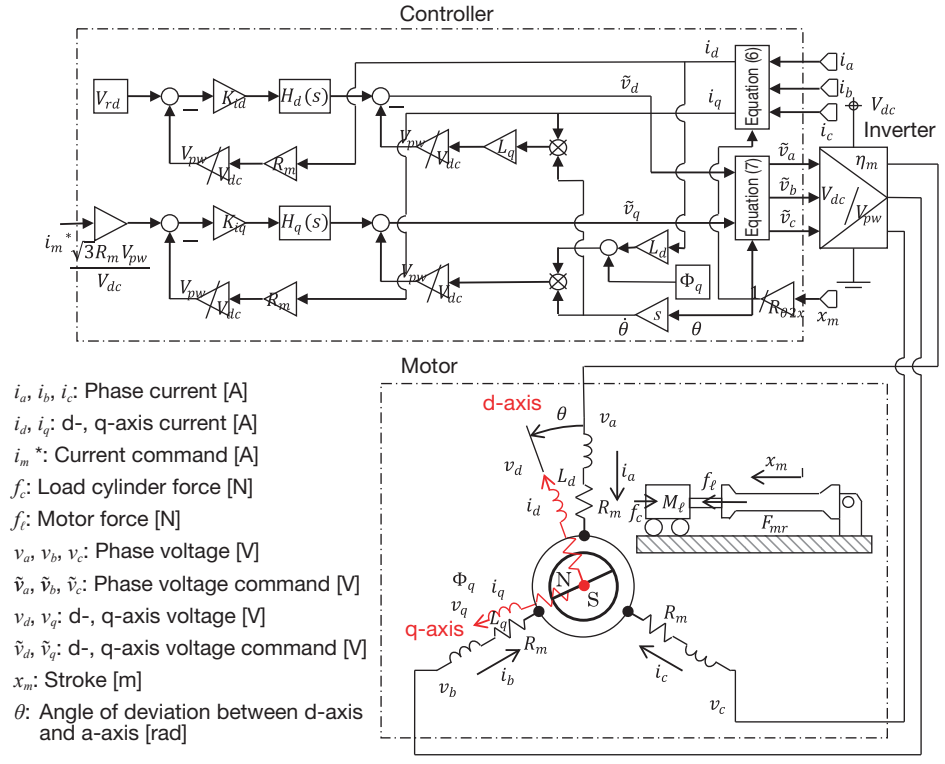

Fig. 8 Dynamic operation model

The PWM operation of the inverter can be approximated by Equation (8):

$$\begin{bmatrix} v_a \\ v_b \\ v_c \end{bmatrix} = \eta_m \frac{V_{dc}}{V_{pw}} \begin{bmatrix} \tilde{v}_a \\ \tilde{v}_b \\ \tilde{v}_c \end{bmatrix} \tag{8}$$

The current compensator for the d-axis can be expressed by Equation (9):

$$\tilde{v}_d = K_{id} H_d(s) \left(V_{rd} - R_m \frac{V_{pw}}{V_{dc}} i_d \right) - \frac{V_{pw}}{V_{dc}} \dot{\theta} L_q i_q \tag{9}$$

Where,

$$H_d(s) = \frac{\dfrac{s}{R_m} + 1}{\dfrac{L_d}{R_m}} \frac{\dfrac{R_m}{L_d}}{\dfrac{s}{2\pi F_c} + 1} \tag{10}$$

The current compensator for the q-axis can be expressed by Equation (11):

$$\tilde{v}_q = K_{iq} H_q(s) \left(\tilde{v}_q^* - R_m \frac{V_{pw}}{V_{dc}} i_d \right) + \frac{V_{pw}}{V_{dc}} \dot{\theta} (\Phi_q + L_d i_d) \tag{11}$$

Where,

$$H_q(s) = \frac{\dfrac{s}{R_m} + 1}{\dfrac{L_q}{R_m}} \frac{\dfrac{R_m}{L_q}}{\dfrac{s}{2\pi F_c} + 1} \tag{12}$$

$$\tilde{v}_q^* = \frac{\sqrt{3} R_m V_{pw}}{V_{dc}} i_m^* \tag{13}$$

Equations (2) through (13) are physical equations expressing the dynamic operation model. For calculation of the damping characteristics, Equation (4) uses $v_d = 0$ and $v_q = 0$ since the a-, b- and c-phase terminals are short-circuited in Fig. 7.

5 Verification Test

5.1 Test Setup

Fig. 9 shows a test setup to evaluate the performance of the tertiary prototype. Table 4 shows the major test equipment. Photo 2 shows how the verification test is carried out.

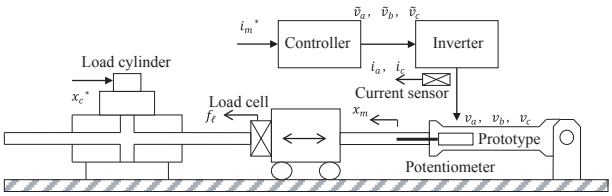

Fig. 9 Test setup

Table 4 Test equipment

	Manufacturer	Model, specifications
Inverter	Myway Plus	MWINV-5022B AC146Arms
Controller	MIS	SEAGALL mini C66 DSP 1.2GHz×4
Load cylinder	Kayaba System Machinery	HTM10-200-07G 10kN, 400mm/s

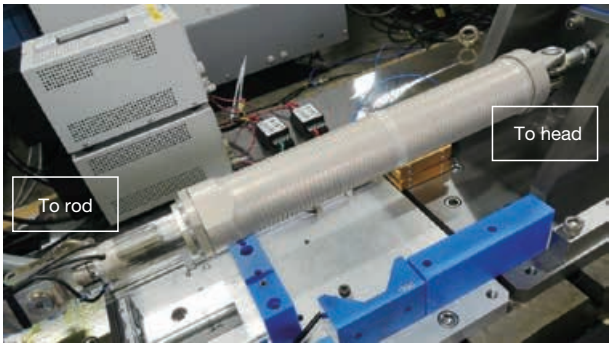

Photo 2 Verification test

A hydraulic load cylinder is located in a position opposite to the prototype and is driven by the stroke control system according to the stroke command x_c*. The load cylinder is equipped with a load cell on the tip to measure the force f_ℓ of the prototype.

The prototype is driven with current control according to the current command i_m via a controller and an inverter. The phase currents i_a and i_c are measured by a current sensor and the phase current i_b is calculated by Equation (14).

$$i_b = - i_a - i_c \tag{14}$$

The stroke x_m of the prototype is measured by the internal potentiometer.

5.2 Low-Speed Operation with Triangular Wave

To verify the sliding property of the armature with the sleeve structure shown in Fig. 4, a low-speed operation test with a triangular wave is conducted. Fig. 10 shows the

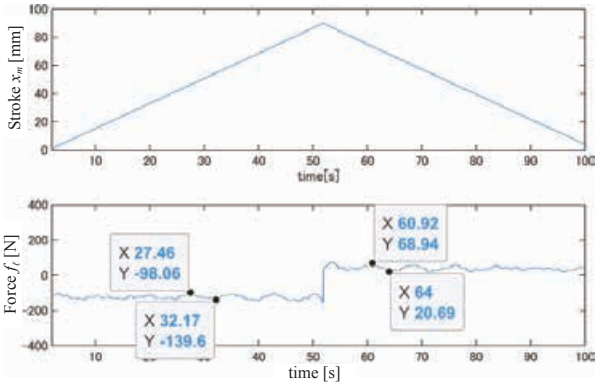

Fig. 10 Low-speed operation with a triangular wave

response, specifically stroke x_m and force f_ℓ, of the prototype when it is forcefully operated by load cylinder with a triangular wave at a frequency of 0.01 Hz and an amplitude of +/-45 mm with the a-, b- and c-phase terminals shown in Fig. 7 left open.

In Fig. 10, the force curve f_ℓ vibrates representing cogging and the rising of the force curve f_ℓ at the turning point of the stroke (about 50 sec.) reflects friction.

Cogging is 41.54 Np-p when the prototype extends or 48.25 Np-p when it retracts, and the normalized cogging with the maximum force described later (in 5.5) is as small as 0.88% to 1.02%. This cogging reduction has been achieved with the 16p18s structure shown in Table 2 and the side piece shown in Fig. 4(b).

The difference between the force during prototype extension and the force during prototype retraction can be used to determine that the frictional force is 163.645 Np-p. Similarly, it can be normalized with the maximum force to be 3.45%, which is not more than the hydraulic actuator friction characteristics (generally 5% to 10%).

It can be determined from the low-speed operation test with a triangular wave (Fig. 10) that the armature with the sleeve structure shown in Fig. 4 has good sliding property.

5.3 Shaking Operation with Sine Wave

To verify that the d-axis current compensator of Equation (9) and the q-axis current compensator of Equation (11) are appropriate, shaking operation with a sine wave is conducted. Using the test setup shown in Fig. 9 with the load cylinder removed from the prototype, the prototype is shaked by the stroke control system using a sine wave at a frequency of 2 Hz and an amplitude of +/-30 mm. The results are shown in Fig. 11.

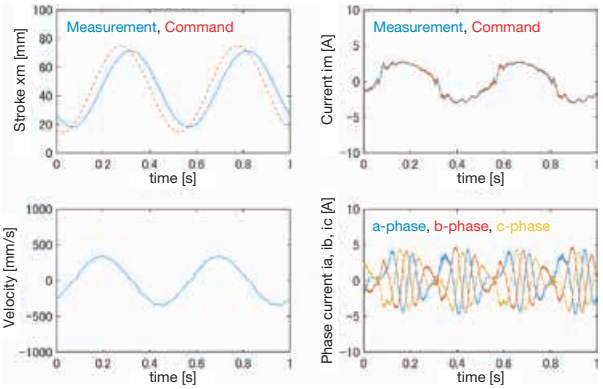

Fig. 11 Shaking operation with a sine wave

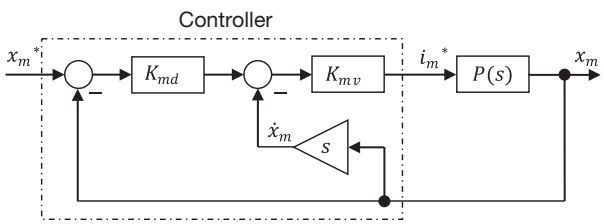

Fig. 12 Stroke control system

Table 5 Constants for stroke control system

K_{md}	Stroke control gain
K_{mv}	Speed control gain

The stroke control system is as shown in Fig. 12 and Table 5. In Fig. 12, $P(s)$ represents the transfer function characteristics from the current command i_m* to the stroke x_m of the dynamic operation model shown in Fig. 8. The stroke control system also has the speed control function as a minor loop. The stroke control frequency has been set to 250 Hz and the speed control frequency to 1 kHz. The current control frequency is 5 kHz and the inverter carrier frequency is 20 kHz in Fig. 8.

According to Fig. 11, the measured value for the current i_m closely follows the command value with no deviation and the phase currents i_a, i_b and i_c do not vibrate, proving that the current control system is stable. Note that the vibration of the current i_m represents a response attributable to cogging.

Based on the shaking operation with a sine wave (Fig. 11), the d-axis current compensator of Equation (9) and the q-axis current compensator of Equation (11) are appropriate.

5.4 Stall Characteristics

The stall characteristics are shown in Fig. 13. The stall characteristics represent the relationship between the current command i_m* and the force f_ℓ when the prototype stroke is retained with the load cylinder and the current command i_m* is given a constant value. Both measured and calculated values for the force f_ℓ represent the average fluctuation in the magnetic pole pitch.

The maximum stall force is 5,034 N @73A during prototype extension and -5,179 N @-73A during prototype retraction, both of which mostly match the calculation results. The non-linearity in the regions of $|i_m^*| > 40$A may be attributable to the magnetic saturation in the armature core.

5.5 Force-Velocity Characteristics

Hydraulic actuators for flight control systems are subjected to a verification test to determine the performance

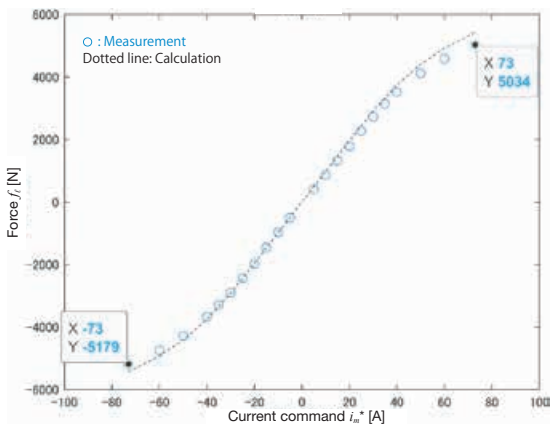

Fig. 13 Stall characteristics

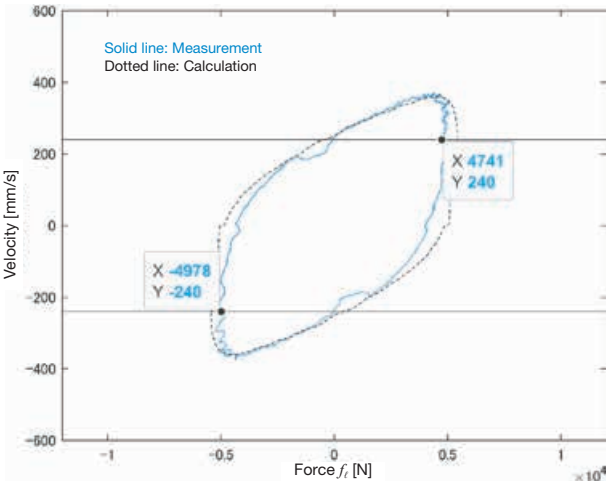

Fig. 14 Force-velocity characteristics

by horizontally applying several hundreds of kilograms of inertia load. Since the application of several hundreds of kilograms of inertia load is dangerous, the load cylinder shown in Fig. 9 is used instead.

The force-velocity characteristics are as shown in Fig. 14. The application conditions can be expressed by Equation (15) and are equivalent to the horizontal application of an inertia load of approx. 200 kg.

$$\left.\begin{aligned} x_c^* &= X_1 \sin(2\pi F_1 t) \\ i_m^* &= I_1 \sin\left(2\pi F_1 t + \tau_1 \frac{\pi}{180}\right) \end{aligned}\right\} \quad (15)$$

Where, X_1 = 30 mm, F_1 = 2 Hz, I_1 = 73 A, τ_1 = -55 deg.

In Fig. 14, Quadrants I and III indicate meter-in operation (power running for electrified operation) and Quadrants II and IV indicate meter-out operation (regenerative). The prototype has the same meter-in and meter-out operation characteristics as those of hydraulic actuators.

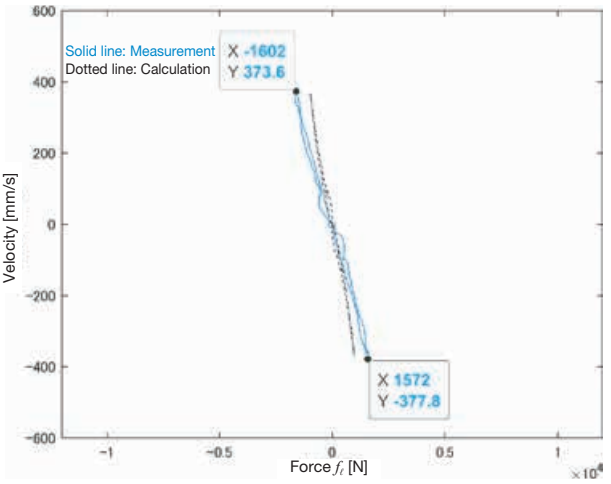

Fig. 15 Damping characteristics

The maximum force is 4,741 N @240 mm/s for prototype extension and -4,978 N @-240 mm/s for prototype retraction. The difference between measurements and calculation may be mainly attributable to the eddy current loss in the armature core.

5.6 Damping Characteristics

The authors assume that the requirements for the electric mechanical actuator to replace the hydraulic equipment relate to the force density as well as the damper operation in case of system shut down. Fig. 15 shows the damping characteristics of the prototype when it is forcefully operated by load cylinder with a sine wave at a frequency of 2 Hz and an amplitude of +/-30 mm with the terminals of the phases a, b and c shown in Fig. 7 left short-circuited.

With a damping factor of 4,224 N/(m/s), the figure indicates linear damping characteristics with small hysteresis. The difference between measurements and calculation may be mainly attributable to the eddy current loss in the armature core as in the force-velocity characteristics. Installing a resistor between the terminals will tune the damping factor to 4,224 N/(m/s) or less, thereby allowing the prototype to be able to serve as a passive damper with a given damping factor in case of system shutdown.

5.7 Force Density

From the maximum force of 4,741 N in 5.5 and the mass of 9.49 kg in Table 2, the force density can be determined to be 499.6 N/kg (= 4,741 N/9.49 kg). The prototypes force density records and the actual data of hydraulic actuators are plotted in Fig. 16. The figure implies that the feasibility of replacing the hydraulic equipment with the electric mechanical actuator has risen.

6 Conclusion

The authors have prototyped the electric mechanical actuator that can be replaced with the hydraulic equipment and carried out a verification test to obtain the following:

(1) The maximum force of 4,741 N @240 mm/s has been achieved through the larger airgap area with the motor structure with the outer stator and inner armature as well as the Halbach arrangement of magnets and the trapezoidal teeth armature.

(2) It has been verified that the prototype shows the friction characteristics not more than those of the hydraulic actuator and the armature has good sliding property thanks to the sleeve structure in which the inner force between the stator and armature is almost zero.

(3) The force density is 499.6 N/kg, which is still below the target level (600 N/kg), but the prototype's force density records and the actual data of the hydraulic actuator's imply that the feasibility for the electric mechanical actuator to replace the hydraulic equipment has risen.

We would like to deeply thank associate professor KANO Yoshiaki of Department of Electrical and Electronic Engineering, Daido University, who designed the motor magnetic circuit for this prototype.

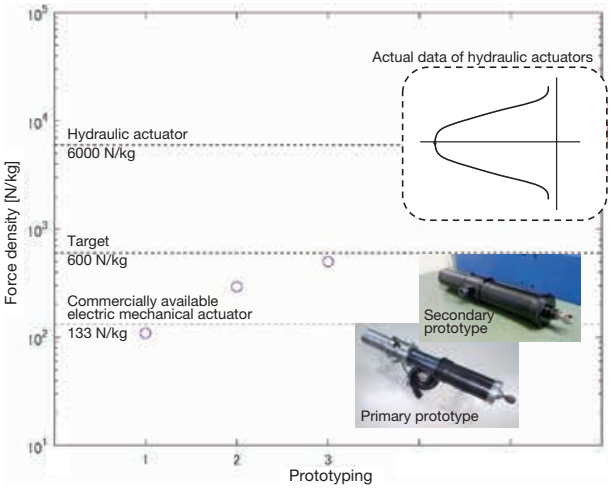

Fig. 16 Force density record

References

1) Michel Todeschi: Airbus-EMAs for flight controls actuation system 2012 status and perspectives, Recent Advances in Aerospace Actuation Systems and Components, Proceedings, (June 13-14 2012).
2) David Blanding: SUBSYSTEM DESIGN AND INTEGRATION FOR THE MORE ELECTRIC AIRCRAFT, Collection of Technical Papers, 5th International Energy Conversion Engineering Conference Vol. 2, (2007).
3) Amine Fraj, Marc Budinger, Toufic El Halabi, Jean-Charles Mare: Modelling approaches for the simulation-based preliminary design and optimization of electromechanical and hydraulic actuation systems, 53rd AIAA/ASME/ASCE/AHS/ASC Structures, Structural Dynamics and Materials Conference, (April 23-26 2012).
4) Yoshiaki Kano, Kousuke Satou: Design and Experimental Verification of a High Force Density Tubular Permanent Magnet Linear Motor for Aerospace Application, AEROTECH EUROPE, (September 24-26 2019).
5) Sato: Development of an Electric Mechanical Actuator for Aircraft with a Cylindrical Linear Motor, KYB Technical Review No.50 (April 2015)

Author

SATO Kosuke

Joined the company in 1984.
Information Technology R&D Sect., Basic Technology R&D Center, Engineering Div.
Engaged in design and development of aircraft equipment.

HAKAMADA Shinichiro

Joined the company in 1988.
Chief Researcher, Information Technology R&D Sect., Basic Technology R&D Center, Engineering Div.
Engaged in design and development of various electronic equipment.

SHIBAHARA Daichi

Joined the company in 2015.
Information Technology R&D Sect., Basic Technology R&D Center, Engineering Div.
Master's degree in engineering.
Engaged in research and development of elements necessary for electrification of hydraulics

Technology Explanation

Semi-Absolute-Type Stroke Sensing Cylinder

NAGAI Yuki

Abstract

In recent years, the electrification of hydraulic actuators and dampers used in hydraulic equipment and transportation equipment has been progressing.

Electro-Hydraulic Actuators (EHA) that drive cylinders with hydraulic pressure generated by electric motors, and active suspension that adjusts damping force and thrust according to the behavior of automobiles and railroad cars, are typical. "Displacement" is one of their control parameters. By detecting the displacement of the hydraulic cylinder in real time, it can be used for more detailed operation and fail-safe mechanisms in case of abnormalities, so its importance is considerable.

On the other hand, hydraulic cylinders are often used in harsh environments under vibration, operating temperature range, etc., so the mounted control equipment is also required to have environmental resistance.

KYB adopted the "Magnetic Scale Method" as a stroke sensor method that can handle such harsh external environments. However, since it is an "Increment Type" sensor that relatively detects the displacement amount of the stroke, there is a problem in that normal output that outputs the "absolute value" of the stroke amount cannot be performed.

"Absolute output" is required as an essential function for hydraulic equipment control.

Therefore, we adopted a magnetic scale that can detect the reference point of the absolute value of the displacement, and developed a Stroke Sensing Cylinder that can output the absolute value of the stroke amount even though it is a magnetic scale method.

1 Introduction

Hydraulic equipment such as actuators and dampers are widely used in transportation equipment including construction machinery, automobiles, railroad cars and aircrafts. From the viewpoint of energy saving and greater functionality, electrification and sophistication of hydraulic equipment, which have been conventionally controlled in a mechanical way, have recently been progressing.

Electro-hydraulic actuators, often called "EHAs", use hydraulic power generated by electric motors, not by conventional diesel motors, to drive hydraulic equipment such as cylinders. EHAs can also use electromagnetic change-over valves to electronically control hydraulic circuits.

EHAs can help achieve higher-efficiency and more-complexed control than before.

For automobiles and railroad cars, more and more active suspensions that can properly control the damping force and thrust in response to the behavior of running vehicles have been used to ensure a more comfortable ride and handling stability.

Both EHAs and active suspensions provide electronic control while detecting the status of hydraulic actuators and dampers (control parameters) with sensors.

One of the parameters detected by sensors is "displacement (or stroke length)" of cylinders.

For electronic control of hydraulic cylinders, the cylinder displacement is an essential parameter to determine where the piston rod is located. The displacement data is normally used by the control system to provide feedback control and is used for a fail-safe mechanism should the cylinder position be out of control.

Particularly for construction machinery and transportation equipment, the importance of such fail-safe mechanisms is considerable because safety is the top priority.

Then, we set about development of a stroke sensing cylinder (hereinafter "SSC") that can detect the cylinder displacement for applications in construction machinery and transportation equipment.

Sensors for use in construction machinery or transportation equipment are required to have high durability under vibration or high/low temperature environment. They also need to be compact because only limited space is available for sensors in many of such equipment.

To meet these demands, we decided to use a design of hydraulic cylinders called "Magnetic Scale Method" in which a sensor can read an evenly spaced magnetic scale

provided on the piston rod to detect the displacement.

However, the magnetic scale based sensor we used was inevitably of increment type because of its physical structure. There arose a problem that the sensor could not output the "absolute value" for the cylinder position.

In general, distance sensors such as a stroke sensor can be roughly divided into "increment" and "absolute" types by their output format.

The former, typified by a pulse counter, counts signals that are input at regular intervals to detect a change in distance from a certain point (displacement). The latter is designed to always output the absolute position from a reference point.

Therefore, the term "absolute output type" means "being able to detect the absolute position of the hydraulic cylinder".

We then developed a "semi-absolute type SSC" using the magnetic scale method that can detect the absolute position of the cylinder with a magnetic scale of a special shape and a sensor signal processing algorism. This paper explains details of the SSC.

The paper also describes later why the word "semi" was added to the general term "absolute type".

2 System Overview

2.1 System Configuration

The semi-absolute type SSC system consists of three components: a piston rod with a magnetic scale, which will be described later, a magnetic sensor that senses the magnetic scale, and a signal processing board that computes signals from the magnetic sensor and converts them into the displacement of the hydraulic cylinder (Fig. 1).

The magnetic sensor is mounted on one of the sides of the hydraulic cylinder and has a sensing member on the tip that is installed in such a manner that can slide with the piston rod. Signals detected by the magnetic sensor are input to the signal processing board installed downstream, where the signals are converted into displacement data and then sent to a higher-order controller that actually controls the hydraulic cylinder.

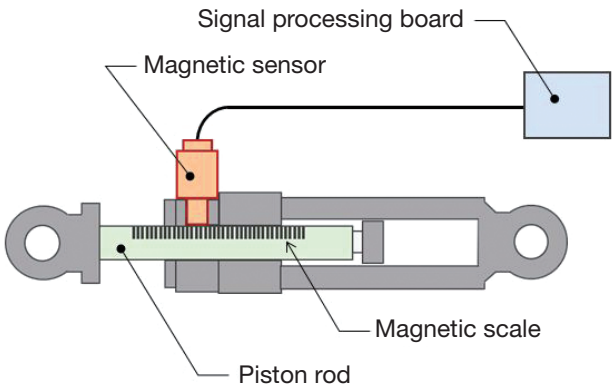

Fig. 1 System configuration

2.2 Piston Rod and Magnetic Scale

Photo 1 shows the appearance of a prototype of the piston rod provided with the magnetic scale. In the photo, the central banded portion is the magnetic scale engraved into the surface of the piston rod to form grooves. The piston rod is then plated with non-magnetic material to fill in the grooves, creating a structure as shown in Fig. 2.

Thus, the piston rod has a cross section where magnetic material and non-magnetic material alternately appear at fixed intervals, constituting a magnetic scale.

The piston rod used in the system introduced in this paper is provided with a 2 mm spaced magnetic scale.

Photo 1 Appearance of piston rod prototype before plating

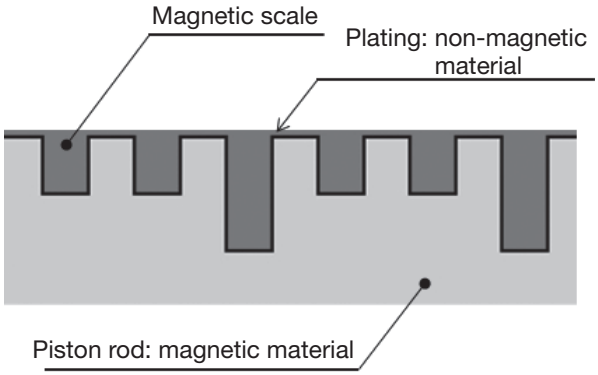

Fig. 2 Structure of magnetic scale

2.3 Magnetic Sensor

The magnetic sensor is designed to detect the magnetic scale by its sensing member installed in such a manner that the tip is made contact with the piston rod.

The sensing member to detect the magnetic scale has an internal structure as shown in the section view of Fig. 3. Lines of magnetic flux from an internal permanent magnet pass through a magnetoresistance IC via a yoke to reach the piston rod surface.

The principle of detection, which will be described in detail later, is that the magnetic sensor detects changes in the number of lines of magnetic flux that occur according to the positional relationship with the magnetic scale provided on the piston rod.

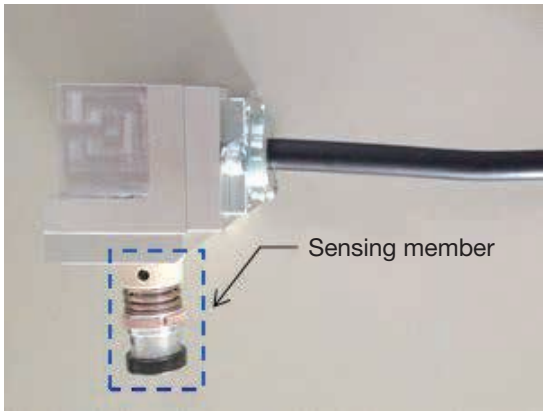

Photo 2 Appearance of magnetic sensor (prototype)

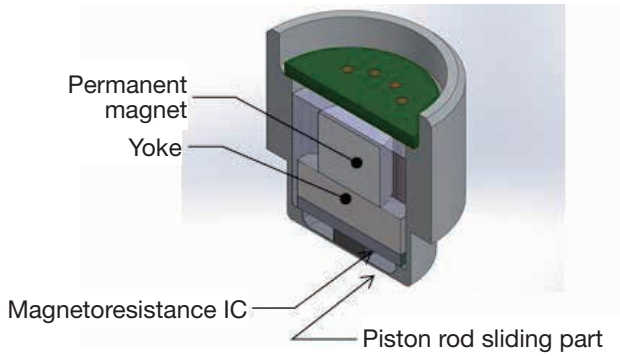

Fig. 3 Section view of sensing member of magnetic sensor

3 Principle of Displacement Detection

3.1 Magnetic Scale Detection with Magnetoresistance IC

The internal magnetoresistance IC of the magnetic sensor has four magnetoresistance elements. These four magnetoresistance elements are spaced at intervals of 0.5 mm, which is 1/4 of the pitch (2 mm) of the magnetic scale on the piston rod. The four elements may be divided into two pairs: one pair is called A-phase magnetoresistance elements and the other B-phase magnetoresistance elements. The A- and B-phase magnetoresistance elements are arranged as shown in Fig. 4.

As mentioned above, the magnetic sensor has a mechanism that lines of magnetic flux from the permanent magnet penetrate the magnetoresistance IC via the yoke. Since more lines of magnetic flux are attracted by magnetic material than by non-magnetic material, the inclination of the lines of magnetic flux passing through individual magnetoresistance elements depends on their position relative to the magnetic scale as in the example shown in Fig. 4.

As the magnetic resistance changes with the inclination of the lines of magnetic flux, the value detected by the magnetic sensor changes accordingly.

Therefore, when the hydraulic cylinder operates to move the magnetic scale, the inclination of each line of magnetic flux changes sequentially.

Assuming that the A- and B-phase magnetoresistance elements output an A- and a B-phase signal respectively, when the piston rod (magnetic scale) moves at a fixed speed, a sine wave output can be obtained, a cycle of which is complete every 2 mm of travel that is equivalent to the magnetic scale pitch as shown in Fig. 5 (for explanatory convenience, hereinafter the piston rod is assumed to travel at a fixed speed unless otherwise noted).

Since the B-phase magnetoresistance element is installed with an offset of 0.5 mm (1/4 of the magnetic scale pitch) from the A-phase magnetoresistance element, the B-phase signal is represented by a cosine wave with a phase-shift of 90 degrees from the A-phase signal.

These A- and B-phase signal values are determined from the difference in the inclination of the lines of magnetic flux between the two magnetoresistance elements. In fact, the sine and cosine waves shown in Fig. 5 may be obtained only with a single magnetoresistance element each. In this case, however, it is difficult to ensure accurate detection because the detected value may change if the gap between the magnetoresistance IC and the magnetic scale fluctuates due to vibration or other disturbance under service conditions. To avoid this, a pair of magnetoresistance elements is used so that the difference in detected values between the two can be taken to eliminate the effect of any variations of the gap between the magnetoresistance IC and the magnetic scale.

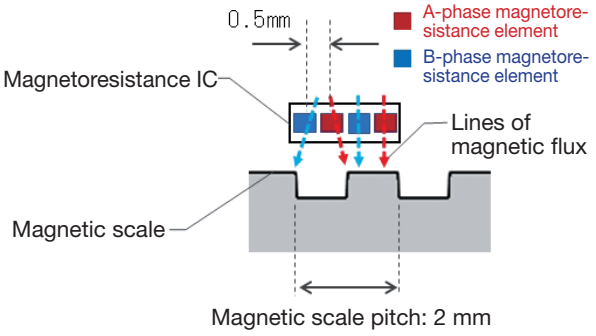

Fig. 4 Positional relationship between magnetoresistance elements and magnetic scale

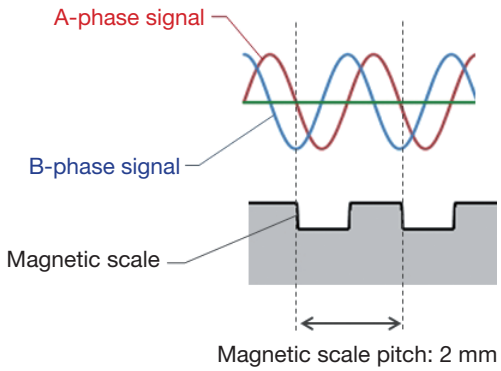

Fig. 5 Magnetic scale and output signal

The A- and B-phase signals greatly depend on the positional relationship between the magnetoresistance IC and the magnetic scale. Therefore, a magnetic field analysis setup shown in Fig. 6 was used to optimize the design.

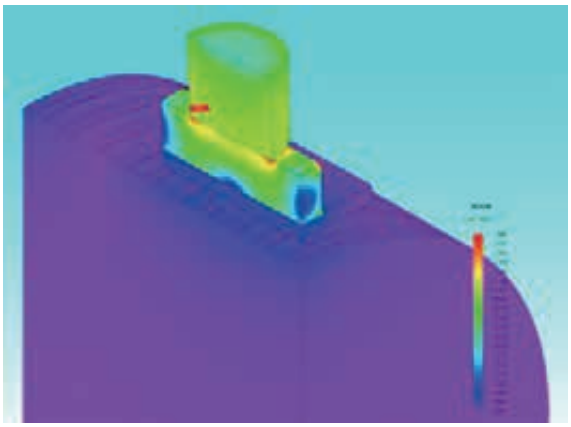

Fig. 6 Magnetic field analysis of magnetic sensor

3.2 Basic principle of displacement detection

The magnetic scale detection signal obtained as described in 3.1 (A- and B-phase signals) are converted into displacement of the hydraulic cylinder by the signal processing board, which is one of the system components.

First, the median value of the amplitude of the A- and B-phase signals is defined as "the zero-crossing level". A pulse generation circuit in which a pulse occurs every time the A- or B-phase signal intersects with the zero-crossing level is provided in the signal processing board. The pulse then is defined as a zero-crossing pulse.

In other words, a zero-crossing pulse takes place every time the piston rod (magnetic scale) moves 0.5 mm (Fig. 7).

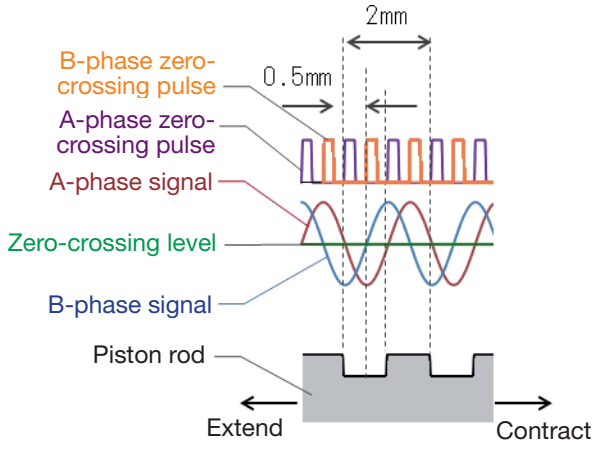

Fig. 7 Zero-crossing pulse

The number of inputs of this zero-crossing pulse can be obtained by a computing unit such as a microprocessor, thereby making it possible to measure the stroke amount (displacement) with a resolution of 0.5 mm.

Which direction the hydraulic cylinder moves (extends or contracts) can be determined by making use of the phase shift between the A- and B-phase signals. When an A-phase zero-crossing pulse is detected, the direction of stroke can be uniquely defined by the combinations of whether the polarity of the A-phase signal changes from positive to negative or vice versa and whether the polarity of the B-phase signal then is positive or negative.

For example, assuming that, in Fig. 7, the motion of the magnetic scale from the right-hand side to the left-hand side is defined as "extension" and the motion from the left-hand side to right-hand side as "contraction", a change-over of the A-phase signal from positive to negative indicates "extension" if the B-phase signal is negative, or "contraction" if the B-phase signal is positive.

Applying similar judgment to the detection of B-phase zero-crossing pulses always allows the judgment of the direction of stroke.

For the displacement detection using this magnetic scale method, the zero-crossing pulse cycle can be uniquely determined by the mechanical dimension. The method brings about a benefit to the system introduced in this paper that an accuracy of +/-0.5 mm can be ensured.

In general, hydraulic cylinders are subjected to a wide range of temperatures because of their frequent outdoor use and/or temperature variations of the hydraulic fluid. Therefore, their related sensors are likely to be affected by a temperature drift.

The possible effect of the temperature drift is almost negligible when the magnetic scale method is introduced. This is also one of the reasons for using the magnetic scale method.

3.3 Semi-Absolute Output

In general, the absolute type sensor refers to a sensor that "always" outputs the absolute value for displacement.

For example, if the hydraulic cylinder is actuated to move to a certain position with the sensor power off (displacement detection disabled), the sensor will be able to output the value for the cylinder position (displacement) immediately after the sensor is restarted.

However, the stroke sensor introduced in this paper is of an increment type that basically measures the displacement by counting the number of zero-crossing pulses as described in 3.2 above. Therefore, it is usually impossible for the sensor to detect the absolute position of the hydraulic cylinder.

Then, the principle below has been utilized to allow the sensor to detect the absolute value.

Firstly, as shown in Fig. 8, two different magnetic scales are engraved into the surface of the piston rod: regular shallow grooves and reference deep grooves. The reference deep grooves are consequentially filled with thicker non-magnetic material, resulting in A- and B-phase signals with a larger amplitude than those from the regular shallow grooves. This difference in amplitude can be used to identify the reference scale.

Secondary, the reference scale has a groove at the absolute zero (0) mm position of the hydraulic cylinder as the

reference point and several others on the both sides of the reference point each. These grooves for the reference scale are located at irregular intervals like one pitch, two pitches and three pitches.

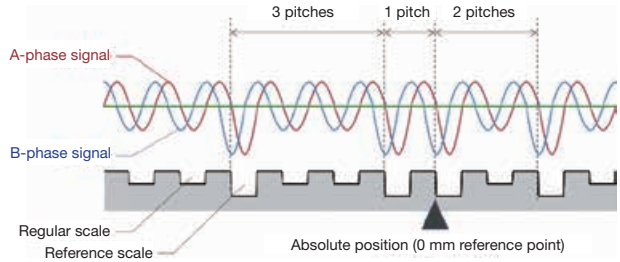

Fig. 8 Example of reference scale arrangement

With this arrangement, when the hydraulic cylinder operates and the magnetic sensor detects any two grooves of the reference scale, the number of pitches between the first and second grooves can be determined from the number of zero-crossing pulses detected during the time, which uniquely determines the second reference groove. That is, the cylinder can be located with its absolute position.

In Fig. 8 for instance, when the magnetic scale moves toward the left-hand side and two pitches of the magnetic scale (two zero-crossing pulses) have been detected until the detection of the second reference groove, this means that the right-most reference groove has been detected. Thus, another absolute position that is 4 mm away from the original absolute position 0 mm is established.

Once established, an absolute position may be used as reference to detect displacement thereafter.

Thus, the SSC in this paper operates as an increment type sensor immediately after the system start-up, but will turn into an absolute type once any two reference grooves have been detected as the hydraulic cylinder operates. That's why the SSC in this paper is called a "semi-absolute type".

In fact, it is theoretically possible to locate the cylinder with its absolute position just by providing only one reference groove at the absolute position 0 mm instead of providing several reference grooves.

However, when assuming actual service conditions, for example, a case in which the SSCs are used for suspension dampers of transportation equipment, the SSCs may extend/contract only with a very small amount of stroke during driving on a flat road where the vehicle is only subjected to small vibration. In this case, the reference scale with only one groove is not necessarily detected and the sensor may be unable to output the absolute position data.

Hydraulic actuators are another example. If the system is started up with its hydraulic actuator located away from the only one groove for the reference scale, the system must be moved by a considerable distance in order for the sensor to detect the reference point.

To solve the problem, several grooves for the reference scale are distributed over the length of the piston rod so that any of the possible reference points can be detected as soon as possible after start-up of the system.

It should be noted that, in the example of Fig. 8, the absolute position 0 mm is located in the midst of the piston rod based on an assumption that the cylinder bidirectionally operates (extension and contraction). For an application where the piston rod is always located at either side during start-up, the location may be given the absolute position 0 mm for one-directional detection.

3.4 Improvement of Measurement Resolution

The sections above have explained the principle of measuring the displacement at a resolution of 0.5 mm by counting the number of zero-crossing pulses obtained from A-phase and B-phase signals.

However, the 0.5 mm resolution may be insufficient to ensure adequate performance control of actual hydraulic cylinders. Then, the SSC has been improved to deliver a finer measurement resolution by means of software computation. Firstly, the zero-crossing pulses as well as the analog voltage values for A- and B-phase signals are simultaneously input to a computing unit such as a microprocessor. These A- and B-phase signals are plotted on the X-axis (horizontal) and the Y-axis (vertical) of a two-dimensional plane respectively and drawing a line sequentially from A1, B1, A2, B2... will create a Lissajous curve as shown in Fig. 9.

As stated in the previous section 3.3, the magnetic scale consists of two different scales: regular and reference. The system can use these scales to output A- and B-phase signals with different amplitudes, producing the curve like a double circle.

A round of the Lissajous circle is equivalent to a cycle of the A- or B-phase, namely, 2 mm displacement. So, a quadrant of the Lissajous circle is equivalent to the zero-crossing pulse interval of 0.5 mm (the sensor output value is shifted by 90 degrees along the trail of the Lissajous circle every 0.5 mm of displacement).

Therefore, determining the angle which forms the line segment from the point on the trail of the Lissajous circle given by the A-/B-phase voltage value obtained to the center point with the horizontal line will allow determine the displacement at a resolution of 0.5 mm or less.

A problem related to this detection of the magnetic scale is that the Lissajous circle is substantially warped in the part of transfer from detection of the regular scale (the inner Lissajous circle) to the detection of the reference scale (the outer Lissajous circle) or vice versa, resulting in a poor accuracy of positional detection.

Still, the system is able to recognize that an A- or B-phase signal being detected is on the warped part of the Lissajous circle when the SSC operates as an absolute type after the establishment of a reference point. So, the effect of the warp can be eliminated by the use of a correc-

tion map or other device specifically prepared for exception handling.

This modified software computation allows the semi-absolute type SSC in this paper to detect displacement with a resolution of 0.1 mm.

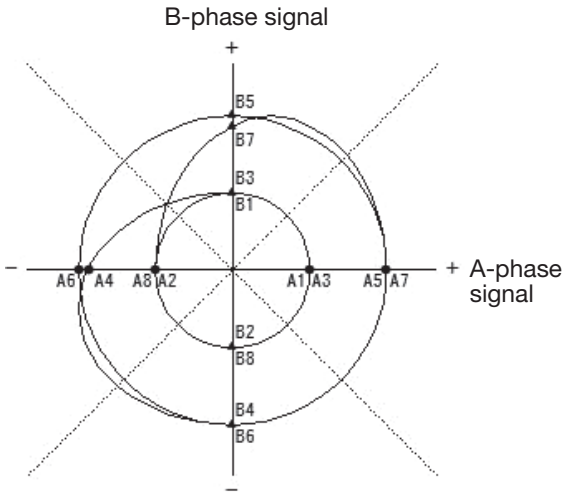

Fig. 9 Lissajous wave of output from magnetoresistance elements

3.5 Automatic Adjustment of Zero-Crossing Level

It is feared that the semi-absolute type SSC in this paper that operates with the piston rod sliding against the magnetic sensor may have wear in its sensing member on the tip of the magnetic sensor due to age deterioration, leading to a larger gap between the magnetic scale and the magnetoresistance elements. Machining variations of the magnetic scale is also another concern.

So, the median value and amplitude of A- and B-phase signals are not always constant.

If the zero-crossing level is out of the median value of A- and B-phase signals, the zero-crossing pulses would not be timed properly, resulting in poor accuracy of displacement detection. Therefore, the zero-crossing level always needs to be adjusted to the median value of the amplitude of actual A- and B-phase signals.

This zero-crossing level adjustment is automatically done by the computing unit on the signal processing board such as a microprocessor by calculating the proper value on an as-needed basis. Fig. 10 shows a block diagram of the zero-crossing level adjustment function:

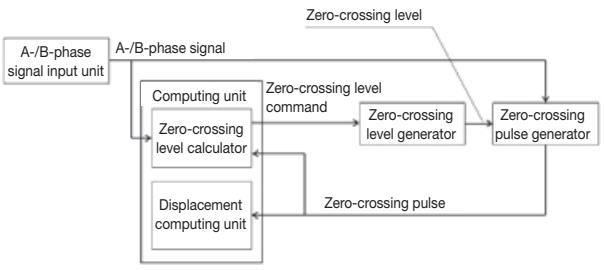

Fig. 10 Block diagram of zero-crossing level adjustment

For example, assume that the zero-crossing level of the A-phase needs to be adjusted. Obtain the value for the A-phase signal at the time when the zero-crossing pulse of the B-phase is input. This value is always a maximum or minimum value of the amplitude because there is a phase difference of 90 degrees between the A- and B-phase signals.

So, these values can be used to calculate the amplitude value for the A-phase signal. Similarly, the amplitude value for the B-phase can be determined by obtaining the value for the B-phase signal at the time when the zero-crossing pulse of the A-phase is input.

Note that this function is only enabled after the absolute type sensor function is enabled with the detection of the reference scale.

The system can recognize which magnetic scale on the piston rod is being read by the sensor only after the SSC turns into an absolute type. Now the system is able to learn amplitude measurements for each magnetic scale.

Based on the amplitude measurement data for each magnetic scale, the system calculates the proper median value of amplitude and then outputs the result as the zero-crossing level.

Continuing to execute this control will allow zero-crossing pulses to take place at proper timing, ensuring the displacement detection accuracy. Also, the automatic correction of the zero-crossing level will allow stable detection of displacement over a long time without manual tuning by user such as zero-point correction, leading to easier maintenance.

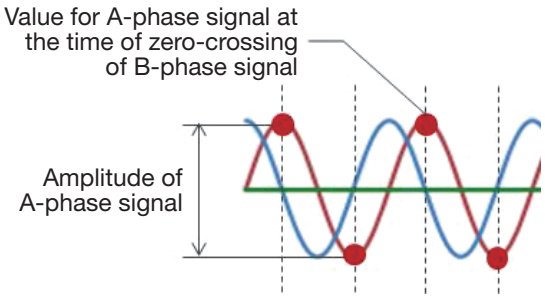

Fig. 11 Obtaining amplitude of A-phase signal

4 Results of Displacement Detection

As an example of detection of the displacement of a cylinder with a reference point (absolute position 0 mm) established in the central part of the piston rod, the cylinder is stroked at a fixed speed by 40 mm in the directions of extension and contraction each. The result is plotted in Fig. 12 with time on the horizontal axis and stroke on the vertical axis.

The output values of a displacement gauge installed as a reference for evaluation (the blue line in Fig. 12) and the

output values of the semi-absolute type SSC (the red line in Fig. 12) overlap one another, which implies that the displacement is stably detected.

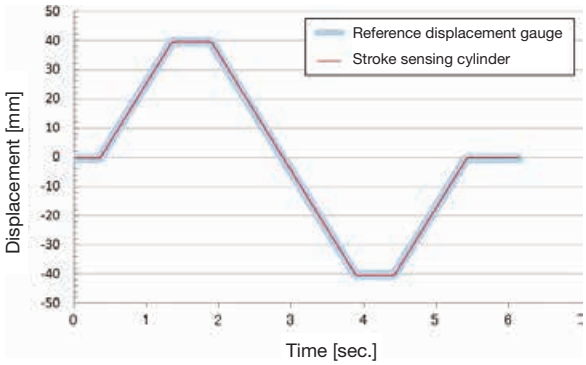

Fig. 12 Example of displacement output

The semi-absolute type SSC outputs the displacement in the form of analog voltage signals. However, it can also support digital output such as CAN and serial communication by adjusting the specifications of the signal processing board to the interface of the main machine.

5 Future prospects

For today's automobiles and construction machinery, new solutions have been developed including remote control through high-speed communications, artificial intelligence (AI) and Internet of Things (IoT).

Among these, hydraulic equipment is required to be even higher value added equipment. Electronic control systems used in such equipment will have to obtain more diverse information (control parameters) than ever from a variety of sensors, in order to be more advanced and more sophisticated.

In this sense, various sensing devices that can detect the status of equipment will be a critical element for hydraulic equipment to have higher-added-value functions. The displacement detection by the semi-absolute type SSC is also one of them.

For example, the conventional suspension of automobiles adjusts its damping force and thrust by estimating the damper behavior according to the magnitude of acceleration (rolling of vehicle) input from acceleration sensors. The active suspension in turn can directly detect the displacement to provide even more accurate control, with which the ride comfort is expected to be further improved.

The developed semi-absolute type SSC is still at a prototype level. For mass production, some challenges must be overcome including the machining process to provide the magnetic scale on the piston rod and the assembly of the magnetic sensor. Still, the SSC is expected to be effectively used as a sensing device that can greatly contribute to higher-value-added hydraulic equipment in the future.

6 Concluding Remarks

Taking a cue from the Industry4.0 proposed by Germany, the Japanese government has also proposed Society5.0.

Under these social circumstances, IoT technology that communicates a variety of information at high speeds and AI technology that processes collected information have rapidly advanced.

These "communications" and "information processing" together with "sensors" are three critical elements of information technology (IT) or may be collectively called "the Three Sacred Treasures of IT". Each of them is very important.

"Sensors" should not be simply used as parts to obtain parameters for electronic control, but should be combined with "communications" and "information processing" to make up "the Three Sacred Treasures", making it possible to build new solutions.

In hydraulic equipment for instance, data obtained with cameras (image sensors) can be transferred to a remote place (communications) for AI analysis (information processing). Some hydraulic equipment using these automated driving and remote control technologies are on their way to be commercialized.

One among them is the semi-absolute type SSC introduced in this paper, whose effectiveness will probably be higher. We would like to make the most of it as an element to build AI x IoT solutions.

Author

NAGAI Yuki

Joined the company in 2008.
Information Technology R&D Sect.,
Basic Technology R&D Center,
Engineering Div.
Mainly engaged in software development for sensors.

Technology Explanation

Thermal Analysis of Electronic Circuits

KAWANO Tomoyuki, SEKINE Nobuyuki, ITO Kensuke, KABASAWA Ryoichi

Abstract

In recent years, due to the "CASE (Connected, Autonomous, Shared, Electric)" technological trend, electronic control units (ECUs) need to be installed at free locations and they need to realize higher performance, have more electronic capabilities, high-density packaging, and integrate multiple functionalities. These requirements crowd heat-generating components and accelerate deterioration. On the other hand, consumer electronic devices such as smartphones are progressing in their complexity and downsizing. These are achieved by saving power through high-performance semiconductors and improving the heat dissipation structure. The thermal design is important to achieve similar performance in ECU. The thermal design makes it possible to secure the required service life, performance, and quality by predicting temperature and dissipating heat, while pursuing the limit of heat generation density. Generally, computational fluid dynamics, which is 3D simulation, is used for the prediction of temperature. However, it is effective to repeat the thermal network method, which is 1D simulation, to verify the feasibility in the upstream area of development flow to prevent rework from the downstream area. This paper reports on detailed modeling to confirm heat phenomena of the electronic circuit and discuss the results of 1D simulation which is accurate and fast.

1 Introduction

In designing Electronic Control Units(ECU) to satisfy upcoming needs for a wide range of high-end applications like automotive or construction machines, it has recently become more important to address thermal issues. In these applications, only limited space is available for such electronic components and the trend of motorization and electronification results in higher power consumption. Naturally, the electronic components reach higher temperatures by internally generating heat, accelerating the deterioration of mounted chips. The trend of in-vehicle electronics packaging technology is shown in Fig. 1:

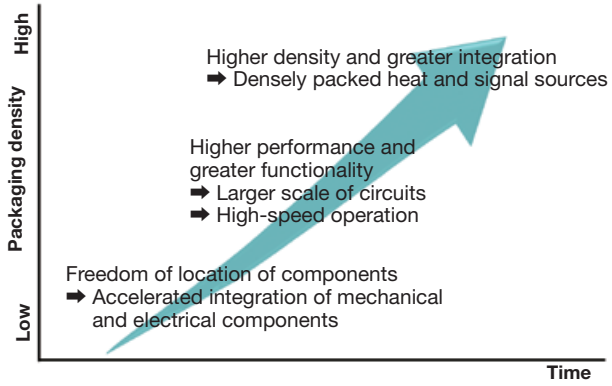

Fig. 1 Trend of ECU packaging technology

To guarantee the service life of products, it is necessary to reduce heat generation through power saving and to lower the temperature by raising the heat dissipation capability. Finer digital circuits have contributed to power saving in such a remarkable way that their processing capability has been doubled in two years while retaining the same power consumption. With the emergence of compound semiconductors such as silicon carbide (SiC) and gallium nitride (GaN), power devices have been downsized with higher switching efficiency and higher switching frequency. Their heat dissipation capacity has also been enhanced. With improved electronics packages and advanced heat transfer materials, today's electronics can be designed to release heat into the atmosphere via their cases to prevent the build-up of heat inside.

Electronics designers need to pursue the limitation of heat generation density in order to improve product competitiveness. Downsizing a product will always decrease its weight, resulting in lower cost. However, the product may also have a higher internal temperature which exceeds the specified service temperature limit or shortens the service life of the components mounted therein. Therefore, it is indispensable to properly estimate the size, weight, cost, life, and quality in the upstream stage of product development.

This paper briefly explains some of our engineering

challenges we have continuously addressed in relation to the above-described estimations. Specifically, with a focus placed on the thermal network method, which replaces heat transfer with an equivalent electric circuit, the following describes an analysis approach using an electronic circuit simulator for calculation.

2 Service Life of Electronic Components

One of the major factors that reduce the service life (Hereafter, service life is represented by life) of electronic components is thermal fatigue. Electronic components may experience failure when a thermal chemical reaction reaches a limit [1].

To predict the life, an acceleration test using the Arrhenius equation (Equation (1)) to predict the chemical reaction speed K at a certain temperature T is widely used:

$$K = A\exp\left(-\frac{E_a}{kT}\right) \tag{1}$$

A: Constant
E_a: Activated energy [J]
k: Boltzmann's constant [J/K]

When the time (life) for product to have a failure at temperatures T_1 and T_2 is L_1 and L_2 respectively, Equation (2) below can be obtained:

$$\ln L_1 - \ln L_2 = \frac{E_a}{k}\left(\frac{1}{T_1} - \frac{1}{T_2}\right) \tag{2}$$

Accordingly, the natural logarithm of the life that was actually measured during the acceleration test is proportional to the plotted inverse of the temperature. This linear relationship is called the Arrhenius plot (Fig. 2). The slope of the line can be used to determine the activated energy E_a. Giving the combined setting of operating temperature and time (temperature profile) of the component as shown in Table 1 enables prediction of the life.

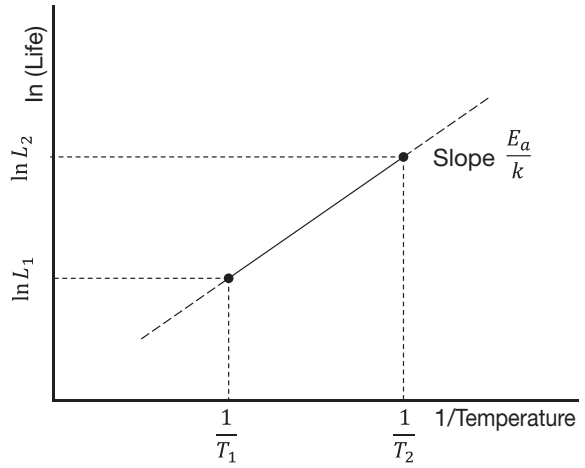

Fig. 2 Arrhenius plot diagram

Table 1 Example of temperature profile

State	Per day				Per 15 years
	tj (°C)	Time (h/day)	150°C-equivalent time (h/day)	Rate (%)	150°C-equivalent time (h)
Active	130	0.05	0.01924	11.00	105
	100	0.95	0.07203	41.17	395
	70	7.00	0.07870	44.98	431
Inactive	25	16.00	0.00500	2.86	27
Total			0.17497	100.00	959
Upper limit			0.18252	100.00	1000

3 Heat Generated by ECUs

The dominant heat generated by an electric control unit (ECU) is Joule heat from the packaged electronic components. This heat is transferred to the ECU casing via the printed circuit board (PCB) and then released into the atmosphere (Fig. 3). This section explains how the heat is transferred with a focus on the PCB, which can efficiently transfer the heat from the electronic component as a heat source.

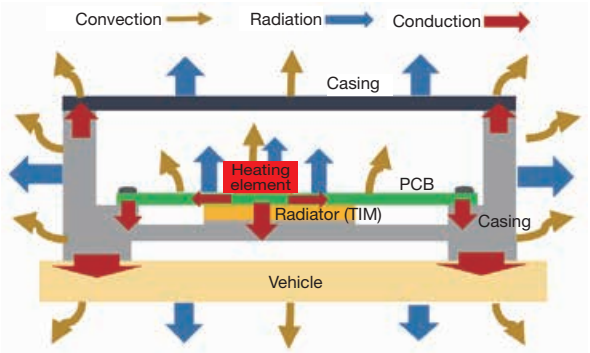

Fig. 3 Heat path of ECU

Once the heat consumption P from the heat source, the atmospheric temperature T_a, and the thermal resistance θ determining how the heat is transferred have been determined, the heat source temperature T can be estimated by Equation (3):

$$T = T_a + \theta P \tag{3}$$

where θ is the total thermal resistance of all heat dissipation paths between the heat source and the atmosphere. In reality, it is complex to calculate the heat source temperature due to the existence of two or more heat sources, two or more heat paths, and the temperature distribution of the atmosphere (Fig. 4). Still, it is possible to determine the heat source temperature simply by determining the thermal resistance of the relevant parts.

When the amount of heat of the heating component and the thermal resistance of the PCB in releasing the heat to the atmosphere are known, the area of the PCB with the required heat dissipation capability can be determined. Since the heat consumption of the electronic component

as a heat source depends on the temperature, it is necessary to use a simulation tool that can support the electric and thermal calculations as a pair.

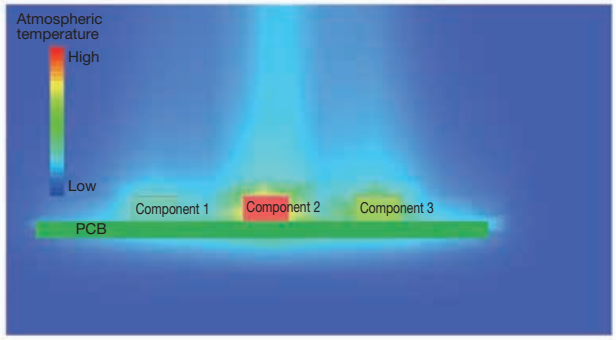

Fig. 4 Heat dissipation to atmosphere

4 Simulation Tool

Thermal analysis is often carried out using dedicated thermal fluid analysis tools. In the conceptual design stage in the upstream stage of product development, where more importance is placed on "guessing," however, it is desirable to carry out a one-dimensional (1D) simulation, not the thermal fluid analysis or another simulation using three-dimensional (3D) profile models. The 1D simulation referred to herein means to replace the heat dissipation path with a thermal network to allow repetitive simulation under variable conditions [2].

What is important in the process of thermal network calculation is the heat consumption of electronic components and the thermal resistance of the heat dissipation path. Conventionally, the heat consumption has been estimated from the standard values included in the data sheets, but depending on the conditions, in some cases the estimation obtained in this method was quite different from the actual heat consumption. This is because the heat consumption of electronic components varies by temperature due to the variations further depending on the manufacturing dispersion of electronic components, and because different electronic components affect each other, resulting in changes in temperature. A solution is to analyze the two kinds of phenomena, namely electric and thermal, along with their interactions.

It may be possible to carry out this analysis through theoretical calculation, but the calculation must be repeated many times. Thus, it is more efficient to use a simulator. For 1D simulation of electronic circuits, we use a simulation tool based on Simulation Program with Integrated Circuit Emphasis (SPICE), which is widely used nowadays. The use of SPICE makes it possible to carry out the simultaneous simulation of both electronic and thermal circuits.

Recently, electronics manufacturers have been providing thermal models for SPICE in some cases. However, thermal analysis requires thermal models of the majority of heat dissipating paths including PCBs and atmosphere to be prepared. The SPICE-based simulators simply calculate any circuits given; thus, they may fail to produce accurate results if an electric or thermal model with poor accuracy is included. Accordingly, it is important to evaluate the prepared circuits and thermal models and then determine the analysis accuracy.

For electric models, electric characteristics should be determined, and depending on the operating conditions, it may be necessary to adjust with consideration given to the effect of temperature.

The shorter time it takes to complete analysis, the better it is. The model representation method depends on whether the temperature is changing over time (transient state) or is stable after an elapse of sufficient time (steady state). Thus, it is necessary to prepare electric and thermal models suitable for the purpose.

5 Thermal Model of Electronic Components

This section discusses a thermal model of the electronic component shown in Fig. 5. The electronic package internally consists of a semiconductor as a heat source and a package material covering the semiconductor as shown in Fig. 6.

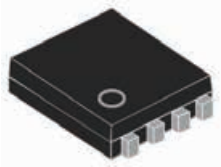

Fig. 5 Semiconductor package

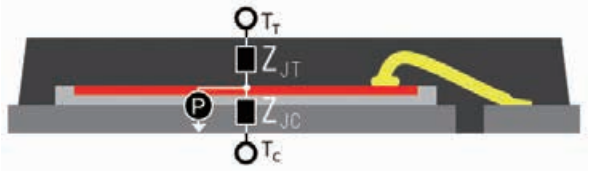

Fig. 6 Internal structure of package

In Fig. 6, P is the heat source, T_T the temperature of the top surface of the package, Z_{JT} the thermal impedance from the p-n junction, colored in red, to the top surface of the package, T_C the temperature of the lower surface (case) of the package, and Z_{JC} the thermal impedance from the p-n junction to the case.

The thermal impedance is the ratio between temperature and heat flow, indicating the resistance of heat to flow in the thermal circuit. There are two types of thermal impedance: resistive and capacitive. These can be represented by the resistance and capacity symbols to form a thermal model of the ladder-type network as shown in Fig. 7(A):

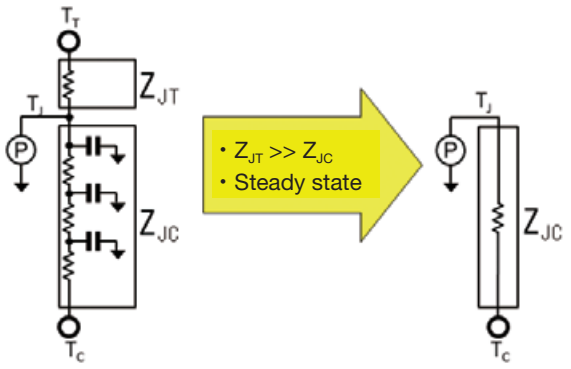

Fig. 7 Thermal model (ladder-type network)

In the steady state, the effect of thermal capacity is negligible. In this example, the network can be simplified into a thermal network only with a thermal resistance shown in Fig. 7(B). The heat consumption P is decided by the power consumption of the devices contained in the package and can be determined from the voltage and current.

If there is any difference between the calculation results and measurements, the model should be modified to improve the analysis accuracy.

5.1 Printed Circuit Boards

The heat generated by electronic components is released into the atmosphere via the PCB (Fig. 8). The thermal resistance of the PCB can be determined from its profile and the thermal conductivity (Table 2) and then can be used as a parameter [3]. The thermal resistance between the PCB and the atmosphere can be determined from the heat transfer coefficient and the surface area of the PCB (Fig. 9).

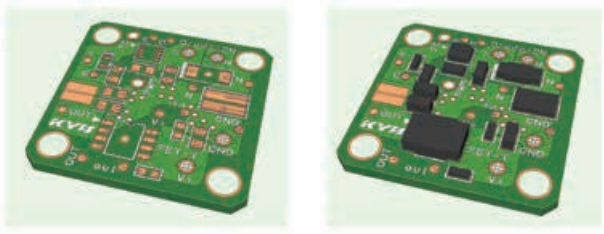

Bare PCB Populated PCB

Fig. 8 PCB

Table 2 Thermal conductivity of PCB materials

Material	Thermal conductivity [W/(m·K)]
Copper	390
Substrate	0.35

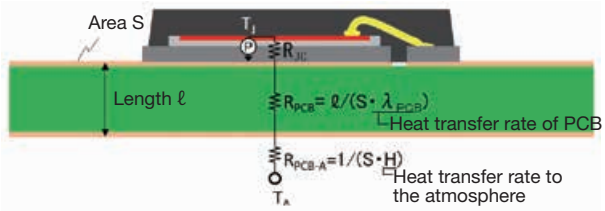

Fig. 9 Thermal model of PCB

5.2 Resistors

When a resistor has a resistance value R, its heat consumption P can be determined by Equation (4) if the current I or voltage V is given:

$$P = VI = \frac{V^2}{R} = RI^2 \tag{4}$$

Multiplying this heat consumption P by the thermal resistance θ of the package material of the resistor will give the temperature difference according to Equation (3), from which the surface temperature of the component can be determined. Electric and thermal models of the resistor are shown in Fig. 10:

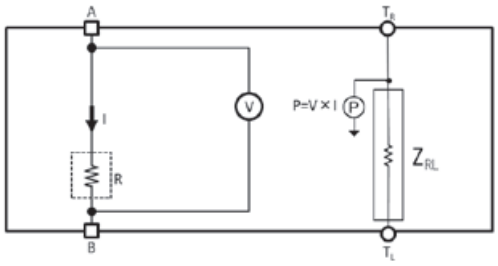

Fig. 10 Electric and thermal models of resistor

5.3 Diodes

A diode is a semiconductor component with two terminals: an anode and a cathode. It conducts current only in one direction, namely from the anode to the cathode, not vice versa.

Diode manufacturers provide SPICE-based thermal models. Using these models, we carried out an electronic circuit simulation and compared the results with the characteristics indicated in the data sheet (Fig. 11).

The diode used for this evaluation has a maximum forward current I_F of 1 A. An electric model is needed to estimate the heat consumption in this region. Since the electric model provided by the manufacturer has a large deviation at a temperature of 125˚C, we decided to adjust the model accordingly (Fig. 12).

This task was difficult to achieve only by adjusting the parameters of the electric model. Accordingly, by using a combination of original mathematical expressions, we adjusted the model to attain an average error of around 10%. To reduce the calculation load, the model has been simplified except for a current region around 1 A, where accuracy is required.

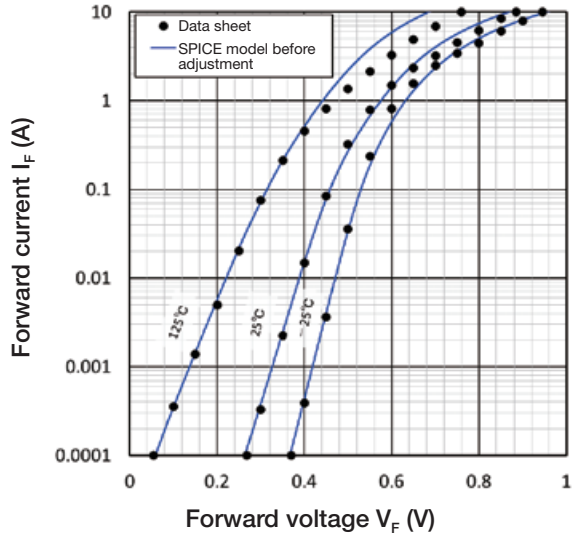

Fig. 11 I_F-V_F characteristics of diode

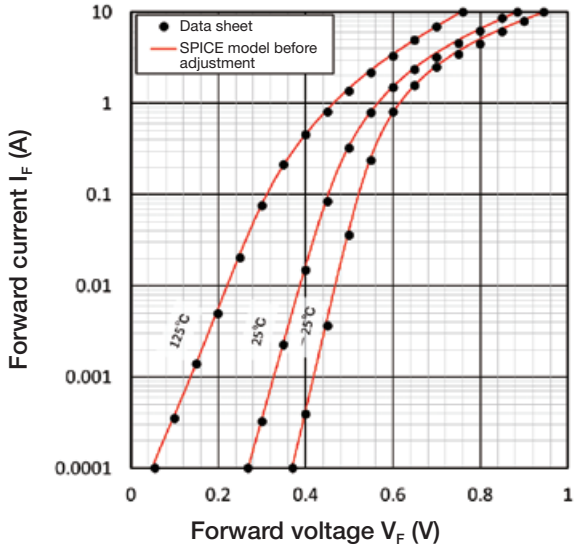

Fig. 12 I_F-V_F characteristics of adjusted diode

The manufacturing dispersion of semiconductors affects how likely they are to generate heat. In consideration of that, we continuously think about the satisfied circuit operation. Since this analysis focuses on heat generation, the forward voltage V_F at which the heat consumption is highest is estimated from the voltage and current indicated in the data sheet (Fig. 13).

We push forward to achieve a circuit design having a design margin that can accommodate the error of the newly estimated electric model and the error (about 10% in average) of the previously adjusted electric model.

Besides the above, diodes also involve adjustment of other characteristics including capacity and reverse recovery. However, this analysis uses the electric model provided by the manufacturer as is. The electric and thermal models of the diode are shown in Fig. 14.

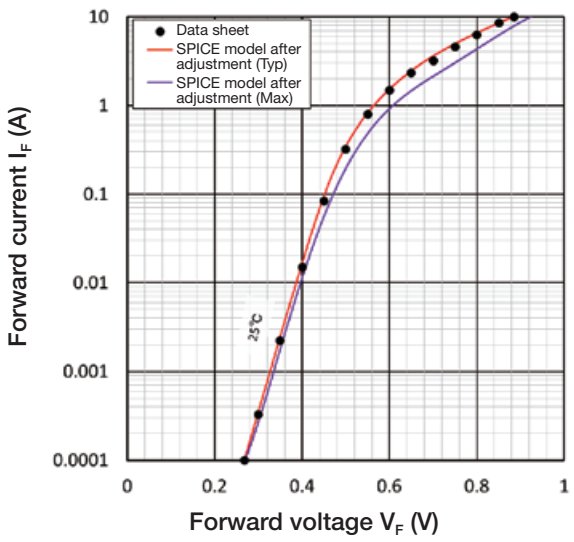

Fig. 13 I_F-V_F characteristics of diode with highest heat consumption

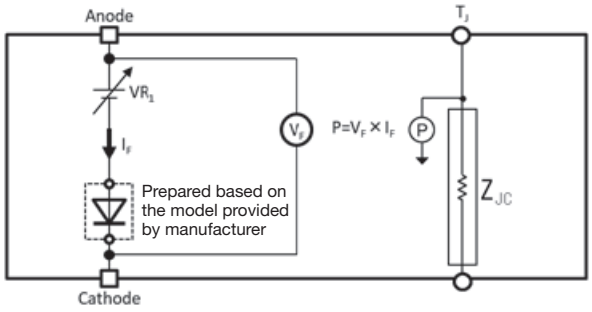

Fig. 14 Electric and thermal models of diode

5.4 FET

The field-effect transistor (FET) is a type of semiconductor components with three terminals: source, gate and drain. FETs control the flow of current between the drain and source by applying a voltage across the gate and source.

FET manufacturers provide SPICE-based electric models of FETs. FETs feature the gate voltage (point Q) at which the current between the drain and source is constant, not depending on the temperature. Fig. 15 shows the V_G-I_D characteristics of an electric model provided by FET manufacturers, in which the characteristics curves at different temperatures do not intersect with each other. In this case, the parameters should be adjusted so that the curves intersect at the point Q as shown in Fig. 16.

The gate-to-source voltage (gate threshold voltage) that is necessary to turn the FET on is dependent on temperature. Since a difference was found between the manufacturer's electric model and the data sheet as shown in Fig.17, the drain current around 1 A, where accuracy is required, has been adjusted (Fig. 18). After the electric model is adjusted, a thermal model should be created (Fig. 19).

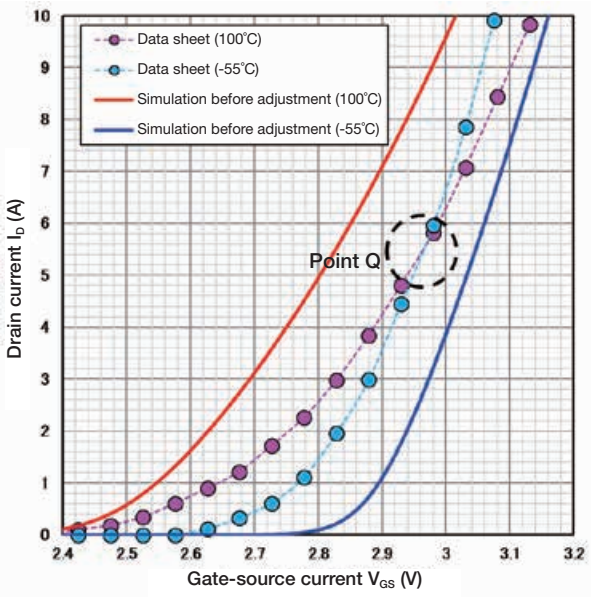

Fig. 15 V_G-I_D characteristics of electric model provided by manufacturer

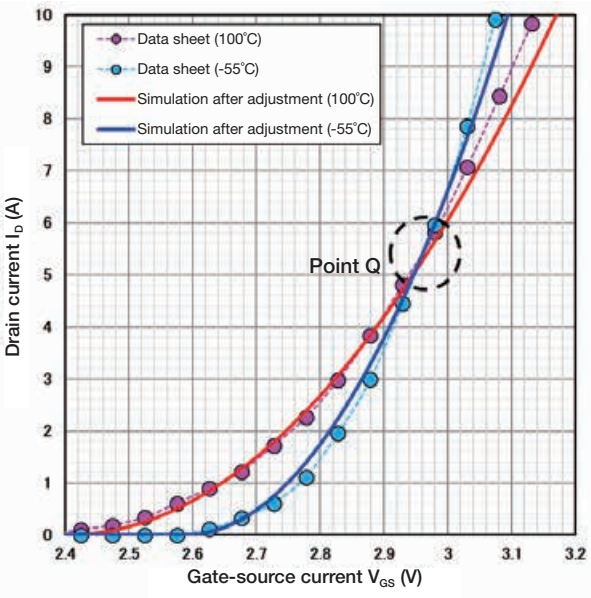

Fig. 16 V_G-I_D characteristics after adjustment

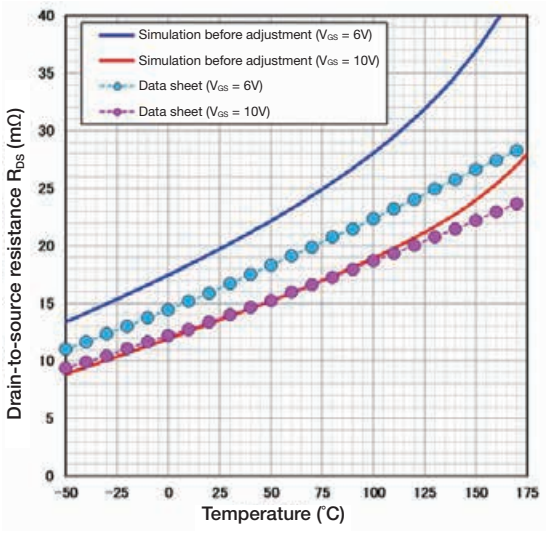

Fig. 17 T_a-R_{DS} characteristics of electric model provided by manufacturer

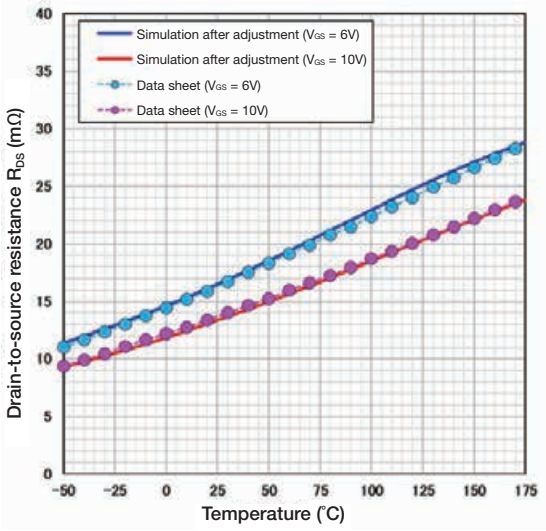

Fig. 18 Adjusted T_a-R_{DS} characteristics

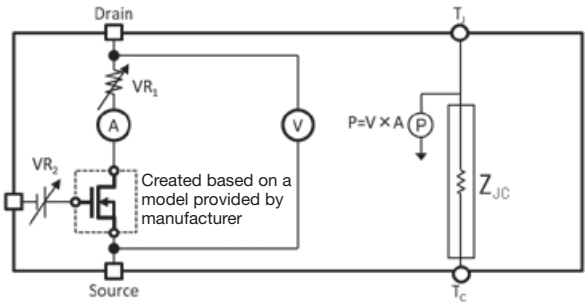

Fig. 19 Electric and thermal models of FET

6 Development Flow

The following lists the flow of development of PCB implementation:

[1] Define the specifications.
[2] Select components and design circuits.
[3] Design a PCB layout.
[4] Design a PCB pattern.
[5] Predict product temperature.
[6] Prototyping and evaluation

If thorough discussion is made in the steps [2] and [3] during the early stage of product development, the number of times of prototyping can be reduced, leading to less rework upon detection of failures during verification tests using actual machines. The following explains the development flow using a specific case of an actuator driving circuit shown in Fig. 20. The FET, diode, and resistance are components that can generate heat.

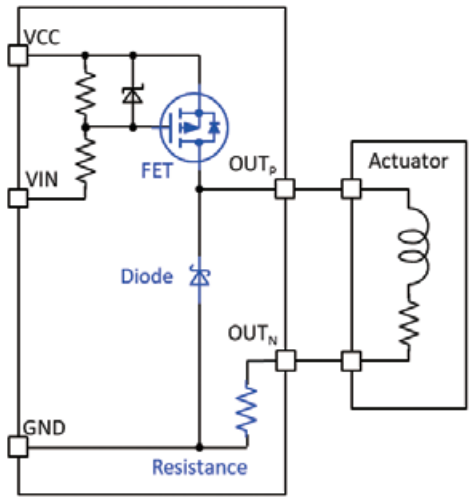

Fig. 20 Actuator driving circuit

6.1 Selecting Components

The key points in selecting components are to satisfy the operating temperature specifications and to ensure the life.

In terms of the operating temperature specifications, components should be selected so that their temperature is within the service temperature range during assumed circuit operation.

The life of components can be estimated from the service environment of the product (a period of time for each temperature range). For example, in-vehicle grade semiconductors are often subjected to a reliability test at 150˚C for 1,000 hours. In order for the semiconductor to satisfy the test conditions, the load current, power consumption and thermal resistance of each electronic component should be estimated and appropriate components should be selected so that the upper temperature limit will not be exceeded.

The power consumption of the overall circuit under the conditions where the selected heat-generating components satisfy the points above should also be calculated, from which the minimum board size can be determined for temporary selection (Fig. 21). Remember that the smaller the board size is, the higher the thermal density is.

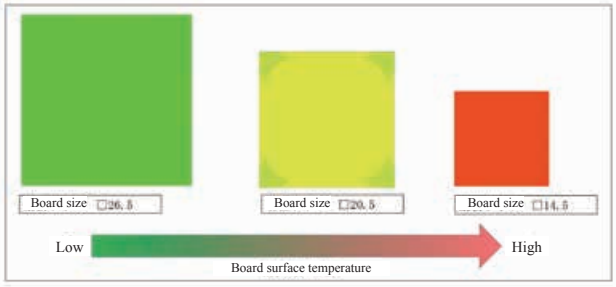

Fig. 21 Relationship between board size and board surface temperature

Boards at higher temperatures need to use high-temperature-resistant components, which are usually expensive. Thus, it is important to consider the balance between cost and size (compactness).

6.2 Designing Circuits

A circuit diagram should be created and the operation be verified through theoretical calculation and using simulation tools. In addition, the source voltage and ambient temperature variations should be determined for improved robustness, and the operation under the worst conditions should be verified with considerations given to variation in components. The worst conditions may be difficult to set up through measurement, but can easily be identified through simulation.

6.3 Analyzing Component Life

The life of the product with the highest heat consumption ("Max." in Table 3) is predicted with a simulation. As an example, the results of a simulation predicting the life of a FET are shown in Fig. 22. It can be determined from the figure that the life is within 1,000 hours at 150˚C, as guaranteed by the manufacturer.

Table 3 Highest heat consumption with manufacturing dispersion

Power consumption (W)		
Min	Typ	Max
0.42	0.54	0.62

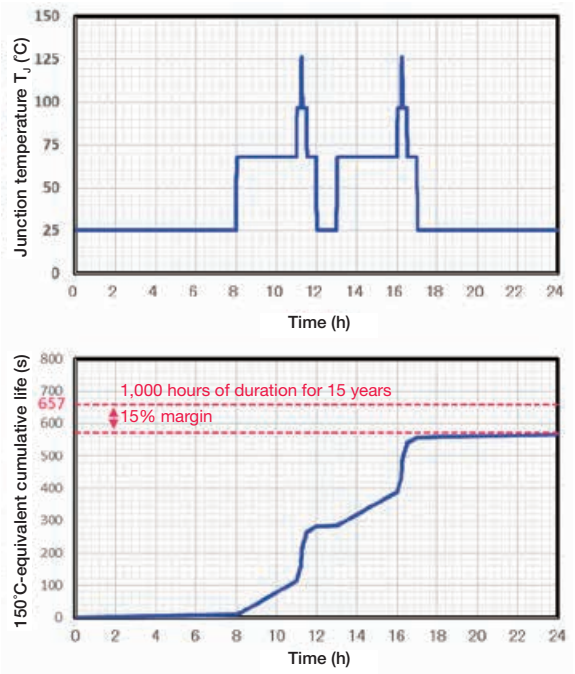

Fig. 22 FET life prediction

6.4 Designing Board Layout

The electric and thermal models using the temporarily selected board size under the worst conditions is analyzed to determine the thermal distribution. If the temperature in a thermally concentrated location is out of the service

temperature range, the arrangement and board size should be adjusted so as to achieve the target temperature. Figs. 23 to 25 indicate the results of 1D and 3D simulations. Fig. 23 shows an example that does not meet the requirements because the component temperature exceeds the upper limit due to an excessively small board. Fig. 24 shows an example in which the board size is larger than necessary while the component temperature is very favorable. Fig. 25 shows an example in which the component temperature and board size are both appropriate.

7 Prototype Evaluation

We have decided the board size based on the results of the 1D simulation and prototyped a board (Photo 1).

We measured the temperature of the on-board components and compared it to the simulation results. The component that showed the highest temperature is the diode, and the difference in temperature between the measurements and the 1D simulation is within 3˚C (Fig. 26). For the most part, the temperature distribution obtained with the 3D simulation represents similar trend to that obtained with actual measurements (Fig. 27).

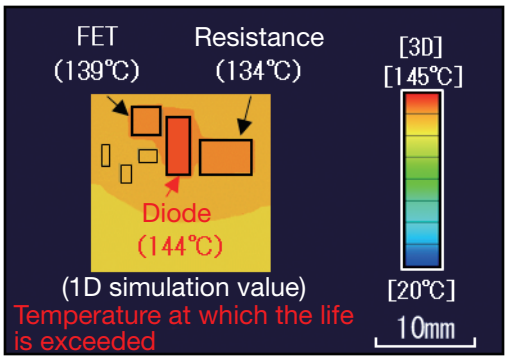

Fig. 23 Excessively small board

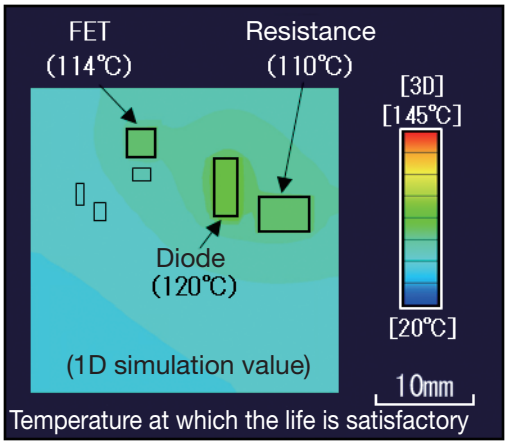

Fig. 24 Excessively large board

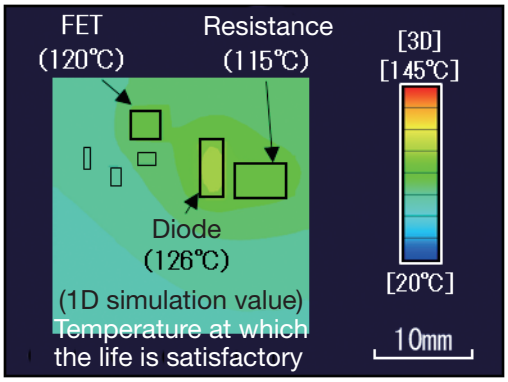

Fig. 25 Board of proper size

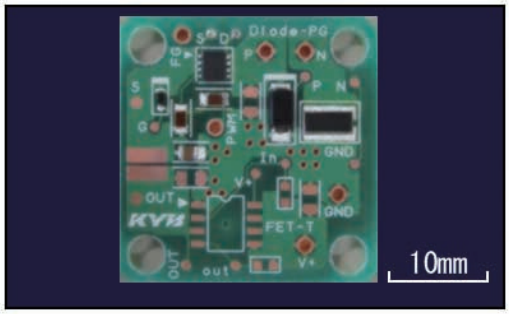

Photo 1 Prototyped board

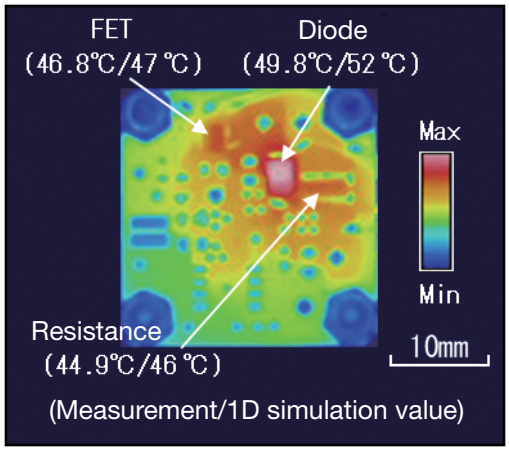

Fig. 26 Comparison between test and 1D simulation

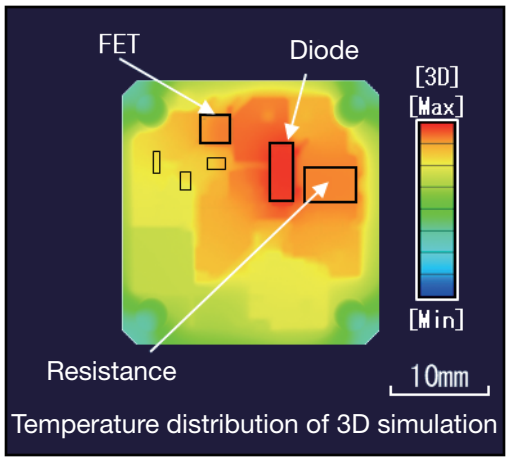

Fig. 27 Results of 3D simulation

Since components at higher temperatures have shorter life, the small difference in temperature of the component with the highest temperature between the measurements and the simulation implies that the results are desirable.

8 Concluding Remarks

We conducted thermal analysis with 1D simulation using electric and thermal models and also carried out actual measurement of the temperature of a prototyped PCB. The results showed that the difference in temperature of heat-generating components between prediction and measurement was 20% or less. We also found that compared to the 3D simulation with thermal fluid analysis, 1D simulation requires a substantially shorter time to obtain calculation results. If it becomes possible to predict the temperature without 3D simulation, the feasibility of a PCB design of a required size can be determined in the conceptual design stage of the initial development phase. This will lead to lower possibility of rework after the 3D profile design has been completed, achieving higher efficiency of total development.

Moving forward, we will accumulate data supported by actual measurements to promote parameter optimization of various models. By improving the accuracy of initial thermal analysis of new products being developed, we are committed to higher efficiency and higher added value for electronics product development.

References

1) Reliability Engineering Association of Japan: Reliability Handbook, Union of Japanese Scientists and Engineers (2014)
2) SHIMADA: ID Simulation, IDCAE, KYB Technical Review No.61 (October 2020)
3) KUNIMINE Naoki: Introduction to Thermo-liquid Analysis of Electronic Equipment, The Nikkan Kogyo Shimbun, Ltd. (2009)

Author

KAWANO Tomoyuki

Joined the company in 2012.
Electronics Technology Sect., Basic Technology R&D Center, Engineering Div.
Engaged in circuit and thermal designs of electronics products.

SEKINE Nobuyuki

Joined the company in 2014.
Electronics Technology Sect., Basic Technology R&D Center, Engineering Div.
Engaged in board and thermal designs of electronics products.

ITO Kensuke

Joined the company in 2015.
Electronics Technology Sect., Basic Technology R&D Center, Engineering Div.
Engaged in circuit and thermal designs of electronics products.

KABASAWA Ryoichi

Joined the company in 2012.
Manager, Electronics Technology Sect., Basic Technology R&D Center, Engineering Div.
Taken present post after working in Development Sect., Electronics Technology Center.

Technology Explanation

The Power of Oil – Influence of Shock Absorber Oil on Vehicle Ride and Handling Performance

SHINJI Kato

Abstract

When the suspension deforms, damping force is generated as the piston of the shock absorber moves, but a time difference occurs before the large hydraulic damping force rises. At the same time the frictional force in the shock absorber is playing an important role in generating effective damping force against deformation of the suspension, the generated force itself is small but its response is high. The frictional force in the shock absorber occurs in reciprocating motion in various speed ranges from amplitude of less than one millimeter to larger amplitudes, its behavior changes dynamically and is non-linear. Recent studies have revealed that controlling the friction is more important than reducing it for improvement of the performance. Because of this we have investigated the dynamic friction characteristics of shock absorber oil and sliding parts, by the means of an own developed device that can measure the speed dependence of friction force in reciprocating motion with high accuracy.

The result of our analysis shows that friction dissipates energy at a speed level of 0.002m/s where hydraulic dissipation is not working yet. By knowing this phenomenon, we have developed different kind of oil types in order to generate various dynamic friction characteristics.

The influence of our developed oil types on the ride and handling performance was tested and analyzed in different vehicles. Subjective assessments and objective measurement show the vehicle performance improvement, which can be generated by using more advanced oil types.

Keywords: shock absorber, damping force, dynamic friction, riding comfort, stability, vertical dynamics

1 Introduction

The damping force of the shock absorbers (SAs) is one of the elements making up the characteristics of the suspension system, and it mainly affects vehicle stability and ride comfort. In recent years, vehicles experience smaller fluctuations in the vertical direction even at high speed as road conditions have improved. Therefore, SAs are often operated at high frequencies with small amplitude, where the direction of SA motion is frequently reversed and the SAs are mainly operated at the low speed.

SA generates damping force by hydraulic oil passing through valves attached to a piston, SA responsiveness is affected by elastic deformation of oil (oil column rigidity) [1] especially at the point where the direction of SAs is reversed. There are new technologies that adjust hydraulic force, for example, a hydraulic valve structure [2] and an electronically controlled SA [3] aiming for generating appropriate damping force according to the road surface conditions by changing hydraulic force. However, these technologies are limited in terms of their ability to improve the damping force when the direction of motion is reversed because of de-formation of oil. The current situation calls for SAs that improve ride comfort and safety (stability, steering response) when driving on good roads as moved very low speed of SAs.

Experience with on-vehicle subjective evaluation of SA performance indicates that ride feeling on good roads can vary greatly with hydraulic oil difference. In this paper, we focus on effect of hydraulic oil on vehicle ride and handling. And then, we developed our own hydraulic oil to adjust the damping force in the very low speed range where direction of motion reverses, in order to clarify the factors that influence the change in feeling.

2 Shock Absorber Design

2.1 Conventional damping force measurement method and its problems

A conventional indicator of the performance of SA is shown in Fig. 1. The right figure is a magnified one of

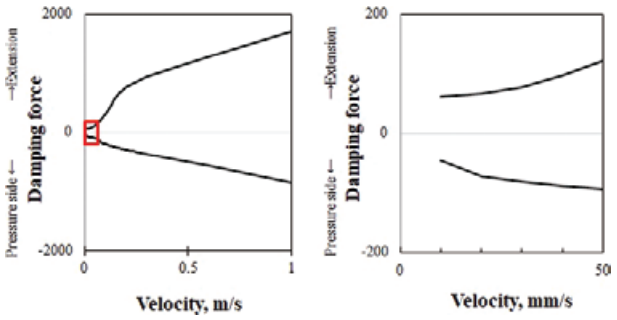

Fig. 1 Damping force - velocity characteristics line diagram

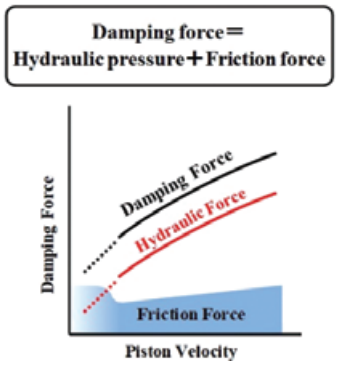

Fig. 3 Relationship between piston speed and damping force

the surrouded area by the red square in the left figure. Here, the performance of the SA is evaluated by a plotting the peak damping force generated by the SA versus stroke speed, which is called "damping force - speed characteristic line diagram". Generally, it does not show speeds of 10mm/s or below. It is a quasi-static characteristics and not suitable for the evaluation of dynamic performance. Hence, in order to evaluate the SA performance on good roads, we believed that it was necessary to evaluate the dynamic characteristics from the time of reversing the moving direction to the very low speed region, which has not been noticed in the conventional performance evaluation.

2.2 Fluid resistance and friction force in damping force

Fig. 2 shows the structure and damping force components of a twin-tube-type SA. As shown in the figure, hydraulic force is generated by the pressure change as hydraulic oil passes through the valves [4], and friction force is generated from the oil seal, the rod guide, and the piston band. The damping force of SAs is the sum of the hydraulic force and the frictional force. We believe that in the very low speed region, a region which has not yet been extensively studied, the hydraulic force would have a smaller impact on the damping force, while the friction force, which has nonlinear characteristics, would have a greater impact [Fig. 3].

In order to understand the relative contribution of hydraulic force and frictional force to the total damping force, we investigated the damping force-speed characteristics. The measurement experiments were conducted as follows.

First, we prepared a valve-less SA by removing valves in order to generate no hydraulic force, and we measured the damping force which now consisted only the friction force. This enables us to determine the speed characteristic of the hydraulic force from the difference between the damping force - speed characteristic of a normal SA and that of the valve-less SA. Fig. 4 shows the changes in the proportion of hydraulic force and the frictional force in the damping force as a function of the piston speed. The figure shows that the proportion of friction force is the highest in the very low speed region where the piston speed is 30mm/s or less.

Next, we analyzed the behavior of the shock absorber on the test course in order to determine their functionality on a good road. In the experiment, we drove a passenger car with a displacement of 1.8L at 60km/h on a test course that reproduced the uneven road surface equivalent to a good road on a national highway. During the experiment, a displacement sensor was mounted in parallel to the SA, as shown in Fig. 5, and the

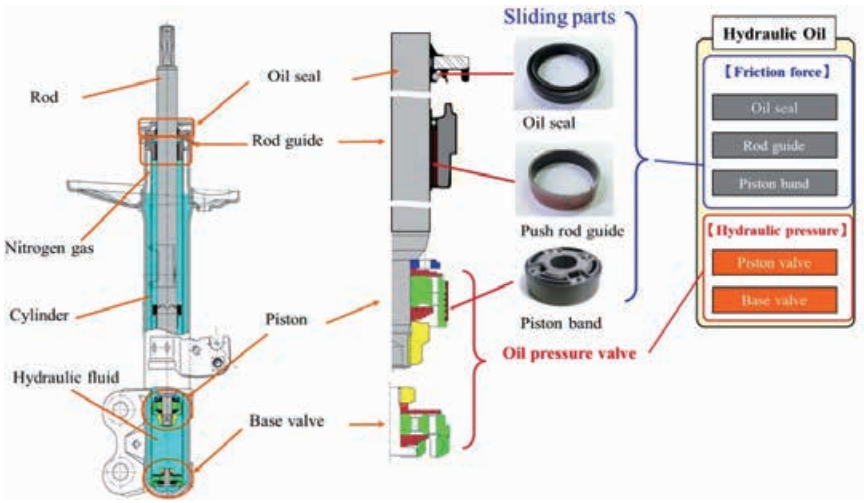

Fig. 2 Twin-tube-type shock absorber structure and damping force component

displacement was measured at 2-kHz intervals, to calculate the frequency distribution of the stroke speed and the displacement. Fig. 6 shows the frequency distribution of the SA speed and Fig. 7 shows the displacement distribution from the neutral position of the SA. We found that for at least 50% of the time on a typical good road, the displacement of the SA would be less than or equal to ± 1.5mm from the stroke center. We also found that for 50% or more of the time, the piston speed was less than or equal to ± 30mm/s, and the most frequent speed was less than or equal to ± 10mm/s.

In these low-speed and low-amplitude regions, little hydraulic force is generated, and the damping force consists mostly of the friction force. In other words, on good roads, the damping force of SAs is largely dominated by the friction force.

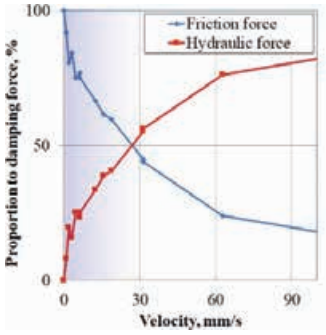

Fig. 4 Speed dependency of load ratio of hydraulic pressure and friction force in damping force

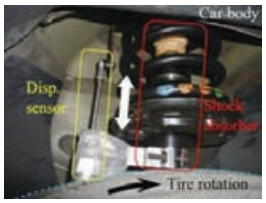

Fig. 5 External view of suspension displacement behavior measurement during actual vehicle running

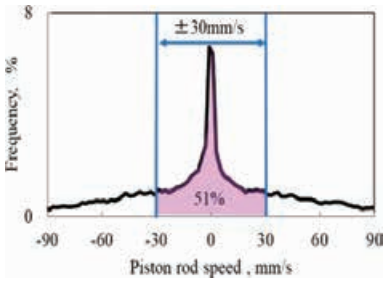

Fig. 6 Frequency distribution of piston speed

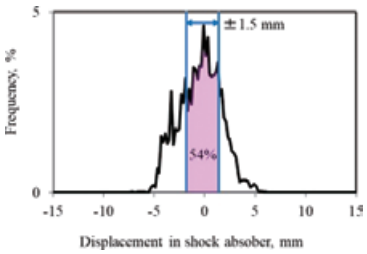

Fig. 7 Frequency distribution of displacement from neutral position

2.3 Evaluation methods and problems in the low-speed operation region

In order to evaluate the dynamic characteristics of the damping force, we use a plotting the force generated by SA versus stroke speed when the SA is operated at a constant frequency and amplitude, as shown in Fig. 8.

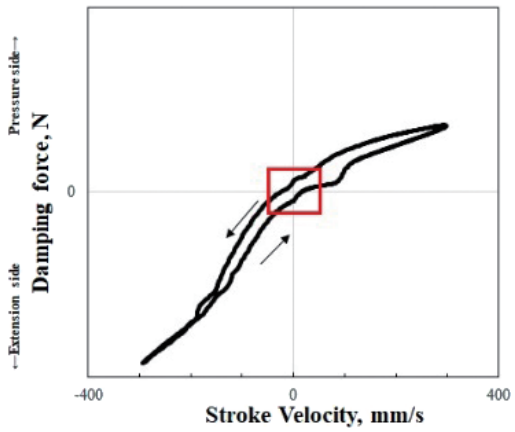

Fig. 8 F-V characteristics

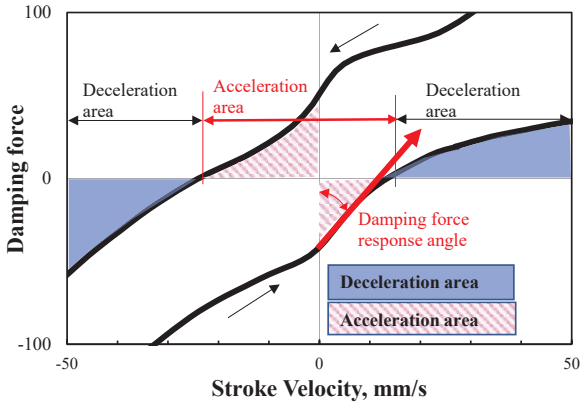

Fig. 9 F-V characteristic around the zero point

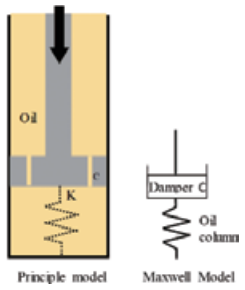

Fig. 10 Influence of oil column stiffness characteristics

The low-speed region around the zero point (surrounded by the red square) in Fig. 8 is magnified in Fig. 9.

Damping force has hysteresis due to the compressibility of the hydraulic oil [1], that works in the form of oil column rigidity as shown in Fig. 10, and in the very-low-speed zone starting at the zero line where the direction of motion reverses, the damping force of SAs is in the direction of acceleration. We believe that the SA response can be improved by reducing this zone.

Friction adjustment using hydraulic oil has been studied in order to improve SA responsiveness, but the response which was observed as the gradient around zero point and the magnitude of the friction force are simultaneously changed as shown in Fig. 11 in order to avoid the occurrence of stick-slip. However, when this method is used, the responsiveness is improved, but at the same time, the ride comfort is deteriorated, and this trade-off characteristics have not been improved. Therefore, we thought that we can improve the responsiveness of SAs without deteriorating the ride comfort by adjusting only the gradient of the friction without changing its magnitude as shown in Fig. 12.

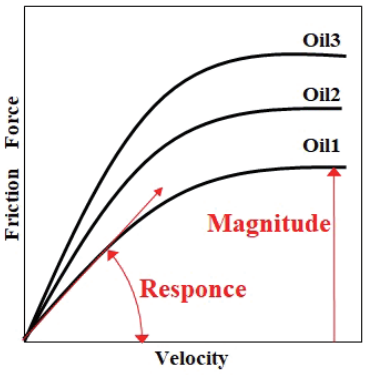

Friction force adjustment
(conventional)

Fig. 11 Technology for changing the magnitude of friction

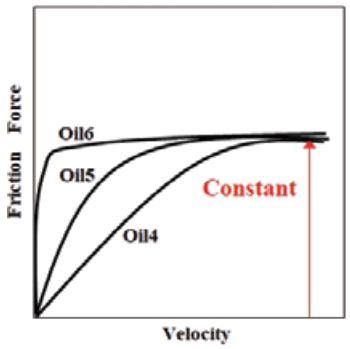

Friction response adjustment
(new technique)

Fig. 12 Technology for adjusting responsiveness

2.4 Friction influence and related components

In order to evaluate friction characteristics while separating friction response and friction force and develop our own hydraulic fluid technology, we developed our own device as shown in Fig. 13 and use it to examine the evaluation index [5].

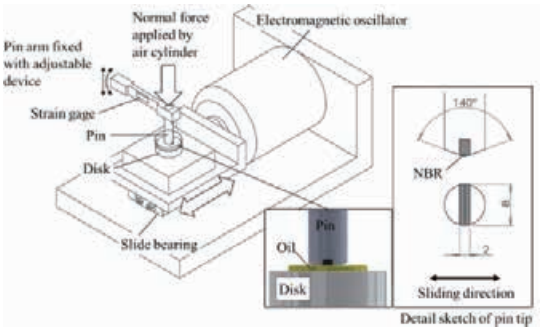

Fig. 13 Schematic of reciprocating force-tester

2.5 Response index

The Response index (RI) was defined as a quantitative index to evaluate the response of friction when the direction of movement was reversed. Fig. 14 shows the range where we extracted the RI in the time waveforms of displacement and friction. Fsa is the maximum friction in the range from the start of motion up to the phase of $\pi/4$ radians (that is, top and bottom dead centers, $\pi/2$ to $3\pi/4$), and normalizes the difference by the average friction. We divided the difference by the average in order to obtain the acceleration-side RI using formula (1).

$$Response\ index\ (RI) = (F_{sa} - F_{ave})/F_{ave}, \quad \pi/2 \leqq \theta \leqq 3\pi/4 \tag{1}$$

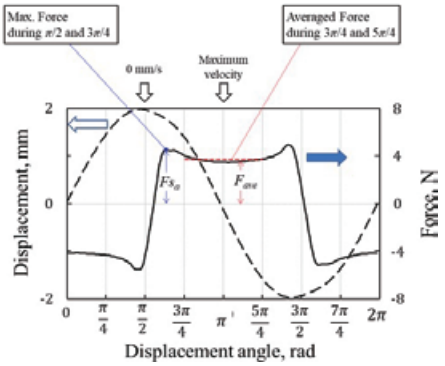

Fig. 14 Calculation concept of the Response index (*RI*)

3 New KYB OIL types and their characteristics

We used our specially made friction test device to develop our own hydraulic fluid technology which can adjust only the response when the direction of motion is

reversed without changing the average friction force. Fig. 15 compares the actual characteristics of the oils that we developed with the conventional hydraulic oil characteristics.

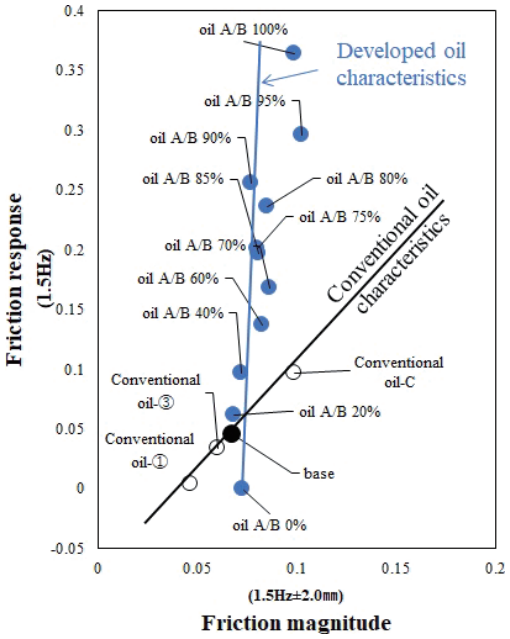

Fig. 15 Characteristics comparison between conventional oils and oils we developed

Hydraulic oil A is a high-response, and the hydraulic oil B is low-response, although the magnitude of friction is almost the same in each case. By changing the blending ratio of these hydraulic oils, it is possible to adjust only the response without changing the magnitude of the frictional force. This technique enables us to investigate the effect of the responsiveness on the basic performance in on-vehicle and bench tests.

4 Oil types Influence on Ride and Handling Performance (Vehicle Assessment Result)

The new KYB oil types and their performance variation on component level were analysed. In order to prove the impact of the oil types on vehicle ride and handling performance, an objective and subjective vehicle assessment is carried out by an engineering service company specialized in vehicle dynamics measurement and assessment.

For this analysis, three sets of SAs with three different oil types, Base (reference, not modified from the original equipment), KYB A/B 100% and KYB A/B 75% are set up. The viscosity of the two KYB oils were adjusted so that it would be the same as the Base specification and the influence of kinematic viscosity and the magnitude of friction would not appear [Table 1].

Apart from the oil, the SA hardware and tuning are not changed. It should be mentioned that by not changing the tuning of the SA while changing the oil, the performance might not be optimally balanced at vehicle level, since the tuning is made usually after choosing the oil. However, since the target of this analysis is to isolate the oil impact on vehicle performance, the tuning is not changed. Fig. 16 shows the damping force-velocity characteristics of the three different SA sets. It can be confirmed that there is almost no difference in damping force characteristics, and one would not expect that the vehicle ride and handling performance will be significantly differing.

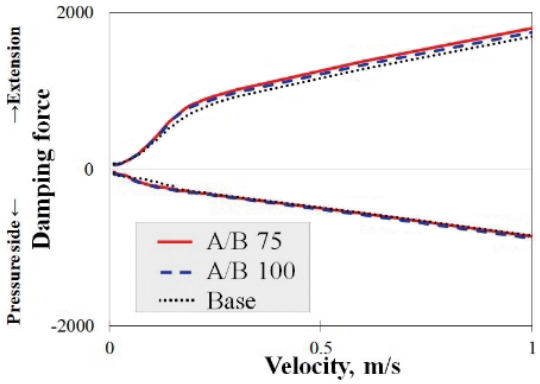

Fig. 16 Damping force-velocity characteristics

4.1 Objective assessment analysis conditions

The vehicle used for this analysis is a Mercedes-Benz A-Class (W177) which was equipped with various acceleration sensors on knuckle/wheel hubs, top mount at all 4 corners and the seat rail. The full sensor setup is shown in Fig. 17.

The test track on which the measurements have been carried out consist of different road surface types: Nevada (smooth tarmac), South Africa (harsh tarmac) and Country-Road (bad local highway) and a special lane with 30mm steps (3 positive and 3 negative). The vehicle speed was varied between 30-50km/h in steps of 5km/h and from 60-100km/h in steps of 10km/h. Measurements were conducted 3times on every lane and at every speed step, and all of the measurements were averaged for the evaluation. All accelerations, body modes and

Table 1 Oil properties

		Base	A/B75	A/B100
Density (15°C)	g/cm^3	0.83	0.85	0.86
Viscosity index		167	168	152
Kinematic viscosity (40°C)	mm^2/s	11.7	12.9	12.9
Kinematic viscosity (100°C)	mm^2/s	3.3	3.9	3.4

movements were assessed for each lane, for low, high, and full speed range.

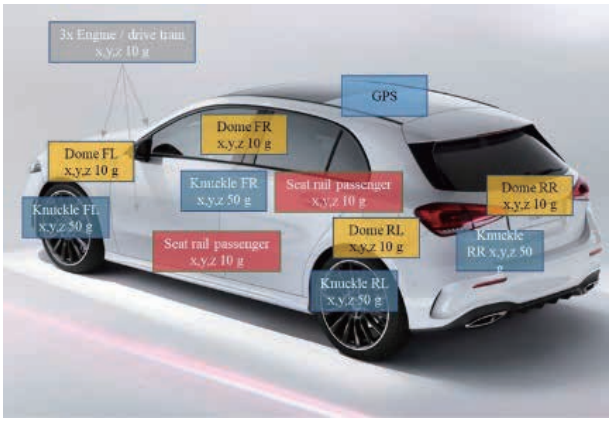

Fig. 17 Vehicle measurement setup

4.2 Objective assessment results

The results of the analysis are shown in Fig. 18-19. Compared the base configuration shown on the dotted line, the A/B 100% oil shown on the dashed line exhibits a smaller body acceleration in the low-frequency region of 1-2Hz on and larger body acceleration in medium-frequency region of 4-15Hz. The A/B 75% oil shown on the solid line exhibits a smaller body acceleration than the base configuration in both the low- and medium-frequency region.

In general, there is a trade-off to be made when using valves to control the hydraulic force. If the body vibration near sprung mass resonance frequency of 1-2Hz is reduced to emphasize safety, the body vibration of 4-15Hz increases. To emphasize ride comfort, the opposite approach is required [6]. The characteristics are contradictory, making it difficult to achieve both goals. These results show that by simply adjusting the friction responsiveness while keeping the characteristics of the damping force unchanged, it is possible to produce a difference in the vibration levels to achieve both ride comfort and handling. The effect of friction response on the body vibration in the region can be summarized as follows.

Compared to the base configuration, our A/B 100%, which has the highest responsiveness, changes the vibration in a way that emphasizes safety. The A/B 75% oil, which has an intermediate responsiveness between the A/B 100% and the base configuration, does not change the vibration of the 7-15Hz region, and yet decreases vibration in the 1-2Hz region. This oil can be said to improve the stability of the vehicle body without impairing the riding comfort. This improvement, which is generally difficult to achieve with hydraulic valves, appears to be the result of the oil's improved responsiveness, which reduces the acceleration zone in the very low speed range.

We investigated the effect of a SA equipped with this more responsive hydraulic oil on an actual vehicle, and we confirmed that it has a significant impact on handling and ride comfort performance.

Traditionally, when the hydraulic force is adjusted to improve the riding comfort, it is at the expense of safety (manoeuvrability and stability), and vice-versa. We were able to enhance both the riding comfort and safety performance by changing the hydraulic oil to adjust the damping force after the reversal of the direction of

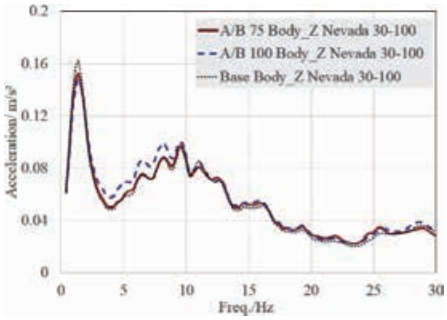

Fig. 18 Vertical Vehicle Body Acceleration for Nevada

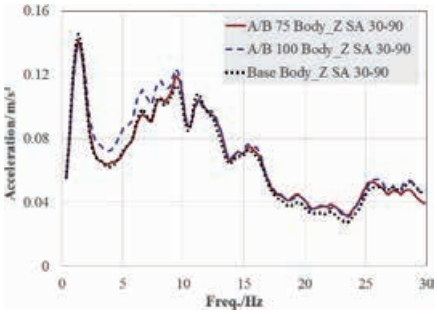

Fig. 19 Vertical Vehicle Body Acceleration for South Africa

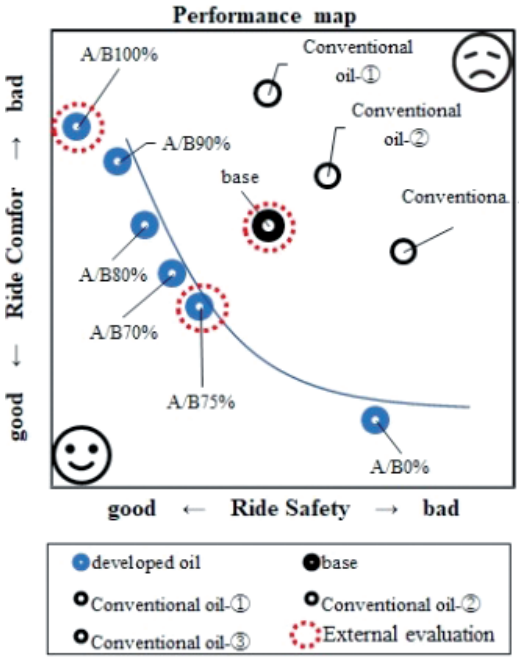

Fig. 20 Response adjustment hydraulic fluid performance

motion in a region where it has been difficult to achieve both goals. The results verified that this is an important technique for meeting the requirements for ride comfort and safety depending on the type of vehicle and the customer's preference.

4.3 Subjective assessment

The subjective evaluation of ride comfort and handling/safety was made on different roads and various conditions such as German motorway (with speed up to 180km/h), well-used roads, potholes, asphalt patches and state roads with conditions between brand new and well-used. Further the assessment was made on the test course containing comfort tracks, simulated state road, single obstacles, handling track, long straight.

As shown in Fig. 20, varying the responsiveness of the oil resulted in significant changes in ride comfort and safety. In addition, we confirmed that it is possible to modify characteristics such as "safety" and "comfort" depending on the purpose and taste of the vehicle.

The subjective assessment of our A/B 100% and A/B 75% oils compared to the base configuration was also commented by the test driver as if a valve setting such as the bypass or bleed area of the SA were modified. Driving the vehicle with the new oils changes the vehicle dynamics like it has a different positioning e.g. a sport type derivate, or a different manufacturer tuning philosophy.

5 Conclusion

1. When driving on good roads, SAs typically operates in a very-low-speed region between zero (where the direction of motion is reversed) and 30mm/s.
2. On good roads, the very-low-speed region of the SA has a greater effect on the friction force than the hydraulic force, which is very important role of the ride comfort and handling.
3. The conventional friction adjustment technique in a very-low-speed region of the SA, which involves varying the magnitude of friction, has drawback in that it negatively impacts the ride comfort.
4. The friction response was confirmed to be an important factor suitable for safety and ride comfort depending on the type of vehicle and customer preferences.
5. The mechanism of our results is considered from improvement in performance produced by compensating for the damping force that is generated by compressibility of the hydraulic oil in the acceleration zone part of the very-low-speed region in which the direction of motion is reversed.
6. Using the KYB developed oils can open a new dimension of creating variations and optimizing the vehicle drive feel. As the result, we developed a technique that adjusts only the friction response and confirmed that it can improve safety without compromising ride comfort.

6 Outlook

In this paper, we proposed a technique for improving the performance using ordinary conventional SAs, but we anticipate that this technique will improve performance even further if applied to a SA with the latest sated-of-the-art valve structure. In the future, in addition to pursuing the practical application of these results, we plan to further study on the relationship between the friction response and vehicle performance, and will continue to develop the potential of this approach as a new performance enhancement technique.

References

1) Ernst, Walter. "Oil hydraulic power and its industrial applications." (1960).
2) KAMAKURA, Ryosuke, et al. "Development of Externally-Mounted Shock Absorber with Adjustable Solenoid Damping Force." (2017).
3) Klinger, Florian, Johannes Edelmann, and Manfred Plöchl. "Characterization and potential analysis of passive and (semi-) active suspension systems by means of equivalent suspension parameters." 10th International Munich Chassis Symposium 2019. Springer Vieweg, Wiesbaden, (2020).
4) Dixon, John C. The shock absorber handbook. John Wiley & Sons, (2008).
5) Kato, Shinji, and Shinya Sasaki. "Effects of hydraulic oil and lubricant additives on dynamic friction properties under various reciprocating sliding conditions." Friction (2019).
6) Kaldas, Mina MS, et al. "Triple-control-mode for semi-active suspension system." SAE International Journal of Commercial Vehicles 8.2015-01-0621 (2015).

Author

Dr. Shinji Kato

Senior Manager Suspension
Engineering Headquarters,
KYB Corporation, 2548, Dota,
Kani-shi, Gifu 509-0298, Japan,
E-Mail: katou-shin@kyb.co.jp

Technology Introduction

Utilization of CAE for Model-Based Development

MITSUSHIMA Koji, NAGAMIZO Yoshiya

1 Introduction

Model-based design (MBD) is a method of developing an embedded software system that effectively uses model-based simulation to reduce development time and improve software quality. As MBD has recently been applied to wider fields including mechanical engineering (strength, vibration, motion, etc.), the term MBD is often used to refer to "on-the-desk" development using computer aided engineering (CAE) [1]. By taking the latter sense, this paper introduces MBD as methodology of efficiently promoting "on-the-desk" development. Industry has a long history of using CAE as a front-loading approach to address problems as early as in the upstream stage of product development. A publication [2] defines the term "design" as "to come up with an idea for a new product with a target quality, fabricate new elements of the product, and combine them to be an integral product," and further "to establish theoretical grounds of the design, prepare many alternatives and efficient assessment methods, and select the best option with active and human design reviews (DRs)."

In relation to "establish[ing] theoretical grounds of the design," easy-to-use physical modeling tools have emerged and been widely used with the dramatic advancement of CAE software technology. To "prepare many alternatives and efficient assessment methods," automation and rationalization of assessments are needed for the earlier selection of excellent ideas. Assessment automation will increase the time and frequency of thinking to come up with ideas while assessment rationalization will allow designers to have the mental capacity to notice a failure in advance [3].

Practicing these in the upstream stage of product development will help efficiently promote MBD in mechanical engineering. As one of the methodologies, the following sections describe the parametric CAE method using parameter design by introducing specific cases:

2 Parameter Design

2.1 Functionality Assessment

First of all, this section discusses how a technology works from the viewpoint of "establishing theoretical grounds of the design." The verb "works" can be replaced by "functions." For example, the function of a hydraulic pump is to input a driving force from outside and to discharge high-pressure oil at a high flow rate. For a mechanical product, the function can be generally represented by energy conversion. A hydraulic pump converts driving energy (revolving speed x torque) into hydraulic energy (discharge pressure x flow rate).

Once a product is shipped to market, it is used under a variety of conditions. A product free of problems at the time of shipment may experience failure or an abnormality when subjected to many different conditions including improper use by the user, adverse temperature/humidity conditions, and deterioration over time. Quality may be defined as stability of the function(s) of a product under various service conditions.

A reliability test for determining the quality of a product usually requires a long period of time. One of the approaches to complete such a reliability test in a short time is a functionality assessment. For a functionality assessment, functions of a target product are measured under the worst conditions reflecting possible various usages of the product in the market area, and then stability of the functions is assessed. As an index of stability assessment, the signal to noise (SN) ratio is used. The SN ratio refers to the ratio between the signal and noise originally used in information engineering and can be defined as "signal/noise." The signal represents the average of signals when subjected to two or more worst conditions, while the noise represents the standard deviation (variation). Using the common logarithm, the SN ratio can be expressed by:

SN ratio = 20 log (average / standard deviation) [db]

The antilogarithm is the inverse of the coefficient of variation.

As an example of a functionality assessment, Table 1 shows the results of an efficiency test on two types of hydraulic pumps A and B when subjected to two levels of

worst conditions: low and high temperatures. Both pumps have identical average performance, but the pump A, having a higher SN ratio, shows higher stability.

Table 1 Example of SN ratio calculation

Pump	Worst conditions		Average	Standard deviation	SN ratio [db]
	Low temp.	High temp.			
A	0.88	0.92	0.90	0.028	30.1
B	0.85	0.95	0.90	0.071	22.1

2.2 Parameter Design and Its Procedure

Next is discussion about "prepar[ing] many alternatives and efficient assessment methods." The parameter design is an approach to determine the design conditions with high stability by implementing a functionality assessment with variable combinations of multiple design parameters. In the example shown in Table 1, two levels of worst conditions have been set against two types of pumps, which means that four experimental runs in total need to be performed. In addition, a number of parameters should be discussed during product development. It is also recommended to apply as many worst conditions as possible with considerations given to actual usage in the market area. If the product were to be tested under all the combinations of conditions, a huge number of experimental runs would be needed. For this reason, the concept of parameter design was established as an approach to substantially reducing the number of experimental runs by applying the concept of experimental design. In parameter design, an orthogonal array is used to reduce the number of experimental runs. As an example, an L18 orthogonal array is shown in Fig. 1:

	Design parameter							
Column #	(1)	(2)	(3)	(4)	(5)	(6)	(7)	(8)
1	1	1	1	1	1	1	1	1
2	1	1	2	2	2	2	2	2
3	1	1	3	3	3	3	3	3
4	1	2	1	1	2	2	3	3
5	1	2	2	2	3	3	1	1
6	1	2	3	3	1	1	2	2
7	1	3	1	2	1	3	2	3
8	1	3	2	3	2	1	3	1
9	1	3	3	1	3	2	1	2
10	2	1	1	3	3	2	2	1
11	2	1	2	1	1	3	3	2
12	2	1	3	2	2	1	1	3
13	2	2	1	2	3	1	3	2
14	2	2	2	3	1	2	1	3
15	2	2	3	1	2	3	2	1
16	2	3	1	3	2	3	1	2
17	2	3	2	1	3	1	2	3
18	2	3	3	2	1	2	3	1

Experimental run #

Fig. 1 L18 (2^1 x 3^7) orthogonal array

In this orthogonal array, up to eight design parameters can be analyzed through 18 runs of testing with an arrangement of 1 factor at 2 levels and 7 factors at 3 levels. Besides the L18 orthogonal array, various orthogonal arrays including L36 and L54 can be used according to the number of design parameters to be analyzed.

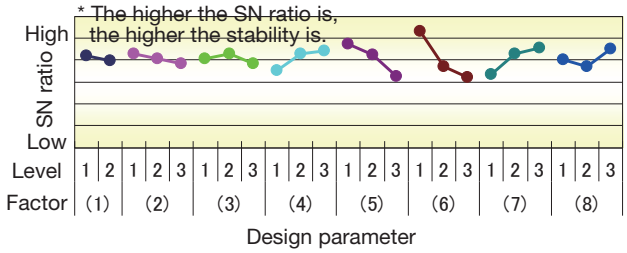

Fig. 2 Factorial effect diagram of SN ratio

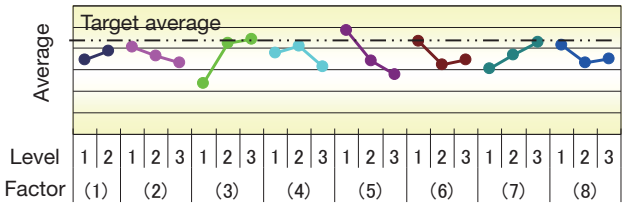

Fig. 3 Factorial effect diagram of average

Design parameters are assigned to an orthogonal array, and experimental runs are carried out under the worst conditions. As in the example of Table 1, the SN ratio of each row is calculated with an experimental run # in the array. The results are statistically processed and the factorial effect for each design parameter is calculated. The results are plotted as shown in Fig. 2. Similarly, the average is calculated and the results are plotted as shown in Fig. 3. From these two figures, a combination of design parameters that is high in stability (high SN ratio) and meets the average target (optimization) is selected.

Note that the optimal value selected from the factorial effect diagrams is the one that has been mathematically estimated from the test results of only some combinations in the orthogonal array. Therefore, it is important to carry out experimental runs by using actual combinations to verify the estimation accuracy. This is called a verification test. If there is no difference between estimation and verification, it can be determined that the testing has been properly done. If there is a difference between the two, it should be determined that the process to evaluate the stability of functionality has a problem. Many of the factors that lower the estimation accuracy involve interaction of output values among the design parameters. If interaction takes place, the output level of specific combinations may be affected, leading to difficulty in adjustment. Good design is based on the idea that individual design parameters reflecting the design concept each exert an effect independent of the output value.

Table 2 Eight steps of parameter design

(1) Select themes - Define the purpose and project scope
(2) Define the functions and create a calculation model
(3) Establish a worst condition strategy
(4) Set up design parameters and assign them to an orthogonal array
(5) Collect data by actual machine testing or CAE calculation
(6) Analyze data using SN ratio
(7) Carry out optimization, estimation, and conformation run
(8) Develop (and document) an action plan

Table 2 shows the parameter design procedure. For more information about the calculation for statistical processing, refer to the reference [4].

3 Examples of Application

Electromagnetic proportional pressure-reducing valves used in the hydraulic system of construction equipment use proportional solenoids. To develop inexpensive high-performance products meeting the market needs, it was necessary to reduce the design man-hours and prevent rework in the development phase. Accordingly, we applied the parameter design and parametric CAE methods to design a proportional solenoid with stabler attraction characteristics. This case is introduced in the following:

(1) Select themes - Define the purpose and project scope

The proportional solenoids are required to:

① have a flat stroke-attraction characteristic;

② have a proportional current-attraction characteristic; and

③ deliver these characteristics stably in actual applications.

Now determine the design conditions that satisfy these requirements at the same time.

(2) Define the functions and create a calculation model

(3) Establish a worst condition strategy

We have given a functional definition of the proportional solenoid as a device to generate an attraction force proportional to the current (Fig. 4).

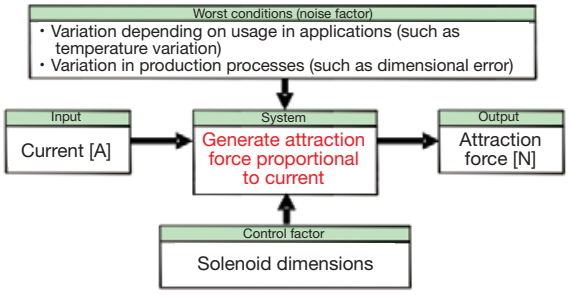

Fig. 4 System chart

For experimental testing, calculation with a CAE model shown in Fig. 5 is carried out. 44 dimensions of this model can be parametrically adjusted for calculation [5]. As a result of engineering discussion, 21 dimensions were selected as design parameters. Since it is not easy with the CAE model to consider product deterioration and wear

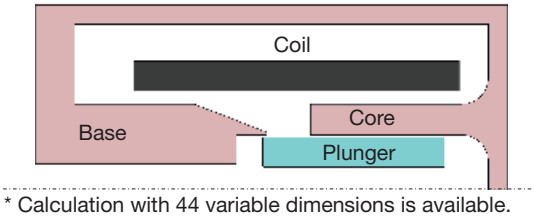

* Calculation with 44 variable dimensions is available.

Fig. 5 CAE magnetic field analysis model

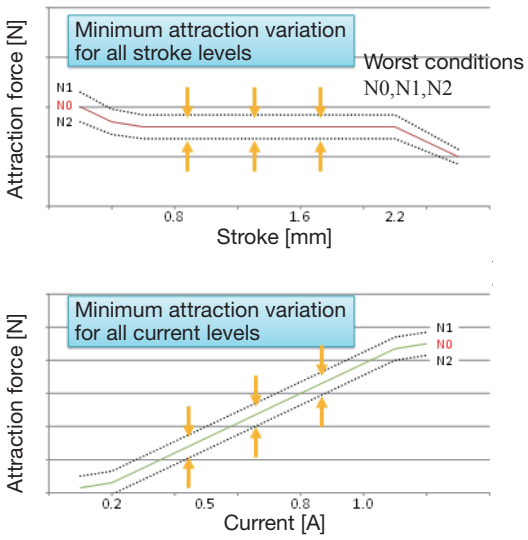

Fig. 6 Characteristics to be stable

during use in applications, the worst conditions have been set to the design parameter tolerance multiplied by a factor [6]. The concept of stabilization of characteristics is shown in Fig. 6.

(4) Set up design parameters and assign them to an orthogonal array

(5) Collect data by actual machine testing or CAE calculation

Since 21 design parameters have been selected, an L54 orthogonal array in which up to 26 factors can be assigned was used. Similarly, 21 worst conditions were assigned to the L54 orthogonal array. The calculation must be repeated for every combination of the design parameters and worst conditions. In total, 2,916 cases (54 x 54 = 2.916) were calculated.

(6) Analyze data using SN ratio

(7) Carry out optimization, estimation and verification test

Statistically process the calculation results and create a factorial effect diagram of each of the three items: SN ratio, magnitude of attraction force, and attraction stability against stroke (Fig. 7). For the design parameters on the horizontal axis, optimal values for three levels are selected so that:

① the attraction variation is small (high SN ratio);

② the magnitude of attraction force is high; and,

③ the attraction force is stable against stroke.

The SN ratio estimation for the optimal condition was 49.9 [db]. The estimation for the reference condition (the initial design condition often used), which had been established for the purpose of comparison, was 44.7 [db]. The difference between the two is 5.2 [db]. The SN ratio is defined by a logarithm and the difference represents the ratio of antilogarithm. 5.2 [db] is equivalent to an approximately 40% decrease in the coefficient of variation. Next, we conducted a verification test (calculation) using actual combinations for the optimal and reference conditions. The results are shown in Table 3:

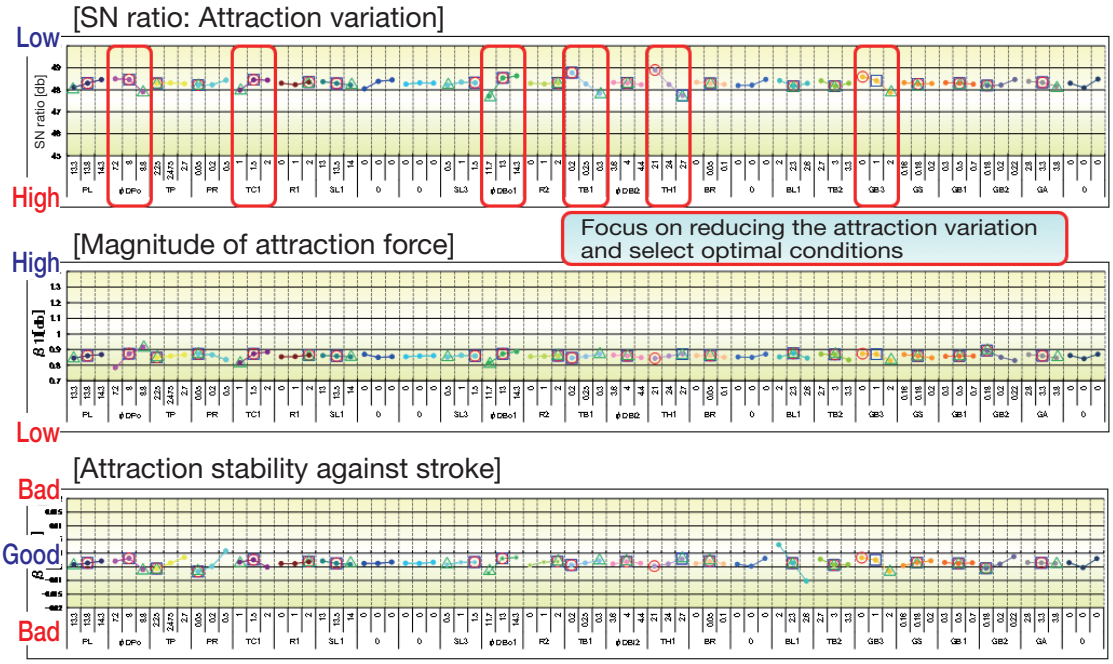

Fig. 7 Factorial effect diagram

Table 3 Results of verification test

SN ratio [db]		
Condition	Estimation	Verification
Optimal	49.9	48.4
Reference	44.7	45.0
Difference	5.2	3.4

The SN ratio estimation roughly matches the verified results. The difference in verified results between optimal and reference conditions is 3.4 [db], which is equivalent to an approximately 30 [%] decrease in performance variation. The variation reduction for different current levels applied is shown in Fig. 8. The difference between the estimation and verification implies that the selection of design parameters is susceptible to improvement, which remains as a future challenge.

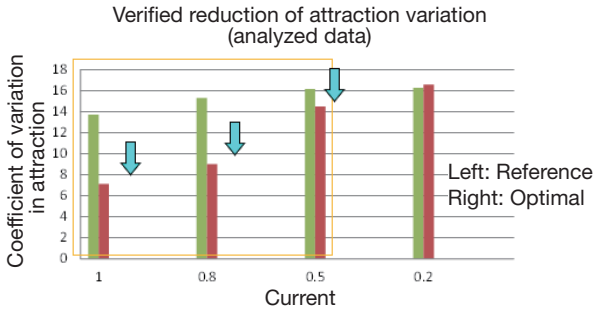

Fig. 8 Reduction of variation in attraction force for different current levels applied

(8) Develop (and document) an action plan

① We have developed a profile with which the performance variation can be reduced by about 30 [%] under the worst conditions in the assumed market.

② We have stablished a magnetic path design method to reduce the performance variation based on a technical analysis of the factorial effect diagram, although it cannot be disclosed because of the proprietary knowhow.

These results will be put into the form of design manuals and effectively used in routine design work.

4 In Closing

The use of parametric CAE using parameter design is effective in increasing the efficiency of MBD in the following points:

① The product functionality can be discussed for stabilization before a problem occurs in the upstream stage of product development.

② A number of design parameters can be adjusted to allow close reviews without making omissions.

③ A well-established procedure can be easily integrated into the development process. For example, the results can be reviewed according to a common method.

In addition, we believe that this approach, as a methodology of pursuing the essence of technologies and allow engineers to be imaginative, can be effectively used to develop young and middle-ranking engineers to be the next-generation of "Monozukuri" manufacturers.

References

1) FUJIKAWA Satoshi, Model Based Development in Mazda, Mazda Technical Review No. 31, pp.44-47 (2013)
2) KISHIMOTO Yukio, Design Method - Approach to Creative Design, Union of Japanese Scientists and Engineers (1988)
3) BABA, CAE Promotion of Analysis Oriented Design, KYB Technical Review No. 39 (2009)
4) TAGUCHI Shin, Data Analysis Method to Imagine Technical Information [Entry-Level Taguchi Method], Japanese Standards Association (2016)
5) MITSUSHIMA, Computer Aided Engineering (CAE) and Quality Engineering, KYB Technical Review No. 41 (2010)
6) SAWADA Ryusaku, Robust Design of Complex Systems - Quality Engineering and Model Based Development (MBD), The Journal of Robust Quality Engineering Society (RQES) Vol. 27, No. 6 (2019)

Author

MITSUSHIMA Koji

Joined the company in 1987.
Manager, DX Dept., Engineering Div.
Engaged in DX promotion after being engaged in CAE analysis and its internal development.

NAGAMIZO Yoshiya

Joined the company in 2012.
CAE Dept., Engineering Div.
Mainly engaged in CAE analysis.

Product Introduction

Development of Control Valve KVSX-12C for Small Size Excavators

FUKUSHIMA Ryo

1 Introduction

Two- to four-ton class small hydraulic excavators are used in many different places and applications including excavation and ground leveling for roadwork, as well as various jobs in building sites in towns. The demand for these excavators has recently expanded. The hydraulic systems for small excavators can be divided into an open-center system and a closed-center system (or load sensing system). The open-center system has a pump continuously discharging a given flow and operates an actuator while letting an adjustable flow drain into a tank using a bleed-off circuit. This system has been used from the early days of commercialization of small hydraulic excavators (Fig. 1).

The load-sensing system includes a variable displacement pump to which the hydraulic pressure is fed back to control the swash plate thereof, keeping the pressure difference over the meter-in orifice constant in accordance with the actuating variable. The system can be controlled only with the minimum required amount of oil (Fig. 2). As the pump is only required to discharge as much as needed, the load-sensing system involves less power loss compared to the open-center system.

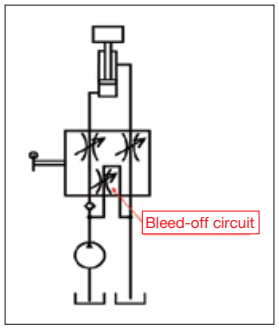

Fig. 1 Open-center system

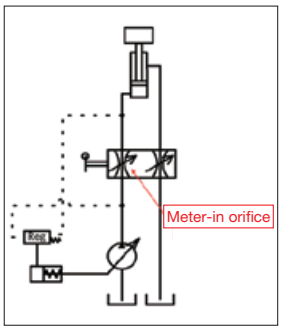

Fig. 2 Load-sensing system

KYB manufactures KVSX-12 Series control valves for load-sensing systems in small hydraulic excavators. In the KVSX-12 Series, Models A and B have been commercialized to this point. To further improve the functionality and performance, KYB has just developed and commercialized a third-generation KVSX-12C (hereinafter referred to as "the new model"). This paper introduces the new model; the appearance thereof is shown in Fig. 3.

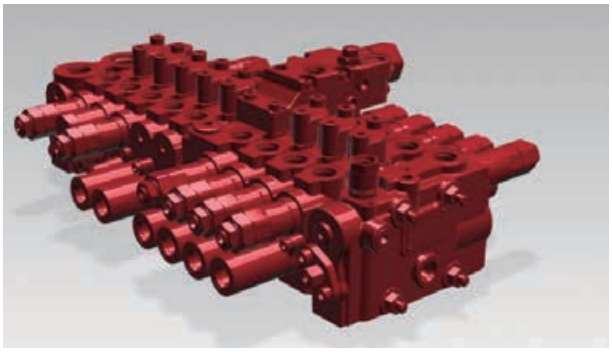

Fig. 3 Appearance of KVSX-12C valve

2 Development Challenges

The development of the new model involved the following challenges:

① Alleviating an operation speed reduction at high temperatures
② Improving fuel efficiency by reducing the pressure loss
③ Reducing the machining cost

In terms of challenge ①, KVSX-12B (hereinafter referred to as "the conventional model") involved a problem in which the operation speed was lower when the oil temperature was higher. For the new model, we have modified the valve structure to alleviate the speed reduction.

With regard to challenge ②, hydraulic excavators are generally required to improve fuel efficiency during actual use in order to achieve higher environmental performance. To reduce the pressure loss in the valve, we have changed the outside diameter of the compensator spool (hereinafter referred to as "the comp. spool") from ø12 (conventional) to ø14 (new).

Challenge ③ was a bottleneck in the valve housing machining process for the conventional model. The process included drawing (oblique machining) to provide the comp. spool with a damping effect. For the new model, we have designed a comp. spool consisting of another set of parts to ensure higher machineability without drawing, in order to reduce the machining cost.

3 Overview of New Model

3.1 Configuration

Fig. 4 shows a comparison of circuit diagrams between the conventional and new models. The new model has been improved in performance with respect to the conventional model in the following points (1) and (2):

(1) Improving warmup performance

The layout of the unload valve has been modified. The conventional model had the unload valve located in the inlet. For the new model, the unload valve has been relocated to the outlet so as to make up a circuit (heating circuit) where the oil supplied from the pump (P) port flows through all the sections and returns to the tank via the tank (T) port even during standby. This heating circuit helps the overall valve body increase in temperature to achieve higher warmup performance.

(2) Improving operability at low temperatures

The conventional model has no LS drain orifice because the model is designed so that the LS passage included in the circuit diagram of Fig. 4 is linked with the tank via the main spool when the spool is in the neutral position. The new model in turn is provided with an LS drain to keep the LS passage constantly connected to the tank (drain orifice type). This new design contributes to higher warmup performance of the LS passage and is particularly unlikely to cause hunting at low temperatures, resulting in higher operability.

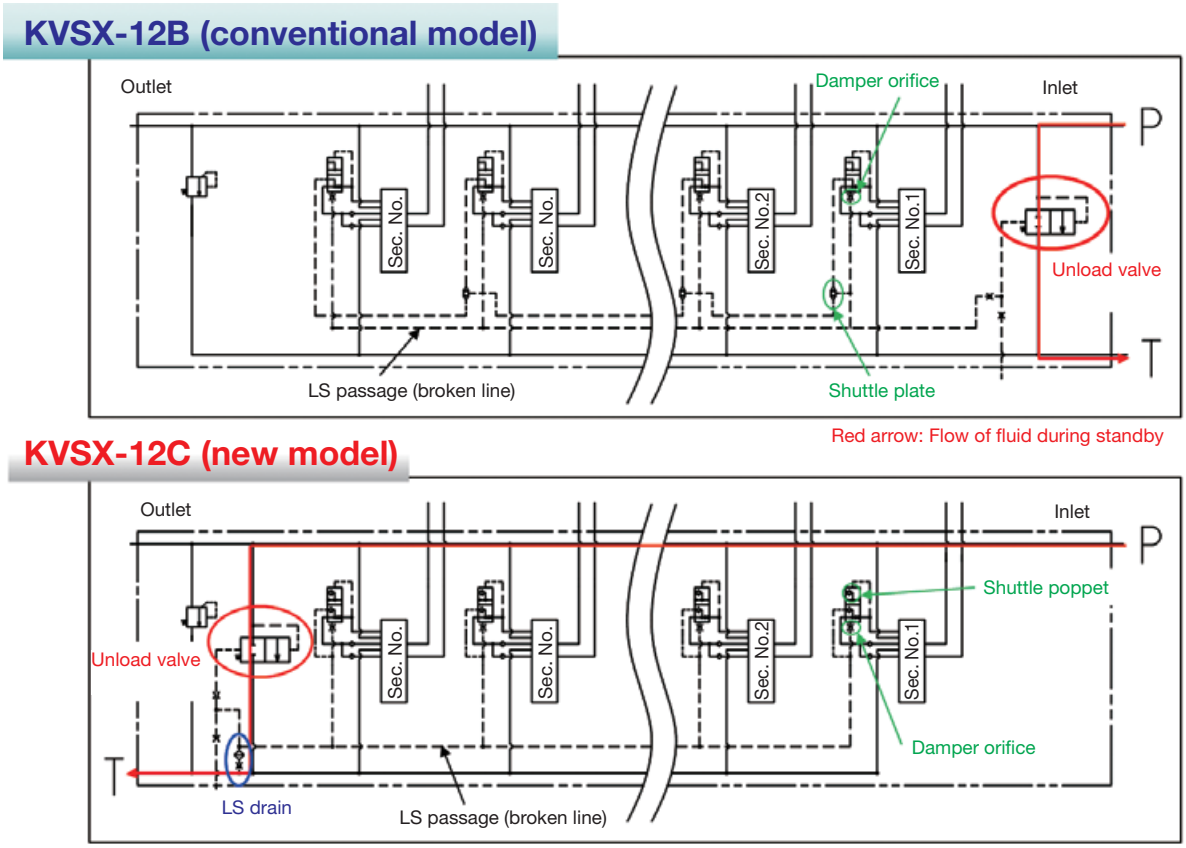

Fig. 4 Circuit comparison

3.2 Alleviating Operation Speed Reduction at High Temperatures

In the conventional model, the high-pressure selection of the LS passage was implemented by a shuttle plate structure (a metal seal system) between the mating surfaces of the valve housing. The LS passage itself also has a metal seal structure between its mating surfaces (Fig. 5). Thus, the likelihood of the valve having internal LS pressure leakage depends on the workmanship related to flatness and surface roughness of the seal sections of the shuttle plate and valve housing. With this structure, the LS pressure leakage would be larger at a higher oil temperature and lower oil viscosity. As the LS pressure decreases due to the leakage, the pressure feedback to the pump decreases. With the lower pressure, the pump discharge decreases, that is, the control flow supplied to the actuator

decreases, because of the characteristics of the load sensing system, which always tries to keep the pressure difference constant. This results in the issue of the operation speed being lower.

The new model has been modified so that the high-pressure selection is implemented by a shuttle poppet structure in the comp. spool, leading to higher seating performance and less leakage. The mating surfaces of the LS passage now use O-ring seals. This sealing system ensures a leak-free structure independent of the workmanship related to flatness and surface roughness (Fig. 6). Thus, the higher seating performance and the modified sealing structure of the mating surfaces have successfully reduced the leakage from the LS passage. The control flow reduction due to an increase in oil temperature has also been improved from approximately 6.8% for the conventional model to approximately 1.5% for the new model.

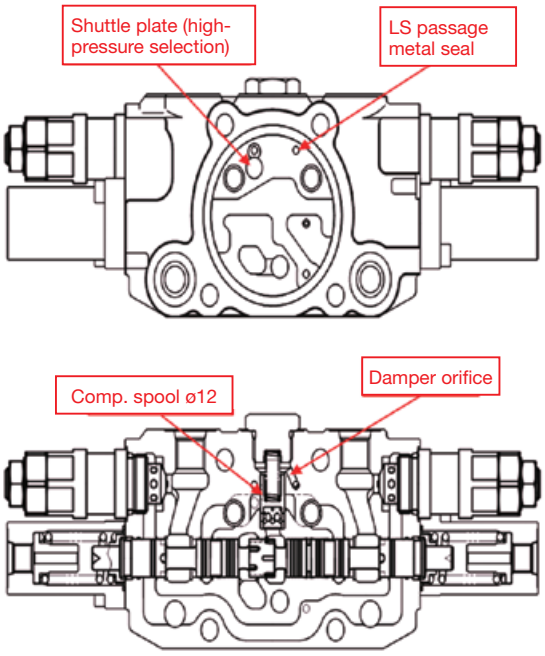

Fig. 5 Section structure of conventional model

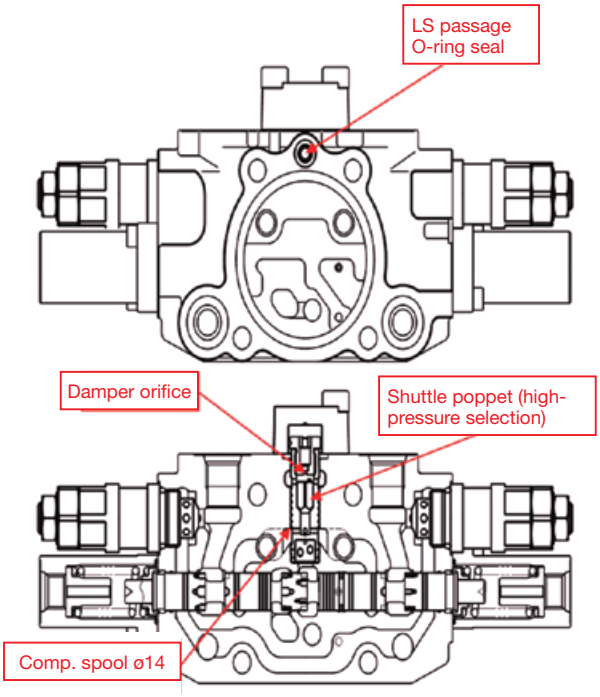

Fig. 6 Section structure of new model

3.3 Reducing Pressure Losses

As shown in Figs. 5 and 6, the conventional model had the comp. spool of an outside diameter (OD) of ø12, which has been enlarged to ø14 for the new model. This OD enlargement is intended to increase the maximum opening area to reduce the pressure loss.

When supplying oil to the actuator at 50 L/min, the conventional model caused a pressure loss of approx. 0.27 MPa during passage through the comp. spool. The new model has the larger opening area to have a pressure loss of approx. 0.16 MPa, which is approx. 0.1 MPa lower than the conventional case.

Since the load sensing system controls the pump discharge to keep the LS control pressure difference constant, the above-described pressure loss reduction enables increasing the operation speed with a control pressure difference similar to that for the conventional model. It is also possible to diminish the LS control pressure difference by the same amount as the decrease in the pressure loss, resulting in energy saving.

In fact, it was feared that the enlarged comp. spool of the new model would require the valve housing to be wider. However, we have optimized the geometry through stress analysis as a front-loading approach, successfully meeting the quality objectives with a valve housing which is the same size as the conventional one (Fig. 7). This means that the new model can offer improved performance while maintaining the same ease of vehicle mounting as the conventional.

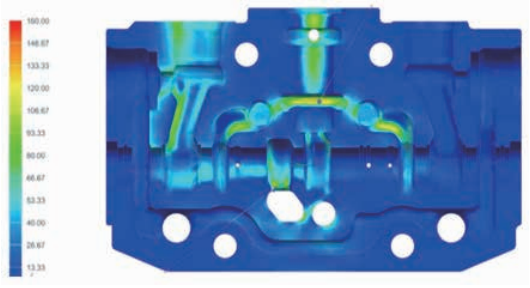

Fig. 7 Results of stress analysis

3.4 Reducing Machining Cost

In the conventional model, the valve housing was obliquely drilled to have an orifice so that the comp. spool would have a damping effect (Fig. 5). For oblique drilling, the machining process needed to be changed, which was

one of the factors in the high machining cost. It is also necessary to change the drill hole diameter according to the required size of the orifice. Thus, a valve housing had to be specified for each specification of the orifice.

The new model has eliminated the oblique drilling by assembling a plug already provided with the orifice into the comp. spool, thereby reducing the machining cost (Fig. 6). Since the orifice is allocated to the plug, it is no longer necessary to specify the valve housing for each specification of the orifice size, making it possible to standardize the machining process. Note that while the above-described shuttle plate structure required machining of the valve housing to create a pocket into which the shuttle plate would be inserted, the shuttle poppet structure introduced for the new model can eliminate the machining, leading to lower machining cost.

4 In closing

This paper has provided an overview of the control valve developed for the load sensing system for two- to four-ton class small hydraulic excavators. In addition to the required functions, the issues with the conventional model have been tackled.

The load-sensing system can be readily adapted to support electronic control for atomization and is expected to be increasingly demanded by the market. The market demand is always changing. By anticipating the market need without falling behind the changes, we would like to continue making efforts to develop competitive products.

Finally, I would like to deeply thank all those from the related departments for their support in developing the product.

Author

FUKUSHIMA Ryo

Joined the company in 2011.
HC Design Sect., Design Dept.,
KYB-YS Corporation
Taken present post after working in
Valve Design Sect., Ueda-Yuki
Engineering Dept., Engineering
Headquarters, Hydraulic
Components Operations.
Engaged in design of control valves.

Introduction

20th Anniversary of KYB Brazil Production Base Establishment in Brazil

YOSHINAKA Hiromi

1 Introduction

KYB has production plants in 24 locations in the world. Among those, the southmost one farthest away from Japan is KYB Manufacturing do Brazil Fabricante de Autopecas S.A. (hereinafter "KMB").

KMB manufactures shock absorbers (hereinafter "SAs") for automobile manufacturers or the after-sales market. As a dominant site in the South American market, which is expected to grow, KMB carries out production activities on a daily basis.

In 2020, KMB celebrated the 20th anniversary of its foundation. Now I would like to briefly look back at the history of KMB and introduce what I experienced there when I was an expatriate employee working for the company.

2 History of KMB

2.1 Foundation

The forerunner of KMB originated in 2000. KYB invested together with ArvinMeritor (hereinafter "Arvin") (investment stake: 75% by Arvin and 25% by KYB), with which KYB formed a technical alliance in Europe, to establish Arvin-Kayaba do Brazil, which started its production in 2002.

The company was located in an industrial park in a town called Fazenda Rio Grande, Parana State, Southern Brazil. The town is adjacent to Curitiba, the capital of Parana State, and is separated from Sao Paulo and Rio de Janeiro, both of which are famous cities in Brazil, by about one-hour of flight (Fig. 1).

Renault, one of our customers at the time, was located in a neighboring town, about 30 minutes by car.

2.2 KYB Wholly-owned Subsidiary - Joint Venture with Mando in South Korea

After Arvin pulled out of the business in 2004, Arvin-Kayaba do Brazil became a wholly-owned subsidiary of KYB named KAYABA Manufacturing do Brazil (hereinafter "KMBR").

KMBR obtained the ISO 14001 certification and began to manufacture OEM products for Renault as well as for the Japanese manufacturer Toyota. The company thus increased its production successfully.

With an eye toward the further expansion of production in the South American market, KMBR conducted investment together with Mando Corporation in South Korea (hereinafter "Mando") to establish the joint venture (JV) KYB-Mando do Brazil Fabricante de Autopecas S.A. (hereinafter the "former KMB") in 2011.

Fig. 1 Location of KMB (Source: Google Map)

2.3 Cancellation of Joint Venture

After foundation, the former KMB increased production for more and more customers including the Japanese-controlled manufacturer Honda Automobile Do Brazil (hereinafter "HAB"), but had frequent quality problems. The former KMB was in difficult position with its current account due to excessively low sales prices for the production cost.

It was also difficult for the former KMB to do business together and share information with its competitor Mando. The joint venture hardly produced the effect the two parties had intended.

In June 2018, the former KMB canceled the joint venture with Mando, thereby establishing KYB's wholly-owned KMB. I fortunately witnessed the moment when KMB started life. On that day, a signing ceremony was held in the room of a hotel, after which I went to the KMB plant. From the signboard bearing the words "KYB-MANDO" mounted on the front building, only the letters "MANDO" were removed. A trace of the letters "MANDO" was clearly left there (Photo 1), which made

me feel that the roughly seven years of our joint venture was not a short time. I remember that I toughened my resolve to reestablish a new company, making a comeback soon as a KYB site.

At the entrance of the plant, a signboard reading "SOMOS TODOS KYB" ("we are all members of KYB") is posted, representing the expectation and hope of all employees of KMB (Photo 2).

Photo 1 Front building with a clear trace of the signboard letters “MANDO”

Photo 2 “SOMOS TODOS KYB” signboard at the plant entrance

2.4 From the 20th Anniversary to the Present

It was November 2018 when I was transferred to KMB. I was mainly engaged in addressing problems particularly related to product quality, promoting improvement, and giving guidance to local staff. Many different problems had accumulated at the beginning, but the quality problems were gradually resolved thanks to support from SA Dept., KYB Gifu North Plant, as well as efforts by the local staff.

With a new order for Toyota Corolla and particularly thanks to the world's first HRS for Toyota [Note 1)], all staff members of KMB managed to start mass production while individually tackling problems, which were small in themselves but quite troublesome. We celebrated the initial shipment, took celebration photos of all those concerned, and shared the happiness with each other (Photo 3). During the period from June to August 2020, for the first time, we marked the achievement of "zero" complaints against the production line for three consecutive months. I was really moved by the celebration participated in all KMB members at that time.

Photo 3 Those concerned gathered for initial shipment for Corolla

In September 2020, KMB finally celebrated the 20th anniversary of its foundation while promoted a structural reconstruction including a painful large-scale layoff carried out in order for the company to survive.

Note 1) HRS stands for Hydraulic Rebound Stop.

Photo 4 Cake and sweets distributed to all employees

Photo 5 Souvenirs distributed to all employees

Unfortunately, Brazil suffered the serious coronavirus pandemic at that time. KMB could not hold a big party with all employees present, but instead distributed cake, sweets, and souvenirs to everyone so that they could celebrate individually in their homes (Photos 4 and 5).

The current number of employees is about one-half that in June 2018, when the company became a wholly-owned subsidiary of KYB.

Still, I expect the small but highly skilled team of staff to make a concerted effort with the aim of achieving No.1 quality among KYB overseas sites and stable management. I believe they can do it.

3 How I Lived in Brazil as an Expatriate Employee

What comes to your mind when you hear the word Brazil? I think everyone knows about the country Brazil, but few people have actually been there.

It usually takes two days to travel from Japan to Sao Paulo and three days to return, partly because you have to cross the international date line. Since the flight time alone is as long as about 24 hours, you may be rather tired just from traveling.

Now I would like to write what I noticed or was surprised by during my stay in Brazil.

3.1 Daily Life

Most aspects of daily life in Brazil, including food, housing and clothes, are not so different from those in Japan. Basically, however, imported goods are so expensive that I did not feel I could freely buy them.

Clothes: Although it may be difficult for you to find many clothes from Japanese manufacturers, shirts and other clothing from Japanese sportswear manufacturers are generally sold in shopping centers. Shoes from popular brands are also available.

Housing: As with most people overseas, Brazilians generally walk through all rooms in their house with their shoes on. What is interesting is that each room or public space has a facility for churrasco (Brazilian barbeque). Anyway, Brazilians love churrasco. Basically, any kind of event always appears to take place along with a churrasco party.

Food: Curitiba, which is located in Southern Brazil, has many immigrants from Europe. There are a lot of Italian and French restaurants as well as Brazilian local Feijoada restaurants (stew with beans and pork). You have a lot of choices.

The culture of Japanese immigrants has taken root in Brazil. A variety of Japanese restaurants can be found, including ramen, Japanese curry rice and sushi. Even Japanese-style taverns (izakaya) exist. I went there often, particularly on weekends, with Japanese businesspersons traveling to Brazil to eat Japanese food such as grilled chicken (yakitori) (Photo 6).

I also cooked for myself. I often cooked Uruguay rice,

Photo 6 Entrance of izakaya in Curitiba

Photo 7 Major Japanese 100-yen shop in shopping mall

which is almost the same as Japanese rice, and stewed Chinese cabbage and fish sausage (Hampen), which are available in supermarkets, to make a Japanese-style stew. Japanese food is available although it is quite expensive. Thus, I seldom felt difficulty with food.

Furthermore, a major Japanese 100-yen shop company recently opened a store in Curitiba. It helped me a lot as commodities made in Japan is readily available, although the goods available are about three to four times more expensive than they are in Japan (Photo 7).

3.2 Communication with Brazilian People

I have an impression of Brazilians that many of them are serious people. They do work seriously once they are convinced of doing so. If they do not get something right, they ask me many times until they can understand it. This is probably because they have boundless curiosity.

Greetings are even more important behavior for them

than for the Japanese. I always greeted and shook hands with local staff when I reported to work. I feel that these forms of communication were an essential item for us to carry out work smoothly.

Brazilian people give high priority to family in any event. On Christmas Day and other events, not only their children but also their parents and grandparents come together to throw a party.

Their typical personality is friendliness. Even when they meet each other for the first time, they will enjoy conversations over a drink just in half an hour.

Brazilians respect Japan and the Japanese. They seem to have learned that Japanese ancestors immigrated to Brazil and developed the land. Curitiba is a town with the third largest population of Japanese-Brazilians in the country after Sao Paulo and Rio de Janeiro. In the vicinity of my condominium there is a park named PLAZA do JAPON where even a three-storied pagoda and a Japanese garden have been built (Photo 8).

Photo 8 Appearance of PLAZA do JAPON (Japanese garden)

4 In Closing

As of January 2021, Brazil, amid the novel coronavirus pandemic, has the world's highest number of patients infected with the coronavirus after the U.S. and India. Nobody can deny that the country's future economic activity is uncertain.

Still, Commercial de Autopecas KYB do Brazil Ltda (KBR), which is one of the major sites in Brazil to sell commercially available products, enjoys successfully increasing sales. I believe Brazil remains a potential market.

I expect KMB to continue growing and I believe the company will absolutely achieve it when I see the KMB staff very positive and avid.

Finally, I would like to thank those concerned from KYB in Japan, KYB expatriate employees in Brazil, and all KMB staff members for their cordial support to me during my expatriate period.

Author

YOSHINAKA Hiromi

Joined the company in 2009.
SA Quality Assurance Dept., Gifu North Plant, Automotive Components Operations.
Taken present post in March 2020 after working for KMB as an expatriate since November 2018.

Essay

Report on Residence in Wuxi, China

KITAMURA Yasuhiro

1. Introduction

Wuxi KYB Top Absorber Co., Ltd (hereinafter referred to as “KWT”), one of the KYB Group’s production bases in China, is located in Wuxi, Jiangsu Province, China, and mainly manufactures suspensions for motorcycles. I was stationed at KWT for three years and eight months from April 2016 as a technical manager. In this essay, I would like to describe about my efforts to achieve both product development and sales promotion there.

This was the first time for me to be stationed abroad since I was engaged in the development of suspensions for motorcycles, and it has been a very valuable and unparalleled experience for me as an engineer. I hope this essay can provide useful information to young engineers who will open the door to the world.

2. Wuxi Information

Wuxi City is located approx. 130 km northwest of Shanghai, and it takes about 1.5 to 2 hours by car from Shanghai Hongqiao Airport by expressway. The most convenient way to get to Wuxi from Shanghai by train is to take the high-speed train from Shanghai Railway Station or Shanghai Hongqiao Station, which takes about 50 minutes . An express bus service is available to Wuxi from the long-distance bus terminal near the station.I never felt inconvenience in traveling between these cities. When you take a flight from an airport in Japan in the morning, you can arrive at KWT in the afternoon on the same day. The location of KWT is excellent for expatriates.

Wuxi City has an area of 4,788 km^2 and is the "city of water," with abundant lakes and canals. The Grand Canal, which was initially constructed during the Sui dynasty, runs through the city even today and ships sail gracefully in the canal.

The total population of the city has exceeded six million, which can be compared in scale to a Japanese prefecture with a government ordinance-designated city. Wuxi is also famous for its industry. Many Japan-based companies have built manufacturing plants mainly in the Development Zone with a lot of Japanese expatriates, although I have heard that there has been a trend toward lower number of such expatriates.

The downtown is lined with high-rise buildings and condominiums, forming an urban landscape. People walking in the city were so energetic at that time, making me strongly feel the economic growth of China.

In addition to Standard Chinese or Mandarin, the local people speak Wuxi dialect when they talk with each other. Wuxi dialect may sound quite aggressive to Japanese people. In my early days working as an expatriate in Wuxi, I was astonished by how they were talking every time I heard them, and I thought they were quarreling. Sooner or later I no longer cared about how they talked, saying, "Oh, it has just started again." That might be the time I got used to life in Wuxi.

Another famous topic concerning Wuxi is that it is the home town of "Wu," one of the famous ancient Three Kingdoms in China described in the Romance of the Three Kingdoms. Wuxi had flourished as a tin-producing area in the ages of "Yin" and "Zhou" before Christ. Ancient people aggressively dug out tin for bronze ware until it ran dry. That's why the city was called Wuxi (literally meaning "no tin" in Chinese). The city's famous souvenirs include earthy dolls called "Wuxi clay dolls." Local farmers used to knead mud to create dolls and dry them in a fireplace or sun-cure them before painting. They exchanged the dolls for food to survive. This type of doll can be found everywhere in China, but the Wuxi clay

Photo 1 Wuxi clay dolls

dolls have a history of over 400 years. It is now customary to give Wuxi clay dolls as a souvenir to expatriates who are returning to Japan.

3. Life in Wuxi

A typical Wuxi food I remember is Wuxi spare ribs. These stewed sweet pork ribs, similar to Japanese braised pork belly (kakuni pork), and was my favourite. Another famous Wuxi dish is silver fish (very similar to Japanese icefish) from Taihu Lake. Which is generally sweetly seasoned and therefore suitable for Japanese people who do not like spicy Chinese food.

In China, eating crayfish with a glass of beer with a group of friends in the heat of summer is a regular event. At first, I was hesitant to eat crayfish, but once I took a bite, I could not stop. We would quickly devour a heap of crayfish. The experienced local people can delicately pick meat from the head and claws, but this may be a little bit difficult for the Japanese to master.

In the cold winter months, hot pot is a must. They pour a special soup in a big pot and throw a variety of ingredients into the pot. After simmering for a couple of minutes, they eat it with a dipping sauce and their favorite topping. The soup includes a good amount of spices and tastes very hot. I frequently had a bad stomachache next day, but I found the hot pot really delicious when I familiarized myself with the taste. I've heard that the number of hot pot restaurants is increasing in Japan these days. I'd like to go there if I have the chance.

Photo 2 Crayfish dish

The famous liquor in Wuxi is baijiu. Baijiu is an original Chinese white liquor mainly made from grains such as corn, potato, or rice. This strong liquor, having about 50% alcohol, has a unique flavor that goes well with heavy Chinese food and I really liked it, although it might not be good to pair with Japanese food. If you have glasses of baijiu one after another while getting carried away with dancing songs for drinking, you may black out, ending in a difficult situation. It might be better for you to be cautious about baijiu when you try it for the first time.

Talking about food is endless, so I would like to move on to housing. My house was located in a suburban district a little bit away from the Wuxi downtown. Many Japanese lived in and around the district. I enjoyed a good environment: it was safe to live in and a supermarket nearby sold food imported from Japan. There is a restaurant mall called "guang chang" (literally meaning "town square" in Chinese) just a 20-minute walk from my house. I could drop by there after work to have dinner and a drink, and I think it was a blessed environment for a foreign resident businessmen. For your information, the restaurant mall has a "deep" atmosphere where the Japanese might get the feeling of the Showa era, and is very popular to Japanese expatriates in KWT. The mall is very large in scale and might be the area where the highest number of Japanese restaurants are densely packed in China. The mall was also a peaceful place for me because I felt as if I was in Japan and relaxed when I came into the area at times when work wasn't going well. I would like to thank all those who took care of me in the area.

Speaking about transportation in the city, I usually used taxis or local buses at that time. Local buses can take you almost everywhere you want to go if you are familiar with

Photo 3 Chinese Hot Pot

Photo 4 Restaurant mall

them, but they may be better used by experienced people because of the complexity of the route map and bus numbering. I recommend those who visit the city for the first time to use a taxi. With a base charge of 10 yuan (equivalent to about 150 Japanese yen) fare at that time, a taxi will take you anywhere you want simply by using body language to show tell the driver where you want to go. Recently smartphone-based taxi booking apps have started to be popularly used there. You may need to have a good command of using such apps.

Electronic banking systems using social network systems (SNSs) had already become popular. Even street vendors post QR codes on their front, and a mobile phone is all that is needed for everyday life. That way of life was so convenient to me as well, but I quickly returned to the way of life carrying a wallet and a coin case since I came back to Japan.

In springtime, Wuxi City is adorned with marvelous cherry blossoms . The locals say that it is one of the three most famous cherry blossom viewing spots in the world, but strangely no one can tell you where the other two were. What is different from the Japanese-style viewing of the cherry blossoms is the wonderful nighttime cherry blossoms lit up with illumination. It was a very Chinese presentation. Japanese may have the impression it is somewhat over the top, but it was really fantastic and remarkable to actually see the lit-up cherry blossoms at night. Please visit and give it a try if you have an opportunity.

Photo 5 Night cherry blossoms in Wuxi

4. Motorcycles in China

When hearing the word China, the first to come to mind for Japanese people may typically be the numerous bicycles flooding streets in Beijing. This is not the case nowadays. In the coastal regions of China, motorcycle riding is prohibited in order to comply with environmental control regulations.Electric scooters have instead become popular as a means of transport for citizens, flooding the roads. A variety of electric scooters from various manufacturers are available, ranging from those of a maximum speed of around 40 km/h to high-performance vehicles with a maximum speed of not less than 80 km/h. Reasonable models are sold in supermarkets at about 2,000 yuan (about 30 thousand Japanese yen) just like home appliances. In my early days of working as an expatriate in Wuxi, I felt my blood freeze so often electric scooters approaching from behind without making a sound. Partly due to instructions from the government, traffic laws for wearing helmets have been improved and the awareness of users has risen.

On the other hand, electric scooters, which have lower power, are actually close to useless in heavily contoured inland areas. People living in such an area still use engine type motorcycles. I rarely found large motorcycles: to illustrate how small they were, the largest model I found was 250 cc. However, the demand for large motorcycles has recently risen. Various motorcycle manufacturers, from leading manufacturers to emerging ones, exhibit their large motorcycles and accessories in domestic motor shows, grabbing the eyes of user visitors.

Emerging motorcycle manufacturers aimed at this market had sprung up in various parts of China, and a very active and attractive market was beginning to be formed. Since these domestic large motorcycles used suspensions imported from European suspension manufacturers at that time, the domestic motorcycle manufacturers really wanted suspensions for large motorcycles to be produced in China.

The stage for KWT to address the market had been almost set.

Photo 6 Chongqing Motor Show

5. Product Development in China

Among the motorcycle suspension components, KWT manufactures two components: the front fork (FF) to be mounted on the front wheels and the rear cushion unit (RCU) to be mounted on the rear wheels. Particularly, FF is a critical functional component that must have the required strength and rigidity as part of the bodywork: it

needs to absorb shock from the road surface for improved ride comfort, to grasp the front wheels securely so as to transmit the steering input to the front wheels, and to serve as a bumper to absorb impact during collision. Therefore, the development of FF needs to be promoted simultaneously with the development of bodywork. Thus, KWT promotes product development under mutual deep relationships with vehicle manufacturers.

In Japan, roles of vehicle manufacturers and suspension component manufacturers including KYB have been defined over many years of development, and the tasks to be carried out by both parties are clearly defined. Among such tasks, suspension tuning to ultimately achieve ride comfort and handling stability is difficult to decide only by Engineering. Rather, test riders from vehicle manufactures carry out sensory evaluation through actual riding and the results are converted into technical terms such as damping force and sliding property, which are then fed back to Engineering and Manufacturing again for optimization.

A major challenge for KWT Engineering, was how to proceed with the promotion of this series of development tasks with Chinese vehicle.

First of all, it was necessary to propose suspensions of appropriate size and materials in accordance with the bodywork strength requirements. It was relatively easy for us to translate these aspects into proper specifications based on the experience and standards of the both parties.

One problem that occasionally arose was the requirement for surface treatment. In the initial stage, we often failed to determine the proper requirements for color tones, weatherproofing, and corrosion resistance due to insufficient discussions or adjustments. However, once we had an accurate understanding of the customer’s requirements, we were able to propose appropriate specifications based on the experience and know-how of the KYB Group without specific problems.

What we had difficulty with was how we should tune handling stability and ride comfort. Since motorcycles other than electric scooters were not permitted to be driven on the public roads in Wuxi to begin with, KWT Engineering staff, who had not driven a geared large motorcycle before, to translate what the test riders communicated about how they had felt regarding faulty conditions of the target motorcycle into technical terms. As a result, they had no idea which direction they should take the vehicle properties and had difficulty making a proper decision. The test riders were certainly able to determine which vehicle they preferred better when they drove two vehicles for relative evaluation. However, it seemed very hard for them to determine to what extent they should specify related properties in many cases since they did not often have an absolute evaluation standard.

That was where I, as an expatriate employee who had experienced that kind of thing in Japan, came in, but I could not properly grasp what the test riders from customers exactly demanded during the initial stage. In spite of repetitive comments given, I had a hard time, as I was unable to propose improved specifications that could convince the riders. Language barriers certainly existed, but those were not the main reason. When looking back, we had failed to establish a common framework or procedure for what we should do under what kind of circumstances, which resulted in indiscriminately increasing test samples and man-hours. This is what I have realized now.

To overcome these problems, I held an internal workshop with Engineering staff on the correlation between the feeling of test riders during test runs and the suspension physics. I provided an opportunity for the staff to actually ride a motorcycle in a vacant space in the company site to feel, though in a quite simple way, the vehicle's behavior in response to the rider's control. These test rides were just at the entry-level, but common grounds for basic understanding were established in my opinion.

These grounds should have been documented to develop a systematic procedure. However, customers would not wait for us. So we unavoidably started improving empirical values in actual orders from customers. We all discussed the direction of improvement every time an incident occurred and added the results to the proposed specifications.

Partly due to these efforts, we reached a mature level of tuning where we could tune the related properties to some extent according to comments from customer's test riders. Still, this was insufficient. We ultimately failed to attain perfect customer satisfaction. Customers also seemed to be hardly able to determine how far they should specify properties as actual vehicle evaluation proceeded, and were once again at a loss regarding what to do. Accordingly, I consulted a senior employee to receive advice on what we should do in order to progress to the next stage. After wondering, I finally decided to take on a challenge. That was to invite test riders from Japan and ask them to ride vehicles together with Chinese customers so as to derive challenges and resolve problems. Thus, we decided to carry out so-called "a joint test" in China.

6. Joint Test in China

The idea was great. But it cannot be realized without obtaining the understanding and cooperation of all those concerned, of course.

First, I prepared proposals to clarify the necessity of a joint test and the effects expected to be brought about by the test (higher evaluation level, its appeal, and receiving new orders). With the proposals, I passionately persuaded management with enthusiasm and finally obtained the approval of top management.

Then, I requestd KYB Motorcycle Suspension (KMS) in Japan to send test riders to China. I sincerely appreciate

that the KMS staff expressed a willingness to accept the proposal in spite of their busy work schedules.

Second, we made a presentation to customers. This was where KWT Sales Department was to make the most of its strengths. The staff members rushed to customers in unison to explain their proposals and then successfully obtained their approval. I really appreciate that the customers positively accepted the proposals.

Once the stage was set, we got down to work for specific preparations. A detailed two-week plan was drawn up to ensure the safe and efficient implementation of the joint test, which would cover a total distance of 2,000 km, visiting customer sites in the coastal East China and the inland Chongqing region. Over 20 staff members were involved in this program. To establish a common conceptual image of purpose and results, they discussed details many times to finalize the program.

Two test riders were invited from KMS in Japan. Safety first was the top priority to begin with. In order to ensure the safety of the riders in the event of a fall, the same safety equipment as in Japan was used, and the itinerary was adjusted to allow for adequate rest.

For safety purposes, an auto race circuit was rented for exclusive use to test vehicles in each region, ensuring an environment for closed testing.

As a preparation to sample disassembly or specification changes on site, we rented a full-size trailer equipped with a damping force testing machine from KYB Group in Zhenjiang Region, China. The joint test team was supposed to travel along with the trailer over the entire itinerary.

After having made all possible preparations, the actual joint test finally arrived and turned out to be a great success. Both customers' and KMS's test riders drove identical vehicles and directly communicated with each other, which disclosed difficulties or events that had not been understood well and allowed us to verify the measures against them and the resulting effects, although I cannot unfortunately give detailed information here because the test runs were confidential. I feel that the communications between the two parties, which were the most important thing for tuning, have been greatly improved. The joint test was also well received by the customers. I believe that the customers actually felt the KYB Group's precision.

After the test runs, we discussed a variety of topics with engineering staff from both parties, leading to higher motivation in KWT engineering staff. I remember the gleam in their eyes vividly even now after coming back to Japan.

Photo 7 Trailer for tuning

Photo 8 Test run

7. In Closing

Fortunately, the current domestic sales of KWT in China are brisk. I heard that KWT was selected as one of the China's top ten motorcycle component manufacturers. I hope that this activity has contributed to the selection. As an engineer, my work has really paid off.

Photo 9 shows how the KWT and KMS colleagues from each country were praising each other in an after-party of the whole joint test itinerary. This photo is a source of my bravery. I'm proud that I was a member of such a marvelous event.

Finally, I would like to appreciate anew the customers who extended cooperation to this program, all those who gave me an opportunity to study abroad, my boss who allowed me to take on this challenge, and the local staff who pulled together with me. Thank you very much, everyone!

Photo 9 Colleagues from each country praising each other

Author

KITAMURA Yasuhiro
Joined the company in 1996.
Manager, Operations Planning Dept., Motorcycle Headquarters, Automotive Components Operations.
Taken present post after being engaged in design operation in KYB Motorcycle Suspension (KMS) and working as an expatriate in Wuxi KYB Top Absorber Co., Ltd.

Glossary

Thermal Model of Thermal Network Method

Refer to Thermal Analysis of Electronic Circuits (page 25)

KAWANO Tomoyuki, SEKINE Nobuyuki, ITO Kensuke
Electronics Technology Sect., Basic Technology R&D Center

KABASAWA Ryoichi
KYB Technical Review Editor

1 Introduction

This Glossary describes the Thermal Model used in the thermal network method, which is an approach to thermal design. With a focus on similarities between heat conduction and electrical conduction, the thermal network method relies on the substitution of a heat transfer route by a thermal circuit consisting of thermal resistance and thermal capacity as shown in Table 1, from which temperature and heat flow can be calculated for thermal design.

Table 1 Relationships between thermal conduction and electrical conduction

Thermal	Unit		Electrical	Unit
Temperature	K	→	Voltage	V
Flow	W(=J/s)	→	Current	A
Resistance	K/W	→	Resistance	Ω(=V/A)
Capacity	J/K	→	Capacitance	F(=A・s/V)

Heat transfer can take place in three different modes: "heat conduction" in a solid body, "thermal radiation" by means of electromagnetic waves, and "heat convention" from a solid to a fluid. Heat itself is a kind of kinetic energy of molecules and atoms. To create a thermal model, it is necessary to understand the materials used in electronic components and determine how they physically behave at the atom/electron scale. On the other hand, product design only requires a simplified model for rough estimation of heating temperature, not an accurate model based on a strict physics theory. Simply creating an appropriate circuit model with materials and geometry taken into account will enable the quick calculation of heating temperature using an electronic circuit simulator. How to configure a circuit model is the key to obtain results approximating actual temperatures. The following explains the knowhow with expressions that are as accurate as possible while giving higher priority to introducing of the model in an easy-to-understand way.

2 Temperature, Movement of Atoms, and Thermal Capacity

Assume that an atom having a mass m moves at a velocity v in a gas at a temperature T. According to the principle of equipartition, the kinetic energy E of the atom can be expressed by Equation (1):

$$E = \frac{1}{2}mv^2 = \frac{3}{2}kT \tag{1}$$

where k is a physical constant called Boltzmann's constant of 1.38 x 10^{-23} J/K. If T = 300 K, the energy of the single atom at room temperature (26.85˚C) can be expressed by Equation (2):

$$E = \frac{3}{2}kT = 6.21 \times 10^{-21} \tag{2}$$

For copper, for instance, the mass m of the atom is 1.06 x 10^{-25} kg. From the energy value expressed by Equation (2), the average velocity v of the atom is 342 m/s as expressed by Equation (3):

$$v = \sqrt{\frac{2E}{m}} = 342 \tag{3}$$

Next, assume there is a Japanese 10-yen coin at room temperature (Fig. 1). The copper atoms constituting the coin have kinetic energy equivalent to the average velocity indicated by Equation (3). These copper atoms are bound together with adjacent copper atoms by metal-to-metal bonding and can only vibrate within a limited range. In this case, it can be said that the kinetic energy

proportional to the temperature has been accumulated in the 10-yen coin. In other words, the 10-yen coin serves as a capacity to store the heat. The total kinetic energy U of the atoms is proportional to the temperature T and can be expressed by Equation (4). The proportionality constant C represents thermal capacity and is defined as the amount of heat required to increase the temperature of an object by 1 K. The unit is [J/K].

$$U = CT \tag{4}$$

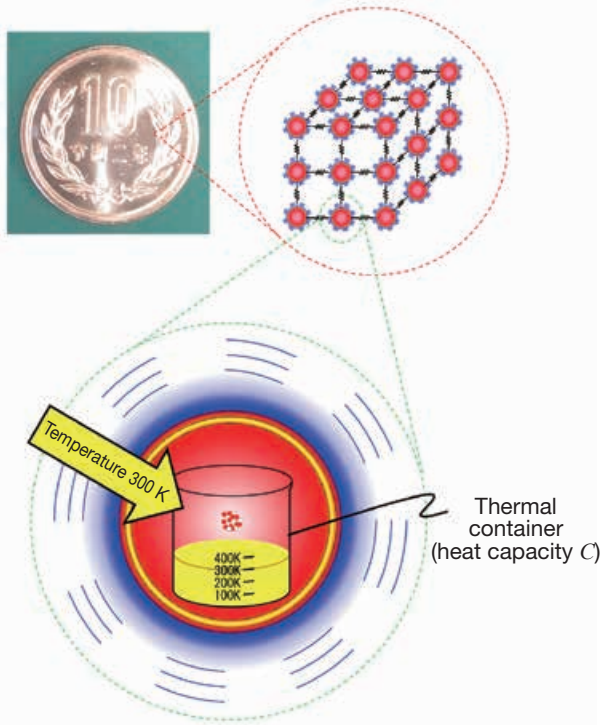

Fig. 1 Movement of copper atoms constituting a 10-yen coin

3 Mutual Vibration and Thermal Resistance of Atoms

Next, consider the force to bind atoms of a solid body together (Fig. 2).

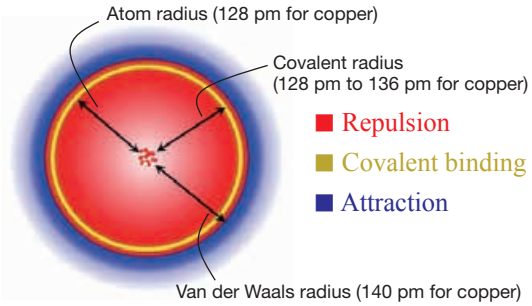

Fig. 2 Distance from the center of the atom and forces applied

Atoms (ions not included here) a certain distance away from each other are held together by forces of attraction (the Van der Waals force). When these atoms come closer to each other, the forces of attraction are replaced by the forces of repulsion at a certain distance between them (the Van der Waals distance). When they come still closer to each other, they share electrons of neighboring atoms to have covalent bonding, keeping their distance at a fixed length (covalent distance). If they are forced to be even closer to each other, they strongly repel against each other in the manner of a rigid body (atomic radius). These forces exerted among the atoms are used to transfer the vibration energy among the neighboring atoms (Fig. 3).

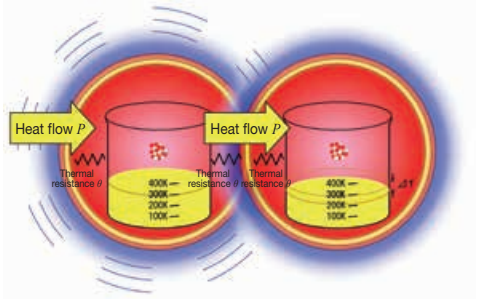

Fig. 3 Distance from the center of the atom and forces applied

Since the vibration energy is gradually transferred with the forces of attraction and repulsion, there arises a time difference in propagation, hindering the heat conduction. Assuming this is thermal resistance θ, the relationship between the heat flow P and temperature change ΔT caused by the flow can be expressed by Equation (5):

$$\Delta T = \theta P \tag{5}$$

This relationship may be substituted by an electric circuit and can be expressed by a multi-stage filtering circuit with the capacitance stated above, as shown in Fig. 4:

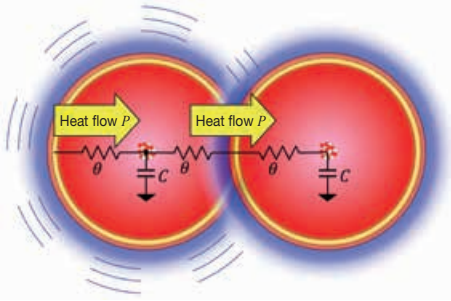

Fig. 4 Heat conduction model of atoms

Fig. 5 shows another model of a greater number of atoms, expanded from the two-atom model shown above, representing how the heat flow P sequentially propagates to neighboring atoms:

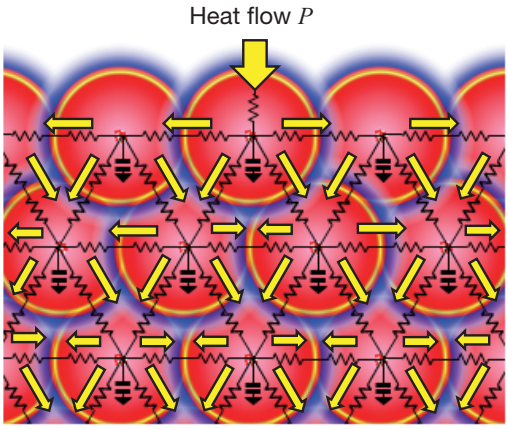

Fig. 5 Heat propagation model of multiple atoms

4 Modeling of Heat Conduction Within a Solid Body

A heat conduction model of a solid body may be created by joining a number of heat conduction models of atoms. For such a model, however, the calculation load is very high. For this reason, it should be converted into a simpler model with similar behavior.

Fig. 6 shows an example of such models. When an atom receives the heat flow P, it transfers the heat to its neighboring atom. This operation is similar to a bucket brigade. If a single atom is replaced by a thermal circuit, these models can be substituted by a T-type low pass filter (LPF). Several LPFs can be combined to create a thermal network.

The first resistance to receive the heat flow P may be omitted in a case of calculating from the temperature T_1 of the first atom. Two resistances that bind two atoms may be put together as a single resistance.

Furthermore, the n-stage LPFs for atoms can be approximated by a primary LPF if the conditions are met.

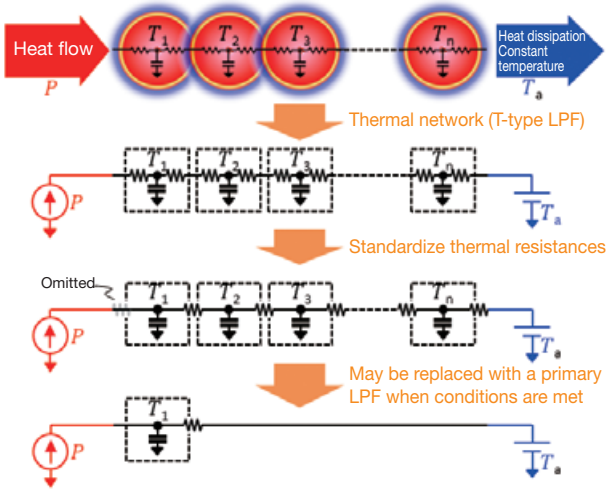

Fig. 6 Simplified heat conduction model of solids

Assuming that the input heat flow is P, the input temperature T_1, and the output temperature T_a, Equation (6) for a primary LPF consisting of resistance θ and capacity C can be obtained:

$$\frac{T_1 - T_a}{P} = \frac{1}{sC + \frac{1}{\theta}} = \frac{\theta}{sC\theta + 1} \tag{6}$$

In the steady state (s → 0), the effect of the thermal capacity C is negligible. The calculation can be made by Equation (7):

$$T1 - Ta = \theta P \tag{7}$$

A tip for modeling is to replace atoms with an LPF of an appropriate order based on the materials and geometry of the elements.

5 Modeling of Conductive Heat Transfer with Free Electrons

Heat conduction in a solid body involves heat propagation with lattice vibration as well as the action of free electrons if the body is metal. Metal is popularly used as heat dissipating materials such as heat sink and substrates and is an indispensable element of the heat conduction model.

Fig. 7 shows a metallic square pole of a cross-sectional area S, a length l and a thermal conductivity λ. The thermal resistance θ on both sides of the metallic pole is defined by Equation (8). The temperature change can be expressed by Equation (9) using the thermal resistance and heat flow P:

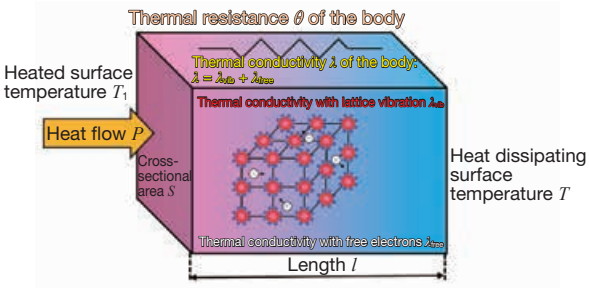

Fig. 7 Thermal conduction model of metal

$$\theta = \frac{l}{S\lambda} \tag{8}$$

$$T_1 - T_a = \theta P = \frac{l}{S\lambda} P \tag{9}$$

The electrical and thermal conductivities of metal show a coefficient of correlation as high as 99.6% as shown in

Fig. 8, known as the Wiedemann-Franz law. The law implies the high contribution of free electrons to the thermal conductivity of metal.

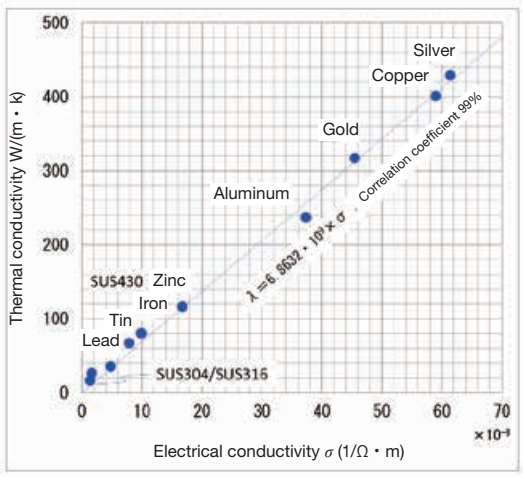

Fig. 8 Relationship between thermal and electrical conductivities of metal

6 Modeling of Thermal Radiation

Thermal radiation is a phenomenon in which thermal energy is emitted from an object as electromagnetic waves. According to the Stefan-Boltzmann law, heat flow proportional to the temperature to the 4th power is released. Since thermal radiation takes place on the surfaces of a solid body, this is an important mode of heat dissipation on a surface exposed to the atmosphere.

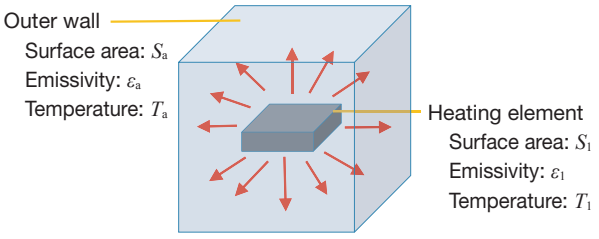

Fig. 9 Illustration of thermal radiation

As shown in Fig. 9, the thermal flow radiated from the outer wall of a surface temperature S_a, a temperature T_a, and an emissivity ε_a of a component having a surface area S_1, a surface temperature T_1, and an emissivity ε_1 to the atmosphere can be expressed by Equation (10). The emissivity ε_1, ε_a is a correction factor between 0 and 1 and is decided by the material and roughness of the surface of the solid body. σ is the Stefan-Boltzmann constant and takes a value of 5.67 x 10^{-8} W/(m^2 • K^4). If $S_a \gg S_1$, that is, heat is transferred to a distance, it can be approximated by Equation (11) and the surface temperature of the solid body can be determined by Equation (12).

This relationship can be substituted by an electric circuit with a constant voltage source and resistances as shown in Fig. 10:

$$P = \frac{\sigma}{\frac{1}{\varepsilon_1} + \frac{S_1}{S_a}\left(\frac{1}{\varepsilon_a} - 1\right)} S_1 (T_1^4 - T_a^4) \tag{10}$$

$$P = \varepsilon_1 \sigma S_1 (T_1^4 - T_a^4) \tag{11}$$

$$T_1 - T_a = \theta P = \frac{1}{\varepsilon_1 \sigma S_1 (T_1^2 + T_a^2)(T_1 + T_a)} P \tag{12}$$

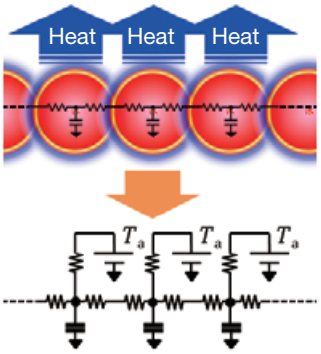

Fig. 10 Thermal radiation heat transfer model

7 Modeling of Convective Heat Transfer

Convective heat transfer involves the transfer of heat from one place at a higher temperature to another at a lower temperature. For an electronic component that generates heat, the heat should be released to the atmosphere to cool the heated component. This heat dissipation is convection.

Since most electronic components are solid, the following discusses heat transfer from a solid to a gas.

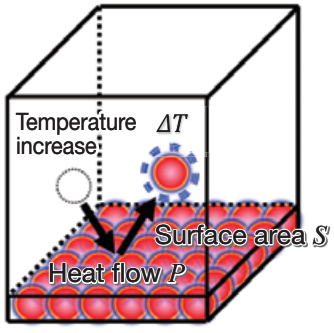

Fig. 11 Illustration of convective heat transfer

On the surface of a heat-generating solid body the atoms are thermally vibrating. When the surface of the solid body is exposed to a gas, the gas receives the thermal vibration, thereby increasing in temperature. After giving off the energy from the surface, the solid body has less thermal vibration, thereby decreasing in temperature. This process takes place repeatedly with a number of molecules to achieve cooling (Fig. 11).

Assuming that the surface temperature of the solid body is T_1, the atmosphere temperature T_a, the surface area of the solid body S, and the heat transfer coefficient h, the heat flow can be expressed by Equation (14) according to Newton's law of cooling (Fig. 59):

$$P = hS(T_1 - T_a) \tag{13}$$

$$T_1 - T_a = \theta P = \frac{1}{hS} P \tag{14}$$

The heat transfer coefficient refers to the amount of heat that is transferred per unit of time in unit of area when the difference in temperature between the surface of a body and its surrounding atmosphere is 1 K. Practically, 5 to 10 W/(k • m^2) is generally used. A lower value may be used in an enclosed space.

As in the case of thermal radiation, the convective heat transfer model can be substituted by an electric circuit with a constant voltage source and the resistances shown in Fig. 10.

References

1) KUBOTA Naminosuke, Basics of Heat Transfer, Nikkan Kogyo Shimbun (2009)
2) TANISHITA Ichimatsu, Industrial Thermodynamics for University Students, Shokabo (1968)
3) KUNIMINE Naoki, Perfect Introduction to Thermal Design for Electronics, Nikkan Kogyo Shimbun (1997)

Glossary

Electronic Linear-Actuator

Refer to Prototype of Electric Mechanical Actuator for Replacing Hydraulic Equipment (page 8)

SATO Kosuke
Information Technology R&D Sect., Basic Technology R&D Center

1 Actuators

The term "actuator" is defined by the Japanese Industrial Standard (JIS) [1] as "a device such as a motor or cylinder that converts hydraulic energy into mechanical energy ." This definition implies that the actuator is a type of energy converter. The JIS definition that only covers hydraulic equipment can be expanded to provide a wider scope of definition: "a device that converts energy, often hydraulic, electrical, or thermal, into kinetic energy such as rotation, linear motion or vibration, or vice versa."

Fig. 1 gives an overview of actuators with the form of energy on the horizontal axis and kinetic energy on the vertical axis. Arrows that appear along the horizontal or vertical axis indicate a direction of flow of energy. A conversion in the forward direction from the horizontal axis (form of energy) along the vertical axis (kinetic energy) is called a power operation (for electrical energy) or meter-in operation (for hydraulic energy), while a conversion in the reverse direction is called a regenerative operation (electrical) or a meter-out operation (hydraulic). More strictly, hydraulic cylinders and linear motors are energy converters that can support conversion in both the forward and reverse directions.

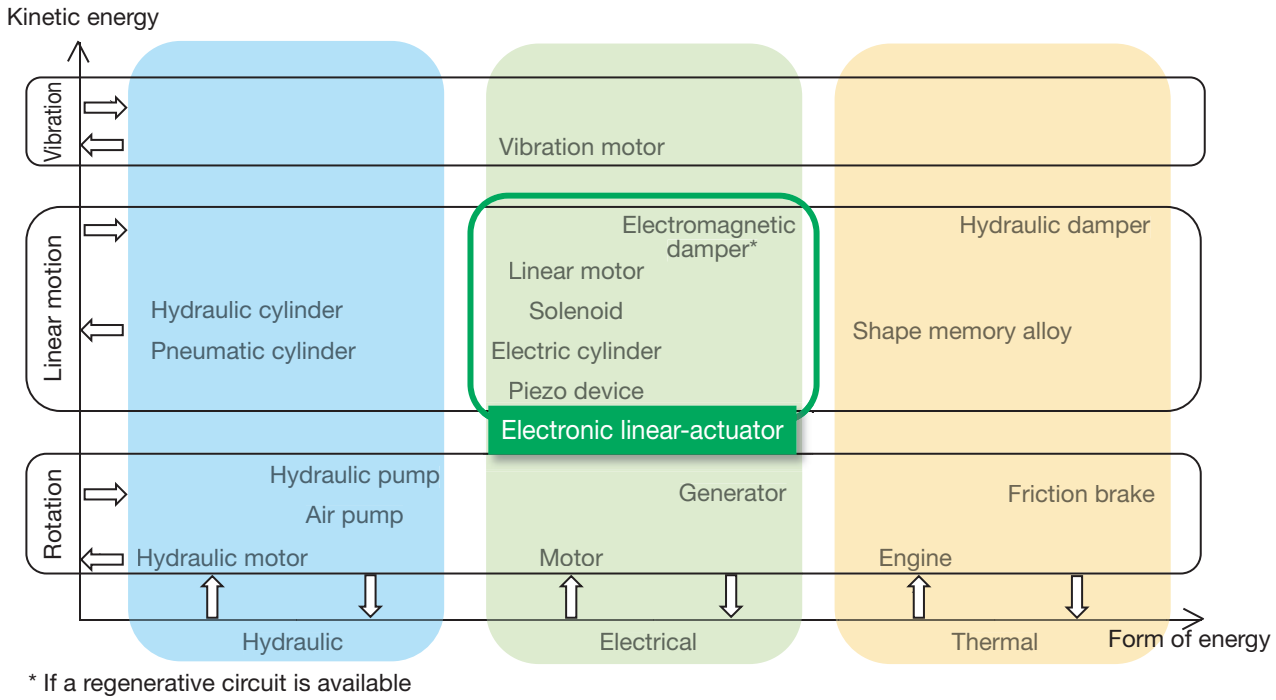

Fig. 1 Overview of actuators

2 Electronic Linear-Actuator

Electronic linear-actuators are those boxed in a green frame in Fig. 1. The electronic linear actuator is "a device that converts electrical energy into linear motion kinetic energy or a device that converts linear motion kinetic energy into electrical energy." Electronic linear-actuators are synonymous with electric mechanical actuators. The paper uses the term "electric mechanical actuator."

The electronic linear-actuator is available in two different configurations: "motor + ball screw" and "linear motor + sliding mechanism." Fig. 2 shows these configurations of electric linear-actuators from the viewpoint of energy conversion. The linear motor has the advantage of energy conversion takings place only once and potential energy efficiency being high, and has the disadvantage of having a magnetic section that would not contribute to the thrust at the moment of a stroke (Fig. 3). Note that the motor, which is a rotary machine, uses all the magnetic sections to deliver torque.

The relationship between the electronic linear-actuator and the linear motor is shown in Fig. 4. The linear motor is included in the electronic linear-actuator. Particularly in order for the electronic linear-actuator to replace the hydraulic cylinder or damper, the strut function corresponding to the sliding mechanism in Fig. 4 is important.

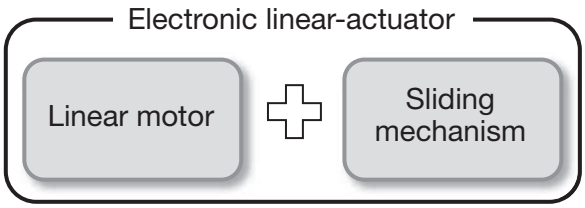

Fig. 4 Electronic linear-actuator and linear motor

3 Actuators in IoT

Recently, the Internet of Things (IoT), which connects a number of things and people over the Internet and creates new added value, has become popular worldwide. IoT consists of applications, clouds, security, networks, sensors, and actuators [2]. Among these, actuators play the role of the limbs of IoT. Electronic linear-actuators that are congenial to IoT are becoming more and more important.

References

1) JIS B 0142: 2011, Fluid Power Systems and Components - Vocabulary
2) KATAYAMA Akio, et.al, Textbook for IoT Engineers, Gijutsu-Hyohron

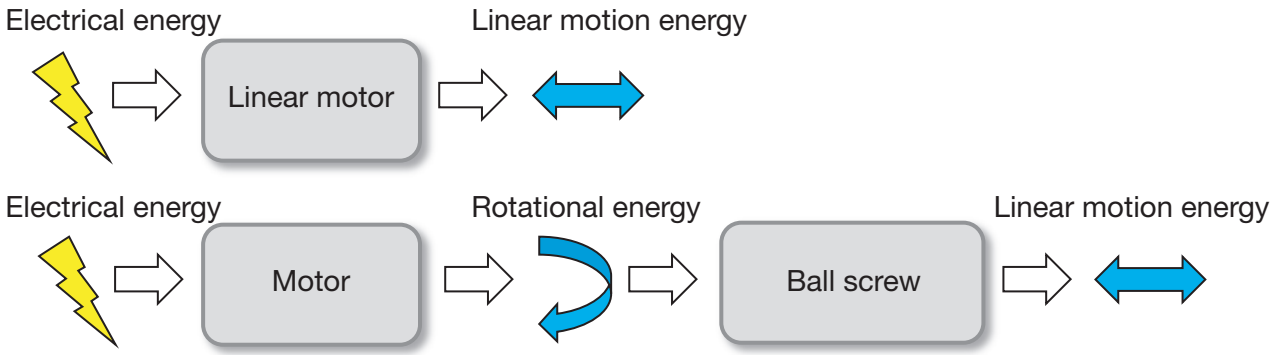

Fig. 2 Configurations of electronic linear-actuators

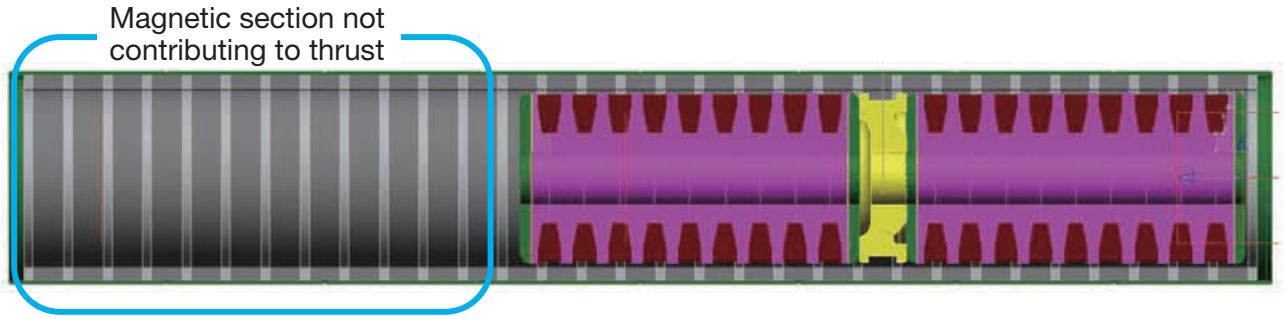

Fig. 3 Linear motor

Glossary

Open-center System/Closed-center System

Refer to Development of Control Valve KVSX-12C for Small Size Excavators (page 46)

FUKUSHIMA Ryo
Valve Design Sect., Ueda Engineering Dept., Hydraulic Components Operations

1 Open-center System

1.1 What is the Open-center System?

The open-center system consists of a bleed-off circuit, a meter-in circuit, and a meter-out circuit (Fig. 1). The bleed-off circuit controls the flow of oil from the pump to the tank. The meter-in circuit controls the flow of oil from the pump to the actuator. The meter-out circuit controls the flow of oil from the actuator to the tank.

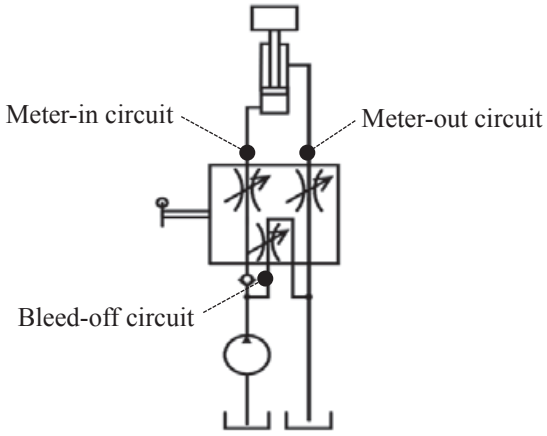

Fig. 1 Open-center system circuits

When the spool is in the neutral position, the bleed-off circuit is open while the meter-in and meter-out circuits are closed. The actuator is disabled in this condition.

Switching the spool position with a control lever closes the bleed-off circuit and opens the meter-in and meter-out circuits, operating the actuator.

1.2 Features of Open-center System

With a constant discharge from the pump, when the actuator load has any pressure variation, the distribution ratio between the bleed-off and meter-in circuits changes, affecting the supply flow to the actuator. In other words, if the actuator load has pressure variation even with the control lever held in a fixed position, the actuator speed changes (Fig. 2).

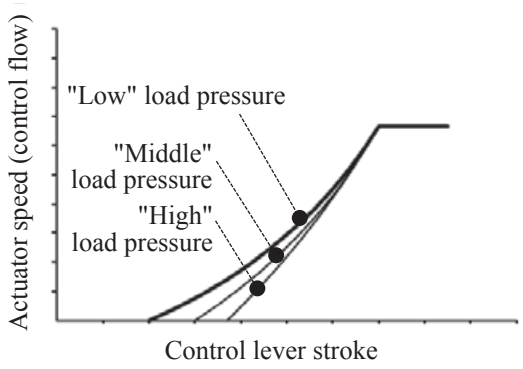

Fig. 2 Relationship between control lever stroke and actuator speed

This can be expressed by the orifice flow equation $Q = C\ A\ \sqrt{\Delta P}$ (Q: Flow rate, C: Capacity coefficient, A: Orifice area, ΔP: ¬Pressure difference). ΔP indicates the pressure difference over the meter-in orifice. To follow the pressure variation of the actuator load, the flow rate to the actuator Q changes.

If you were to compare this system to driving a car, your car slows down on a slope even if you keep pressing the accelerator to a certain depth.

1.3 Types of Open-center System

Small excavators are usually used in combination with a fixed displacement pump that discharges fluid at a fixed flow rate all the time. Medium-sized excavators in turn are generally combined with a variable displacement pump that discharges a given flow of fluid according to

input signals. For the open-center system combined with a variable displacement pump, the system can be controlled in two different ways. One is negative control for which an orifice is provided downstream from the bleed-off circuit to feedback the downstream pressure to the pump in order to control the discharge flow. The other is positive control for which a signal (pressure or current value) corresponding to the spool actuating variable is fed back to the pump to control the discharge pressure.

The both systems are of energy-saving type that can minimize the pump discharge according to the actuating variable.

2 Closed-center System

2.1 What is the Closed-center System?

A typical circuit of closed-center system is a load-sensing system.

Unlike the open-center system, the load-sensing system has no bleed-off circuit. It mainly consists of a meter-in circuit and a meter-out circuit and is combined with a variable displacement pump (Fig. 3).

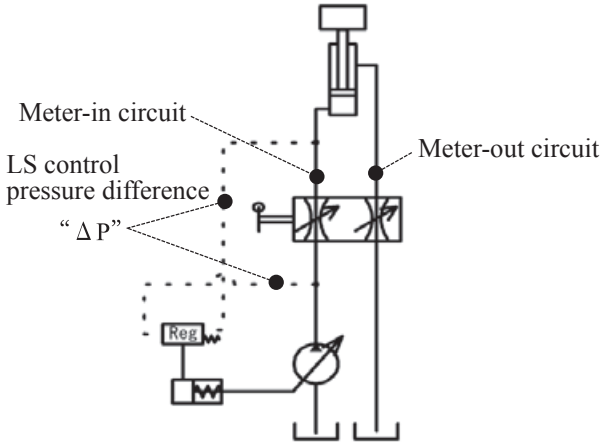

Fig. 3 Load-sensing system circuits

When the spool is in the neutral position, the meter-in and meter-out circuits are closed, disabling the actuator. In this case, the pump discharges fluid at a stand-by flow rate to the tank via an unload valve and other devices.

Switching the spool position with a control lever will close the unload valve and open the meter-in and meter-out circuits, operating the actuator. Thus, the pressure of the actuator load is fed back to the pump so that the pressure difference over the meter-in orifice ΔP is constant, controlling the discharge flow. This ΔP is defined as the LS control pressure difference.

2.2 Features of Load-sensing System

The flow rate of fluid supply to the actuator does not change even if the actuator load has pressure variation. In other words, if the actuator load has pressure variation even with the control lever held in a fixed position, the actuator speed does not change (Fig. 4).

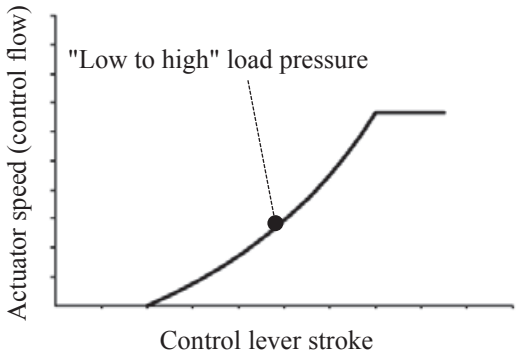

Fig. 4 Relationship between control lever stroke and actuator speed

This can be expressed by the orifice flow equation $Q = C A\sqrt{\Delta P}$. ΔP indicates the pressure difference over the meter-in orifice. Since the load-sensing system has a constant ΔP, the flow rate Q does not change.

2.3 Trend of Load-sensing System

The load-sensing system is of energy-saving type that can minimize the pump discharge according to the actuating variable and is in increasing demand mainly for small excavators.

With its features of being independent of any pressure variation of the actuator load and having a reliable flow control according to the actuating variable, the demand for the load-sensing system has recently grown not only for excavators but also for hydraulic systems for automation.

Editors Script

Since I am involved in the development of production technology, I mainly collect articles related to production technology. However, since most of the production technology is know-how, it is often impossible to write about it even if I wanted to, and it is always difficult to collect articles. This is the fifth number since I became an editor of the Technical Review. But among the articles of the past five numbers, only about 10% have been related to production technology. Engineers usually want to promote technologies they have developed themselves, but this hope can be seldom materialized. How can you promote your own technology without disclosing the related production engineering knowhow? It may be a point for the editors to show their skills.
(KAWAZOE)

I never imagined these circumstances a little while ago. Now we need to coexist with COVID-19. If you think you have to change or transform your lifestyle or your awareness of your behavior in a negative way, you may find yourself feeling down. I do not like to be nostalgic, but, when looking back at some numbers of KYB Technical Review issued several years ago, I feel that the editors then tried to encourage employees to continue covering topics that what would bear fruits soon or in future, as their mission, without fearing changing something or changing themselves.

Anyway, KYB Technical Review, including its archive of past numbers, is also available on the company's website. I would be happy for you to feel free to visit the site and casually browse the Review, just like me. (OTA)

When looking through the KYB Technical Review, you can readily notice that the company has carried out research and development in truly various fields. Editors are often responsible for editing articles or papers related to a field of expertise that is not their own, so they have trouble understanding the contents before editing. On a personal note, I took a qualification test last year and its notification of acceptance arrived at my house when I was involved in the editing of this Review.

Actually, I was almost a beginner in the field of the test I took, which is quite different from my area of specialization. With nearly three months of self-learning, I fortunately passed the test on my first try. The fact that I put forth effort in a field of expertise other than my own may be useful in my future editing work or my efforts for new research and self-development.
(OKADA)

KYB TECHNICAL REVIEW No.62

Published on April 1, 2021
Editor and publisher: KYB Technical Review Editorial Board
Publishing office: KYB Corporation
(In October 1, 2015, Kayaba Industry Co., Ltd. changed its trade name to KYB Corporation.)
World Trade Center Building,
4-1 Hamamatsu-cho 2-chome, Minato-ku, Tokyo 105-6111
TEL: 03-3435-6451
FAX: 03-3436-6759
Published by Shobi Printing Co., Ltd. (Hakusan, Tokyo)

Notification regarding website release

Thank you for supporting KYB TECHNICAL REVIEW. Since the 50th edition (issued in April of 2015), we have been releasing these reviews on our website with the aim of enabling more people to read them.
We will also continue to publish the booklets as usual, so please read the printed version and/or the website at your convenience.

<KYB website>
http://www.kyb.co.jp/
(Please click on the KYB REVIEW banner on the home page).